

The Monitor Project: Stellar rotation at 13 Myr

I. A photometric monitoring survey of the young open cluster h Per.

E. Moraux¹, S. Artemenko², J. Bouvier¹, J. Irwin³, M. Ibrahimov⁴, T. Magakian⁵, K. Grankin², E. Nikogossian⁵, C. Cardoso⁶, S. Hodgkin⁷, S. Aigrain⁸, and T.A. Movsessian⁵

¹ UJF-Grenoble 1 / CNRS-INSU, Institut de Plantologie et d'Astrophysique de Grenoble (IPAG) UMR 5274, Grenoble, F-38041, France

² Crimean Astrophysical Observatory, p/o Nauchny, 98409, Crimea, Ukraine

³ Harvard-Smithsonian Center for Astrophysics, 60 Garden Street, Cambridge, MA 02138, USA

⁴ Ulugh Bek Astronomical Institute of the Uzbek Academy of Sciences, Astronomicheskaya 33, 700052, Tashkent, Uzbekistan

⁵ Byurakan Astrophysical Observatory, 0213, Aragatsotn reg., Armenia

⁶ Istituto Nazionale di Astrofisica, Osservatorio Astronomico di Torino, Strada Osservatorio 20, 10025 Pino Torinese, Italy

⁷ Institute of Astronomy, University of Cambridge, Madingley Road, Cambridge, CB3 0HA, UK

⁸ Astrophysics, Denys Wilkinson Building, University of Oxford, Oxford OX1 3RH, UK

Accepted 20/06/2013

ABSTRACT

Aims. We aim at constraining the angular momentum evolution of low mass stars by measuring their rotation rates when they begin to evolve freely towards the ZAMS, i.e. after the disk accretion phase has stopped.

Methods. We conducted a multi-site photometric monitoring of the young open cluster h Persei that has an age of ~ 13 Myr. The observations were done in the I -band using 4 different telescopes and the variability study is sensitive to periods from less than 0.2 day to 20 days.

Results. Rotation periods are derived for 586 candidate cluster members over the mass range $0.4 \leq M/M_{\odot} \leq 1.4$. The rotation period distribution indicates a slightly higher fraction of fast rotators for the lower mass objects, although the lower and upper envelopes of the rotation period distribution, located respectively at ~ 0.2 - 0.3 d and ~ 10 d, are remarkably flat over the whole mass range. We combine this period distribution with previous results obtained in younger and older clusters to model the angular momentum evolution of low mass stars during the PMS.

Conclusions. The h Per cluster provides the first statistically robust estimate of the rotational period distribution of solar-type and lower mass stars at the end of the PMS accretion phase (≥ 10 Myr). The results are consistent with models that assume significant core-envelope decoupling during the angular momentum evolution to the ZAMS.

Key words. Stars: rotation – Stars: low-mass – open clusters and associations: individual: h Per

1. Introduction

The angular momentum evolution of low mass stars is best characterized by measuring the rotation rates of coeval populations at well-defined evolutionary stages. Star forming regions and young open clusters offer such an opportunity for the pre-main sequence (PMS) and main sequence (MS) evolutionary phases, as they harbour rich stellar populations of known age. Thus, in recent years, thousands of rotational periods have been derived for low-mass stars and brown dwarfs in these environments, covering an age range from 1 Myr to 1 Gyr. A compilation of these efforts was provided by Irwin & Bouvier (2009) and rotational distributions at additional age steps have been further documented since then (e.g., Hartman et al. 2010; Littlefair et al. 2010; Meibom et al. 2011; Affer et al. 2013). These results yield prime observational constraints for the development of stellar angular momentum models (e.g., Gallet & Bouvier 2013). Yet, a major deficiency on the time sampling provided by these studies concerns the end of the pre-main sequence evolution, between 5 Myr (Irwin et al. 2008a) and 40 Myr (Irwin et al. 2008b), which remains poorly documented (Messina et al. 2010, 2011). The goal of the study presented in this paper is to remedy the lack of statistically robust rotational distributions in this age range by

measuring the rotational periods of hundreds of low-mass members of the young open cluster h Per at an age of about 13 Myr (Mayne & Naylor 2008).

H Per, also known as NGC 869, is the westernmost of the Perseus double cluster with χ Per (or NGC884), separated by about $30'$. Visible to the naked eye and probably known since antiquity, this region was first cataloged by Hipparchus as a patch of light in the Perseus constellation in ~ 130 B.C.. Its true nature, however, was only discovered in 1780, well after the telescope invention, when sir William Herschel recognized h & χ Persei as two separate stellar clusters. Since early 1900, it has been the target of extensive photometric surveys using photographic plates (e.g. van Maanen 1911; Oosterhoff 1937) and spectroscopic studies (e.g. Trumpler 1926; Bidelman 1943; Schild 1965), leading to some controversy about the distances and relative ages of h and χ Per. More recent studies (e.g. Keller et al. 2001; Capilla & Fabregat 2002; Slesnick et al. 2002; Uribe et al. 2002; Bragg & Kenyon 2005; Mayne et al. 2007; Currie et al. 2010) are now converging to similar properties for both clusters, with a distance modulus of ~ 11.8 , an extinction $E(B - V) \sim 0.54$ and an age of ~ 13 Myr (Mayne & Naylor 2008). H Per is about 30% more

populous than χ Per with at least ~ 3000 stars within its $10'$ center and has an estimated mass of $\sim 4700M_{\odot}$ (Currie et al. 2010).

The age of h Per samples a critical phase for angular momentum evolution models. By that age, the disk accretion process has ceased, and the stars begin to freely evolve towards the zero-age main sequence (ZAMS). Hence, deriving the rotational distribution of low-mass stars in this cluster allows us to characterize the angular momentum properties of stars at the end of the accretion phase, when they have finally acquired their total mass and their angular momentum evolution is not affected any more by the interaction with the circumstellar disk. The distribution of rotation rates at this age also provides the initial conditions for further evolution to the ZAMS and onto the MS.

The paper is organized as follows. In the next section we describe the observations and explain briefly how the light curves were produced for selected possible candidate members. In Section 3, we present the method we used to measure rotational periods and discuss possible biases and contamination before giving our results. A general discussion on the angular momentum PMS evolution follows in Section 4 and Section 5 summarizes our conclusions.

2. Observations and light curve production of possible cluster members

Within the framework of the Monitor project (Aigrain et al. 2007), we conducted a multi-site photometric monitoring of h Persei during the fall 2008 using 4 different telescopes: the 3.6m Canada-France-Hawaii Telescope (CFHT), the 1.5m telescope in Maidanak (Uzbekistan), the 2.6m Shajn telescope (ZTSh) at the Crimean Astrophysical Observatory (CrAO, Ukraine), and the 2.6m telescope of Byurakan observatory (Armenia). The total amount of time spend to monitor the cluster was ~ 110 hrs, spread over 2 months from Sept. 5 to Oct. 27, 2008. The observations were done in the I -band and the individual exposure times were adapted to reach the equivalent of $i'_{CFHT} \approx 21$ with a signal to noise larger or equal to 10 at each telescope. The details of the observations performed at each telescope are described below. Table 1 provides a summary of all the observations, Figure 1 represents the various field of views and Figure 2 shows the sampling rate of the light curves.

2.1. Instrumentation and observing strategy

At CFHT, the observations were performed in the i'_{CFHT} filter with the $1\text{deg} \times 1\text{deg}$ MegaCam CCD mosaic (Boulade et al. 2003) over two runs (runID: 08BF06, P.I. E. Moraux and runID: 08BH17, P.I. B. Reipurth). Observing blocks of ~ 2 h were obtained over 10 nights in Oct. 1-7 and Oct. 21, 26, 27, 2008, yielding a total observing time of 23h. In total, 698 individual exposure times of 75s as well as 55 short exposures of 20s were obtained. The observing conditions were photometric and obtained during dark or grey time. The seeing was between 0.6 and 1 arcsec. One of the longest observing nights includes continuous measurements over more than 6h (0.25d), which proved very useful to distinguish between long and short period aliases in the period search analysis (cf. Section 3.1).

At Maidanak, the observations were obtained in the I_{Maid} -band filter using the SI 600 Series $4k \times 4k$ CCD camera at the 1.5m AZT-22 telescope. The field of view of the camera is $18' \times 18'$. The images are round and good up to $15'$ arcmin from the center but there is a small coma-like distortion at the edge of the FOV. The individual exposure time was 300s. A total of

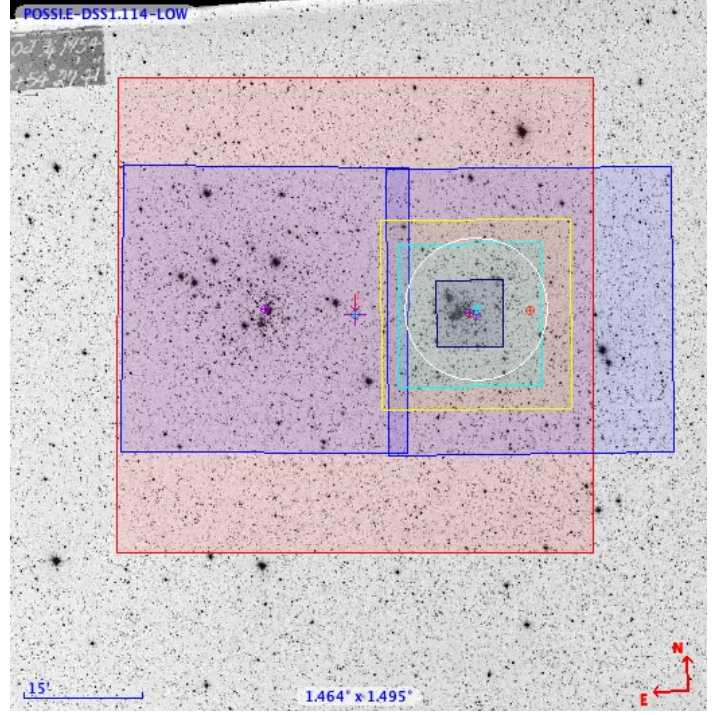


Fig. 1. Pointings of the various instruments used for this monitoring campaign: CFHT/MegaCam (red square), Maidanak (cyan square), CrAO, Byurakan (white circle). The field of view observed in the optical by Currie et al. (2010; blue rectangles) and in the near-infrared with CFHT/WIRCam by Cardoso et al. (in prep.; yellow square) are also shown. Their photometry is used to assess membership (see section 2.3).

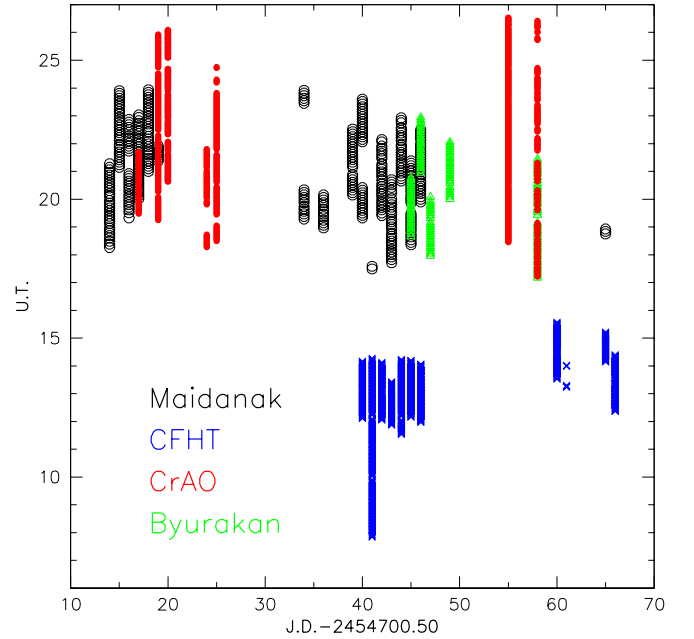


Fig. 2. Temporal sampling of photometric measurements obtained at Mt. Maidanak (black open circles), CFHT (blue crosses), CrAO (red dots), and Byurakan (green triangles) observatories.

Table 1. Journal of the observations

Telescope	pointing	FOV	Dates of observations	Number of nights	Individual exp. time	Total number of exposures	Total hours
CFHT 3.6m	02:20:42 +57:08:00	1° × 1°	Oct. 1-7 Oct. 21-27	7 3	75s (+20s)	698 (+55)	23h
Maidanak 1.5m	02:18:56 +57:08:00	18' × 18'	Sep. 5-9 Sep. 25 - Oct. 7 Oct. 25-26	5 10 2	300s	402	42h
CrAO 2.6m	02:18:56 + 57:08:10	8.4' × 8.4'	Sep 8-16 Oct. 16-17	5 2	120s	992	33h
Byurakan 2.6m	02:18:50 +57:08:45	9' radius	Oct. 6-19	5	120s	142	12h
Total			Sep. 5 - Oct. 27	27		2234	110h

42.3 observing hours (corresponding to 402 individual frames) divided into blocks of ~ 3 hours were obtained over 3 different periods (Sep. 5-9, Sep. 25-Oct. 7 and Oct. 25-26). Only the first two periods benefited from good weather conditions and the data obtained during the 3rd period are not used in our analysis.

At CrAO, the observations were carried out in the I_{CrAO} photometric band, using a FLI PL-1001E CCD camera at the prime focus of the 2.6-m Shajn telescope (ZTSh). The pixel size of the 1024 × 1024 size CCD matrix KAF-1001E is 0.5 arcsec and the field of view is 8.4' × 8.4'. The cluster was imaged during 7 nights on Sept. 8, 10, 11, 15, 16 and Oct. 16, 19, 2008. The exposure time for each frame was 120 seconds and the total time of observations was about 33 hours corresponding to ~ 5 hours per night, yielding a total of 992 images. As weather conditions on September 15-16 were bad, we have excluded these two nights from the subsequent analysis.

At Byurakan, the observations were done at the prime focus of the 2.6m telescope with the ByuFOSC-2 camera, equipped with 2058 × 2063 pix Loral CCD matrix. This equipment provides a scale of 0.5 arcsec/pix and a full view of 17' × 17'. However, due to the absence of correcting optics, the non-distorted FOV is reduced to about 9' × 9'. Images were taken through the I_{Byur} -band filter with an exposure time of 120 sec. The seeing was about 2 arcsec during the observations performed over 5 nights on Oct. 6, 7, 8, 10, and 19, and the observing blocks were 2 hours long except on Oct. 19 where it was 4 hours long, yielding a total of 142 images.

2.2. Light curve production

The data processing and light curve production were performed for each dataset separately following the procedure described in Irwin et al. (2007a). Briefly, a master frame was created by stacking the images taken in the best seeing conditions before using the source detection software. The resulting master catalog containing the positions of the detected objects was then used to perform aperture photometry on all the individual images. For each frame, the difference between each source magnitude and its median (calculated across all frames) was measured to compute the frame offset and correct for seeing variation. A 2-D fit of the residual map was then subsequently removed to account for varying differential atmospheric extinction across each frame. Light curves were extracted for $\sim 219\,000$, ~ 8000 , ~ 2000 and ~ 3000 objects from the CFHT, Maidanak, CrAO and Byurakan images.

For the CFHT dataset, the achieved photometric precision for each data point is very good: it is better than 2 mmag for the brightest objects ($i'_{CFHT} \leq 16$), with a scatter < 1 per cent up to $i'_{CFHT} \approx 19.5$ (see Fig. 3). The detection limit on a single frame corresponding to a signal-to-noise ratio of 5 is reached

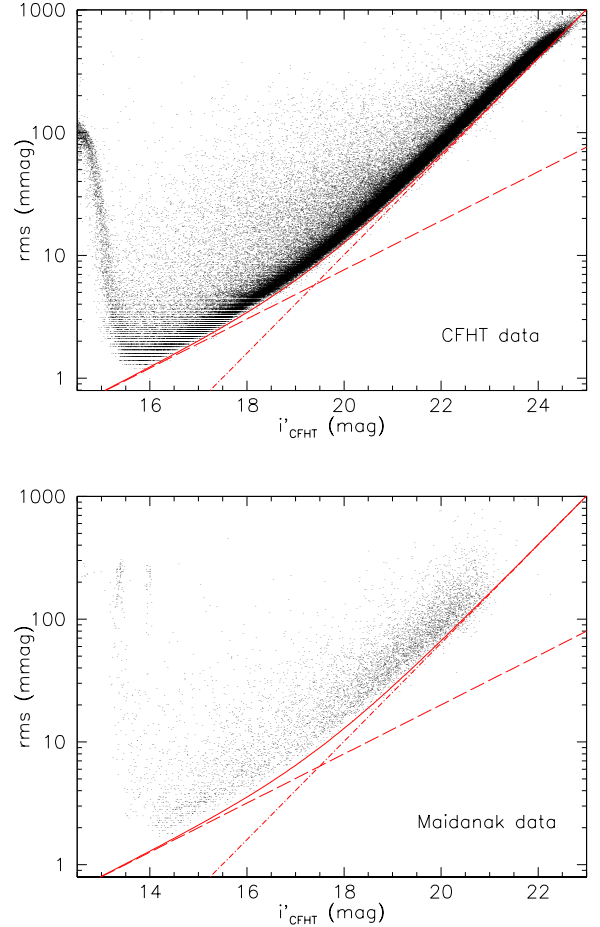


Fig. 3. Plot of RMS scatter per data point measured over the CFHT and Maidanak dataset as a function of i'_{CFHT} magnitude. The diagonal dashed lines show the expected RMS from Poisson noise in the object, the diagonal dot-dashed lines show the RMS from sky noise in the photometric aperture. The solid lines show the overall predicted RMS, combining these contributions.

at $i'_{CFHT} \approx 23.5$. The photometric precision for the Maidanak data is also very good, although not as deep. For the CrAO and Byurakan photometry however, the rms scatter never gets better than 5 mmag even for the brightest objects.

For each possible cluster member (see next section for a description of the selection), a quality check of each data point was performed before combining the light curves of the 4 different sites. If its magnitude was brighter than $i'_{CFHT} < 15.6$

($i'_{CFHT} < 13.8$) for the long (short) exposures of the CFHT images or $i'_{CFHT} < 14$ for the other data, we considered it as saturated (see Fig. 3). If the aperture contained bad pixels, if the frame seeing was extremely bad or if the frame offset was very large (typically if it falls in the worst 5% of the distribution in both cases), the data point was qualified as bad. We also marked all the objects located more than 550 pixels (or 4.6 arcmin) away from the center of Byurakan images due to strong distortion. And finally, we used a sigma clipping to identify all the data points for which the magnitude is more than 3 sigma away from the average magnitude of the 10 closest data points. In all cases, a flag was added to the data point and we kept only those with a flag 0 for our analysis.

For each object, we then computed the median magnitude of each light curve using only the good data points. We normalised the obtained value to the CFHT median taken as a reference by applying an offset, and we combined the light curves. No color term was applied. For the period search described in section 4, we used only the data from CFHT and Maidanak however since the photometric precision is best for these two datasets. The data from CrAO and Byurakan observatory were used *a posteriori* to check the goodness of the period found.

2.3. Possible cluster member selection

We first built a master catalog by cross correlating all the sources detected in any of the monitoring images described above, i.e. from either CFHT, Maidanak, CrAO or Byurakan observatory. Since the field of view and the image quality was better for the CFHT and Maidanak datasets, we decided to focus on the objects that were detected at least in one of these two. The cross-correlation was done by coordinates with TOPCAT (Taylor 2005) using a matching radius of 2 arcsec. This leads to a catalog with 219,642 sources with $i'_{CFHT} \approx 13 - 24$.

We then cross-correlated our master catalog with data from the literature (Slesnick et al. 2002, Uribe et al. 2002, Mayne et al. 2007, Currie et al. 2007a, 2007b, 2007c, 2008 and 2010) in order to get as many photometric and/or spectroscopic information for each source. In particular, we used the V and I_C magnitude from Currie et al. (2010) as the observed field of view is very similar to our MegaCam pointing (see Fig. 1). We also used YJHK CFHT/WIRCam data (Cardoso et al., in prep.) as well as Chandra X-ray data (C. Argiroffi, priv. com.). Again the matching radius was set to 2 arcsec, except for the X-ray data for which we used 2.5 arcsec.

Using all the available photometric data we built colour-magnitude diagrams. Since the cluster sequence is clearly visible in all the CMDs, we defined an empirical sequence to assess membership. As an example, we can see in Fig. 4 the selection that we made in $i'_{CFHT}, V - i'_{CFHT}$. The two solid lines represent the cluster sequence shifted in colours by ± 0.1 mag plus the amount of the photometric error, and by -0.75 mag in i'_{CFHT} for the upper envelope to take into account binaries. All the objects located between the two lines were selected as candidate members. We performed the same selection on all the available CMDs. An object was eventually considered as a possible cluster member if its optical $V - i'_{CFHT}$ colour and/or near-infrared WIRCam colours ($J - H$, $J - K$ and $H - K$) were consistent with membership. Alternatively, if these colours were not available (no detection) but the object was detected in $H\alpha$ (Currie et al. 2007c), or in X-ray (Currie et al. 2009, and C. Argiroffi priv. com.), or was classified as possible member by Currie et al. 2010 (membership flag ≥ 1) or Uribe et al. 2002 based on proper motion, we kept it as a cluster candidate. We ended up with a rather

conservative final catalog of 19,224 sources selected as possible members over the whole field of view. 45,710 objects were rejected based on their photometric colours and 154,708 objects were classified as “unknown” since we did not have any membership information (objects detected only in one filter, usually with MegaCam at CFHT since its FOV is larger than any other h Per survey that has been performed so far).

In order to estimate the level of contamination by field objects in our photometric selection, we used the Besancon galactic model (Robin et al. 2003). We performed the same analysis on our data and on the synthetic catalog to which photometric noise has been added. In both cases the considered FOV was restricted to the WIRCam pointing and we used only two CMDs ($i'_{CFHT}, V - i'_{CFHT}$ and $i'_{CFHT}, i'_{CFHT} - K$) for the selection. This will only provide us an upper limit of the contamination as we actually used more colours for the final photometric selection but this is sufficient for our purpose, especially as these two colours are the most constraining for membership selection. Overall we found a contamination level of 14% after selection on both $V - i'_{CFHT}$ and $i'_{CFHT} - K$ colours (26% if only $V - i'_{CFHT}$ is used, 34% if only $i'_{CFHT} - K$) in the magnitude range $i'_{CFHT} = 15 - 21$. The contamination per magnitude bin is given in Fig. 5. It is interesting to note that the selection drops to zero for the faintest objects. This is due to the fact that the cluster members are much redder than the galactic population in the chosen CMDs for $i'_{CFHT} = 20 - 21$ (see Fig. 4). There is therefore no contamination by field stars in this magnitude range (but by galaxies). For brighter magnitudes, however, the contamination gets larger especially when the cluster sequence joins the dwarf locus.

For the rest of the paper, we restricted our study to the possible members with $i'_{CFHT} > 15.6$ (16,381 objects) to avoid saturation on the CFHT long exposures (the time sampling on the short exposures being too low). Following the work from Cardoso et al. (in prep.), we converted the i'_{CFHT} magnitude of each candidate member into mass using the mass-magnitude relationship from Siess model at 13 Myr (Siess et al. 2000).

3. Period measurement analysis

3.1. Period search

In order to take the best benefit of our sampling, we performed the period search on objects detected in both CFHT and Maidanak images, i.e. with light curves containing more than 800 measurements (and up to 986). This allows us to be sensitive to both short and long periods and to avoid confusion between harmonics as much as possible. The CFHT and Maidanak measurements are spread over 51 nights, from JD 2454716 to JD 2454767, with two large observing gaps from JD 2454720 to JD 2454735 and from JD 2454748 to JD 2454761. The sampling rate is graphically shown in Figure 2. Photometry obtained at other sites is of lower quality and was only used *a posteriori* to confirm the measured periods. Of the 16,381 h Per photometric candidate members located within the CFHT FOV with $i'_{CFHT} > 15.6$, only 2287 were detected in both CFHT and Maidanak data. We thus restricted our period analysis to these sources.

Periodic signals were searched in the light curves using 3 methods : Lomb-Scargle periodogram (Scargle 1982; Horne & Baliunas 1986), CLEAN Discrete Fourier Transform (CLN DFT, Roberts et al. 1987) and String-Length minimization (Dworetzky 1983). In all cases, we probed a range of frequency from 0.05 to 5.0 d^{-1} (i.e., periods from 0.2 to 20 days). The

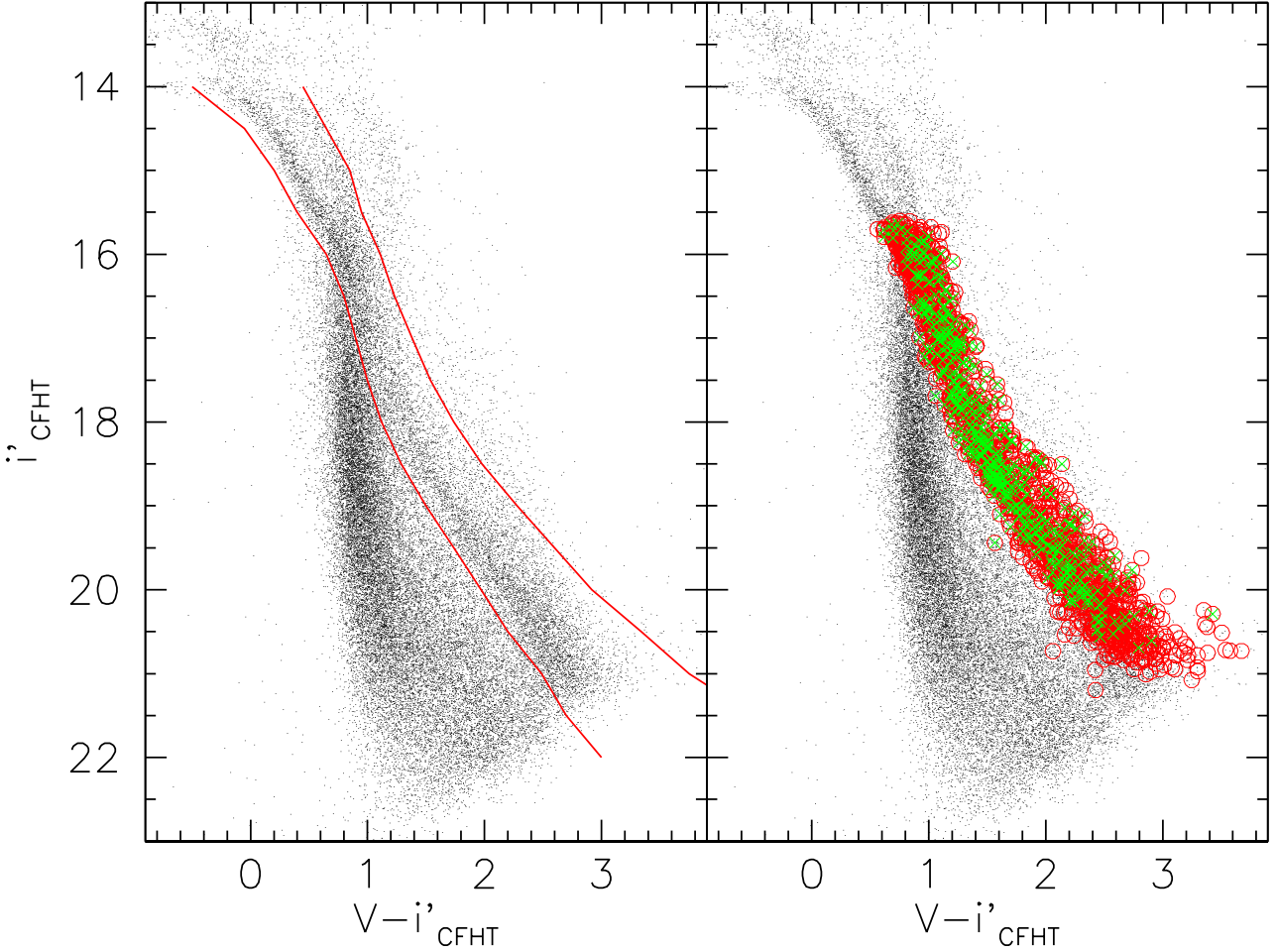


Fig. 4. $i'_{CFHT}, V - i'_{CFHT}$ colour magnitude diagram. *Left:* All the objects located between the two solid lines have been selected as possible cluster members. *Right:* The red open circles show the objects that have been analysed while the green crosses show the periodic objects (a colour version is available on the journal electronic version).

lower frequency limit is about twice the frequency resolution, $\delta f \approx 1/T$ where T is the total time span of the observations. The higher frequency limit was set somewhat arbitrarily to reduce computation time, though we are sensitive to much shorter periods ($f_{max} \approx \delta t^{-1} \approx 20 \text{ d}^{-1}$, see below). The frequency range was explored by step of 0.001 d^{-1} . At every sampled frequency, the power of the periodogram and of the CLEAN DFT, as well as the string-length were computed. For each light curve, we thus derive 3 possible periods corresponding to the highest peaks in the periodogram and CLN DFT, and to the shortest string-length in the phase diagram.

The power of the highest peak recorded in the periodogram of each of the 2287 light curve is plotted as a function of frequency in Figure 6. A clear accumulation of peaks occurs at frequencies around 0.5 and 1 d^{-1} . These peaks correspond to spurious periods resulting from the nightly sampling rate. We therefore removed all periods lying in the frequency ranges $0.48\text{--}0.51$ and $0.95\text{--}1.03 \text{ d}^{-1}$. This left us with 1761 possibly periodic h Per candidate members. As the investigated light curves have nearly the same number of measurements and a similar temporal sampling, the highest peak power also corresponds to the lowest False Alarm Probability (FAP, cf. Scargle 1982).

We derived FAP levels from a control sample (discussed in more details in Section 3.3) of 1307 field stars, i.e., photometric *non* members spanning a similar magnitude and color ranges in the $(V, V - i'_{CFHT})$ color-magnitude as h Per photometric candidate members. The light curves of these 1307 field stars also have a similar temporal sampling as those of the h Per candidate members under analysis. The cumulative distribution of the power of the highest peak in the periodograms of the field stars provides an estimate of the FAP, i.e., the probability that a given peak power merely results from statistical noise. After removal of spurious peaks at frequencies around 0.5 and 1.0 d^{-1} (see above), we are left with 890 field stars, from which we derive a FAP level of 0.01 for a peak power of 116, and FAP of 0.05 for a peak power of 72. These FAPs are illustrated in Fig. 6. As discussed by Littlefair et al. (2010), this approach is more accurate than analytical estimates of the FAP and/or FAP derived from Monte Carlo simulations.

Of the 1761 h Per candidates under analysis, we retained 872 with a FAP level less than 0.05 (604 with a FAP < 0.01) as be-

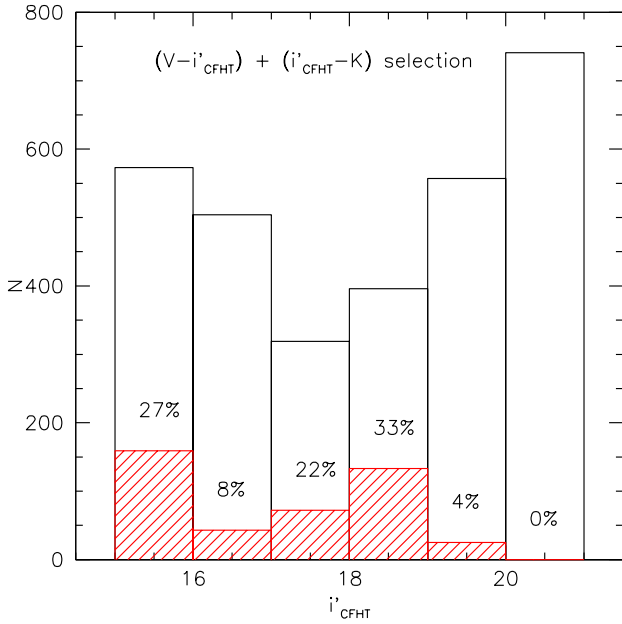


Fig. 5. Photometric contamination level per magnitude bin using the Besancon galactic model after selection in both $V - i'_{CFHT}$ and $i'_{CFHT} - K$ colours. The plain histogram corresponds to the number of objects selected as possible members from our data (and located in the WIRCAM FOV), while the dashed one corresponds to the selection performed on the synthetic catalogue obtained from the Besancon model for the same WIRCAM pointing.

ing possibly periodic¹. Their light curves were phase-folded with period estimates derived from the periodogram, CLN DFT and string-length methods. In most cases, the periodogram and CLN DFT return similar results. Whenever the 3 methods yielded different estimates, we visually relied on the phase diagrams to decide on the best period, if any. CLN DFT proved very reliable to detect the periods of sinusoidal-like light curves, while string-length was found sometimes, though rarely, superior for more complex signals (e.g double-spotted light curves, cf. HPer-195, -243, -431). The FAP analysis is not fully reliable on its own (cf. Littlefair et al. 2010) and must be complemented by eye-inspection of the phased light curves to remove interlopers. A significant fraction of the selected possibly periodic candidate members did not show any convincing phased light curves and we rejected 283 candidates as being non periodic. Among them, 90 had a FAP less than 0.01 while the others (193) had a FAP between 0.01 and up to 0.05. We considered that their phased light curves did not show periodic modulation by surface spots for one of the following reasons: unconvincing periods close to 0.5d or 1d (about 50% of the rejected light curves have periods

¹ Note that using a much lower FAP level, as sometimes done in other studies, may introduce a bias against long periods and small amplitudes.

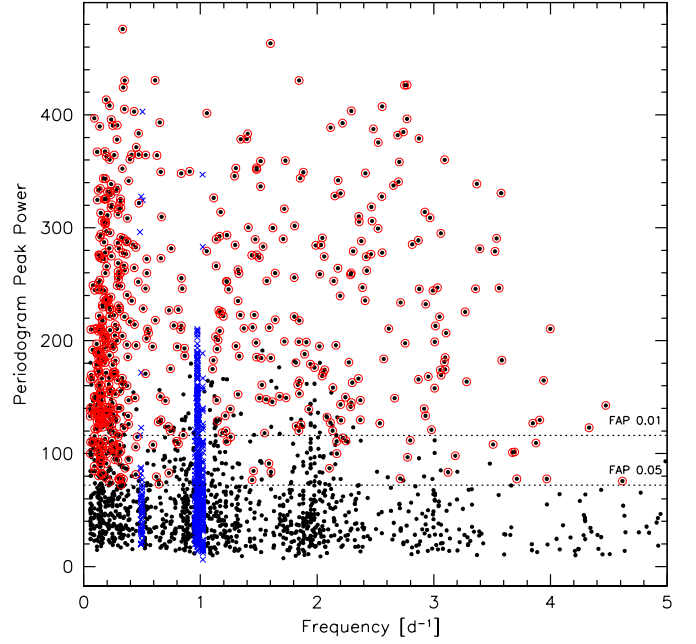


Fig. 6. The distribution of the power of the highest periodogram peak is shown as a function of frequency for 2287 h Per photometric candidate members analyzed for periodicity. Spurious periods occurring at frequencies around 0.5 and $1.0d^{-1}$ (shown as blue crosses) were discarded. The FAP levels computed from a control sample of non-periodic field stars are indicated. The 586 h Per candidate members that were eventually considered as periodic are encircled (red).

in the range 0.4-0.6d or 0.8-1.2d); presence of superimposed low and high frequency modulations, presumably frequency aliases, which do not allow us to reliably assess the true period; discontinuous photometric jumps in the phased light curves and/or systematic offsets between Maidanak and CFHT data; significant discrepancies between CFHT and Maidanak phased light curves; single flares or dips dominating the photometric amplitude.

In order to test the effect of the chosen FAP level, we defined two samples based on two different FAP cuts at 0.01 and 0.05, containing respectively 514 and 586 periodic objects after eye examination. We then compared their period distributions for the 4 mass bins discussed in section 3.5. The KS probability that both distributions are drawn from the same population is larger than 99.99% for the three higher mass bins, and is equal to 82.36% for the lower mass bin ($0.4-0.6 M_{\odot}$), indicating that there is no significant difference between the two samples. Thus, choosing one or the other cut in FAP level would not affect the results of the paper, and we decided to use the less selective threshold ($FAP < 0.05$) allowing to select all the clear periodic variables – in the line with our previous Monitor studies from Irwin et al. (2007b, 2008a, 2008b, 2009).

We finally ended with a sample of 586 periodic h Per candidate members, with a spectral type spanning a range from $\sim F0$ to M6. It is interesting to note that we measured a rotation period for about 50 F stars, which is of the same order than the number of such periodic stars found by Saesen et al. (2010) who investigated the variability of bright stars in χ Per in a similar FOV. Table 2 (available online) lists the periods and photometric amplitudes of all the periodic objects. The rms error

on each period can be computed as $\delta P = \delta v \times P^2$, where $\delta v = 0.0145d^{-1}$ is the average sigma of the gaussian fit to the highest peak in the CLN DFT. The amplitude of variability was derived from a sinusoidal fit to the light curves using FAMOUS². The phased light curves of the 586 periodic variables are shown in the appendix, Fig.[A1]. In some cases, especially for objects with short periods, the phased light curve provides clear evidence for phase and/or amplitude variations over the time span of the observations, indicative of spot evolution and/or surface differential rotation over a timescale of weeks (see e.g. HPer-208, $i'_{CFHT} = 15.72$, as an extreme case).

Note that some periods reported here are shorter than 0.2d, the lower limit of our period search range. This is because visual inspection of some phase diagrams clearly indicated that we had detected a lower frequency harmonic of the true period. In such a case, the period search analysis was repeated with a lower limit of 0.05d. This yielded 5 objects with clear photometric periods shorter than 0.2d, with the 2 shortest ones, amounting to only 0.0662 d (1.59 h) and 0.0982 d (2.36 h), illustrated in Figure 7. The spectral type (F1±2.5 according to Currie et al. 2010), mass (~1.4 M_{\odot}), and low photometric amplitude (~0.008 mag) of HPer-215 suggests δ -Scuti type pulsations rather than rotational modulation (Saesen et al. 2010; Chang et al. 2013). However, the red colors ($V - I_C \sim 4.5$; Mayne et al. 2007) of HPer-513, indicative of a spectral type ~M6, put this object far from expected pulsational instability strips at the age of the cluster (Rodríguez-López et al. 2012; Baran et al. 2011; Palla & Baraffe 2005). The shape of the phased light-curve is somewhat suggestive of a ($P_{orb}=0.19654d$) contact binary (Nefs et al. 2012).

The period analysis above was performed on the combined Maidaanak and CFHT datasets. The CrAO and Byurakan datasets, of lower quality and with a sparser, though complementary, temporal sampling were used to visually confirm the results. In most cases, whenever the S/N ratio of the latter datasets was high enough, the additional measurements adjusted consistently, albeit with a much increased scatter, onto the phased light curve, thus providing further support to the reported periods.

3.2. Period detection, completeness and reliability

We describe here Monte Carlo simulations that we ran on synthetic light curves to estimate the robustness and completeness of the period search analysis presented in the previous section. In order to build synthetic light curves, we first selected photometric cluster non-members in the CMD, i.e., objects running below the lower envelope of the cluster sequence, over the range $i'_{CFHT} \sim 15$ -21 mag. We further selected a subset of these non-members, whose photometric light curves had an rms dispersion lower than the median photometric error at a given brightness. Of this subset, we retained only those with light curves having at least 800 measurements from CFHT and Maidaanak, thus yielding a sampling rate similar to those of the h Per members analyzed above. This procedure resulted in a sample of 1065 light curves for non- (or low-) variable field stars.

To these light curves we then added a sinusoidal signal, with a log-uniform distribution of periods in the range 0.2-20 d and of amplitudes from 0.002 to 0.02 mag, and random phases. The resulting light curves were subjected to exactly the same period search analysis as described above for the candidate members. After removing spurious periodogram peaks at frequencies around 0.5 and 1.0 d^{-1} , thus leaving 941 synthetic light curves,

² based on the frequency mapping FAMOUS, F. Mignard, OCA/CNRS, <ftp://ftp.obs-nice.fr/pub/mignard/Famous>

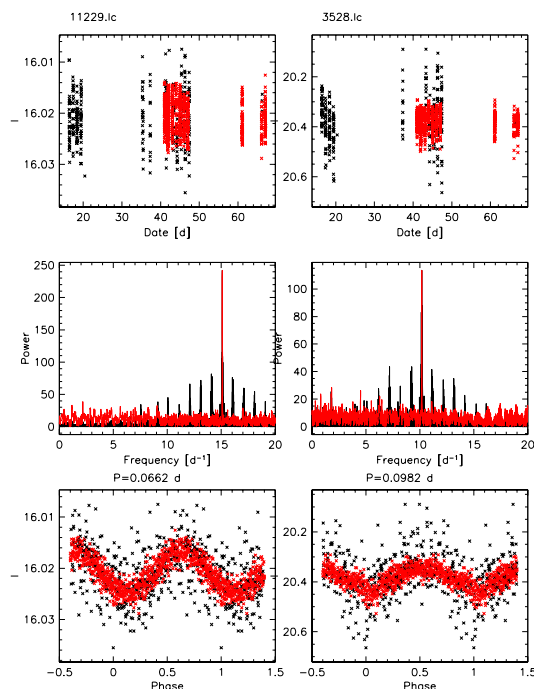


Fig. 7. The light curves of the 2 h Per candidate members with the shortest photometric periods are shown in the top panels (red: CFHT, black: Maidaanak), their frequency spectrum in the middle panels (black: periodogram, red: CLEAN DFT), and their phased light curves in the bottom panels (red: CFHT, black: Maidaanak). *Left* : HPer-215 with a period of 0.06626 d; *Right* : HPer-513 with a period of 0.09827 d.

we retained 592 objects with a FAP less than 0.05 and visualized their phased light curves. We rejected 50 additional objects based on the large scatter in their phased light curves. We were thus left with 542 periodic object from this sub-sample, i.e., a global detection rate of $542/1065 = 51\%$.

Comparing the detected periods to the input periods thus allows us to estimate the period detection rate as a function of period, amplitude and brightness, and to assess the sensitivity of the method to aliases and harmonics. Note that the production of synthetic periodic light curves has been done by one of the authors, and the search for periods has been performed by another two who ignored the input parameters so as not to bias the results. The results are shown in Figure 8. The completeness plot, i.e., the number of detected periods divided by the number of input periods in a given period bin, indicates that the period detection rate is relatively uniform over the 0.2-20d range (Fig. 8, panel a). Figure 8 (panel b) also indicates that the period detection rate is quite sensitive to the input amplitude, increasing from about 20% for amplitudes of 0.002 mag to nearly 80% for amplitudes of 0.02 mag. A sinusoidal fit to the light curves with detected periods recovers the input amplitudes to within 1.1 mmag rms. The period detection rate is equally sensitive to the stellar magnitude (Fig. 8, panel c), decreasing from ~80% at $i'_{CFHT} \approx 15.5$ to a mere 5% at $i'_{CFHT} \approx 19.5$, where the photometric noise becomes comparable to the injected amplitudes (see Fig. 3). We should stress, however, that for the large surface spots expected for low mass stars at the age of h Per, the photometric amplitudes are likely to be larger than ~0.01 mag, thus alleviating the issue of photometric noise for faint members.

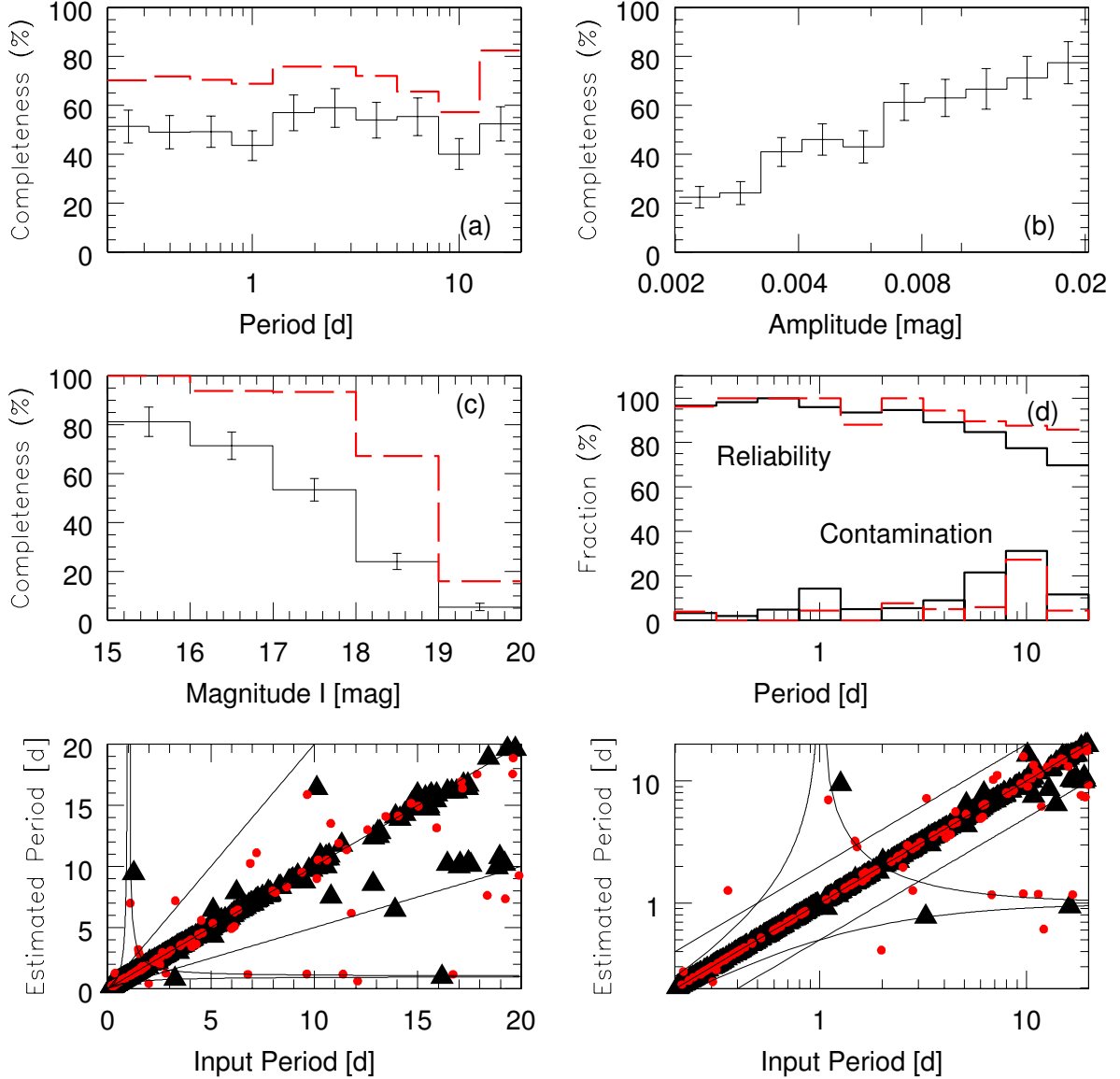


Fig. 8. Period detection completeness and reliability for sinusoidal signals with amplitudes from 0.002 to 0.02 mag (black histograms) and from 0.01 to 0.02 mag (red dashed histograms). The period detection completeness is shown as a function of period in panel (a), photometric amplitude in panel (b), and stellar magnitude in panel (c). The reliability of the recovered periods is shown in panel (d). Reliable periods are defined as those within 10% of the input periods (shown as a function of input period). Contaminating periods are those that differ from the input period by more than 10% (shown as a function of detected period). The lower left and right panels show the estimated periods as a function of the input periods on a linear and log scales, respectively. Periods recovered with a $\text{FAP} \leq 0.01$ are shown by large (black) triangles, while those with $0.01 < \text{FAP} \leq 0.05$ are shown by small (red) circles. The straight lines show the locus of equal periods and factor of 2 harmonics and the curves show the location of 1d period aliases.

It is quite noticeable that a large fraction ($490/542=90\%$) of the recovered periods agree with the input ones to better than 10% (cf. Fig. 8, panel d). The contamination of the recovered period distribution by incorrect periods is generally small ($\leq 10\%$), except in the period range around 1 day and from 5 to 11 days. The excess of periods around 1d mainly results from aliases of longer input periods (7-17d), while the excess of periods in the range 5-11d arises partly from harmonics of longer input periods (12-20d) (cf. Fig. 8, lower panels). This illustrates the fact that the sampling of the light curves is not optimal for the detection of long periods, mostly due to a large gap of about

20 nights in the observing window, between the Maidanak and CFHT datasets (cf. Figure 2). Finally, we note that detected periods with a $\text{FAP} \leq 0.01$ have a recovery rate of 95%, while those with $0.01 < \text{FAP} \leq 0.05$ have a recovery rate of 74% (cf. Fig. 8, lower panels).

The simulations we ran include very small amplitudes and long periods, none of which may be characteristic of such young stars as the 13 Myr-old h Per members. Therefore, the actual period detection rate for h Per members is likely to be significantly larger than what these simulations suggest. To illustrate this, restricting the completeness analysis to input light curves

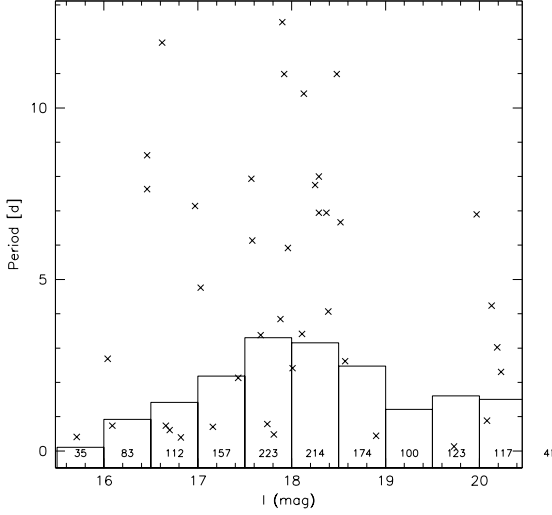


Fig. 9. The distribution of 40 periods detected in a sample of 1347 field stars is shown as a function of i'_{CFHT} -band magnitude (crosses). The lower histogram shows the magnitude distribution of the field star sample. The number of field stars is indicated in each bin.

with amplitudes larger than 0.01 mag raises the period detection rate from 51% to 71%, and brings the recovery rate to 90% or more for all periods smaller than 10d. Indeed, what is most important here is not so much to reach a high completeness level but rather to be able to measure reliable periods in an unbiased way over the whole period range between 0.2d and at least 10d. The Monte Carlo simulations presented here suggest that the combination of Maidanak and CFHT datasets allows us to derive such a relatively robust and largely unbiased rotational period distribution for h Per members over this period range.

3.3. Rotational contamination by field stars

The sample of 2287 h Per photometric candidate members we selected for period analysis includes a fraction of contaminating field stars as estimated above (cf. Section 2.3). In order to investigate the pollution of the h Per rotational distribution by unrelated periodic field stars, we selected a control sample of photometric *non* members. Among the 45,710 photometric non members, 3169 have at least 800 data points from CFHT and Maidanak in their combined light curve. Of these, 1347 have been selected in the $V, V - i'_{CFHT}$ CMD as lying in a locus parallel to the cluster sequence, either above its upper envelope up to 0.7 mag redder, or below the lower envelope down to -0.7 mag bluer. The control sample thus encompasses a similar magnitude and color range as the sample of h Per photometric candidate members. We then applied to the control sample the same period analysis as we did for the photometric members. Sorting the results by decreasing periodogram peak power, we visualized the phased light curves to decide on periodic and non-periodic objects. Over 1347 objects, we retained 40 objects as being periodic. The remaining 1307 non periodic field objects were used to estimate the FAP levels discussed above (cf. Sections 3.1, 3.2).

The distribution of periods for the control sample is shown in Figure 9. Periods typically range from 0.4 to 12d over the brightness range 16-21 mag. The shortest periods ($P \leq 1d$) we detect in the control sample probably relate to synchronized field

binaries and the longer periods of a few days may pertain to the young stellar population of the galactic field (cf. e.g. Briceño et al. 1997). In any case, the period detection rate is very low for field stars, amounting to a mere $40/1347 = 3\%$. The photometric contamination of the sample of 2287 h Per candidates by field stars is estimated to be 18.7% (cf. Section 2.3), i.e., about 428 field stars are included in this sample of candidate members. We expect to detect a period for 3% of the contaminants, yielding 13 periodic field stars. We thus estimate the contamination of the h Per rotational period distribution by field stars to $13/586$, i.e., 2.2% over the mass range $0.3-1.6M_{\odot}$. Furthermore, since the period distribution we obtain for field stars appears relatively uniform in the range 1-13 days, this low level of contamination is unlikely to introduce any significant bias in the period distribution of h Per candidate members. We notice, however, an apparent excess of field stars with periods shorter than 1d, presumably short period binaries.

3.4. Rotational bias due to synchronized binaries

As synchronized binaries are expected to have a different angular momentum evolution than detached systems and single stars, we investigate how the former may impact on the period distribution we derive for h Per candidate members. To this aim, we first identify photometric binaries in our sample of 2287 h Per candidate members from their location in the $i'_{CFHT}, i'_{CFHT} - K$ CMD. In this diagram, the binary sequence is fairly well separated from the single star sequence and we defined the empirical boundary as follows:

$$\begin{aligned} i'_{CFHT} - K &= 0.475 i'_{CFHT} - 5.625 & \text{for } i'_{CFHT} < 19 \\ i'_{CFHT} - K &= 0.3 i'_{CFHT} - 2.3 & \text{for } i'_{CFHT} \geq 19 \end{aligned}$$

391 objects are redder than this limit and have been classified as binaries.

Among the 586 periodic h Per candidate members, 142 are identified as photometric binaries. The distribution of periods as a function of mass is shown in Figure 10 for the subsamples of photometric binaries and of single stars. There is a clear excess of short period binary systems over the whole mass range from 0.3 to $1.5 M_{\odot}$, which is particularly conspicuous in the mass range above $1.2 M_{\odot}$. The cumulative period distribution of single and binary stars is shown in Fig. 10 in 2 mass bins, on either side of $1.2 M_{\odot}$. A Kolmogorov-Smirnov test indicates that the probability for the binary and single star period distributions to be drawn from the same distribution is 9.10^{-6} in the higher mass bin and 6.10^{-3} in the lower mass one. Clearly, the excess of short period binaries strongly skews the overall rotational distribution of the h Per candidate members.

Indeed, when removing rapid rotators with $P < 1d$ from the period distribution, a KS test on the remaining single and binary period distributions indicate they are the same with a probability of 0.77 in the higher mass bin and 0.58 in the lower mass one. This suggests that, unlike synchronized binaries that have a specific rotational evolution due to tidal effects, the components (or at least the primary) of wider binary systems appear to undergo a similar angular momentum evolution as single stars. A similar result was reported for binaries in the Pleiades cluster (Bouvier et al. 1997).

In order to avoid the bias introduced by synchronized binaries, we thus remove the 79 photometric binaries detected with $P < 1d$ from the sample of 586 periodic h Per candidate members. Since the period distribution of wider binary systems appears to be statistically similar to that of single stars, we keep

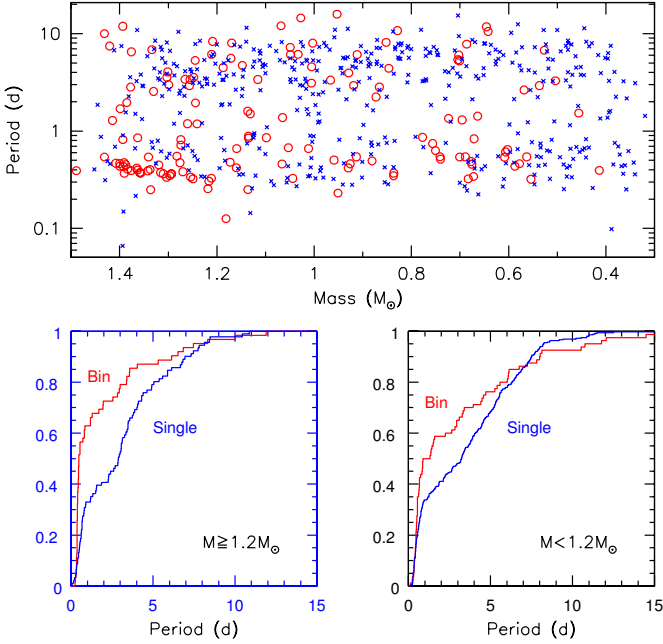


Fig. 10. *Top panel* : The distribution of periods is shown as a function of stellar mass for h Per *photometric binary* candidates (red circles) and for h Per candidate members lying on the cluster’s single star photometric sequence (blue crosses). *Bottom panels* : The cumulative distribution of periods for photometric binaries and single stars in 2 mass ranges (*left*: $M \geq 1.2 M_{\odot}$; *right*: $M < 1.2 M_{\odot}$). In the 2 mass bins, there is a clear excess of short period binaries compared to short period single stars (see text).

them for the following analysis. This leaves us a sample of 508 h Per candidate members with measured periods over the mass range from 0.3 to $1.5 M_{\odot}$, which we can use to investigate stellar rotation at 13 Myr and angular momentum evolution prior to the arrival on the main sequence.

3.5. Period distribution

The period distribution of h Per candidate members is shown as a function of mass in Fig. 11. It extends widely from ~ 0.2 to ~ 12 days at all masses, from ~ 0.3 to $\sim 1.4 M_{\odot}$, and its lower and upper envelopes do not show any clear dependence with mass. We have divided our sample of periodic objects in 4 mass bins, centered on 0.5, 0.75, 1.0 and $1.25 M_{\odot}$, respectively, and plot their distributions in Fig. 12. In each mass bin, most of the periods lie in the range 2-10 d, with a tail of slower rotators extending up to about 20 days, and a peak of fast rotators, with periods less than 1d. This peak is particularly conspicuous at the lowest masses and becomes weaker in the highest mass bin. The fraction of objects rotating faster than 2 days is $47 \pm 8\%$, $31 \pm 6\%$, $35 \pm 7\%$ and $34 \pm 5\%$ from the lowest to the highest mass bin. On a log scale, the period distributions in each mass bin appear somewhat bimodal, especially at low masses again, with a primary peak around 8-10 days, and a secondary peak at a fraction of a day. Such bimodal period distributions, albeit on a linear period scale, have previously been reported for young stars in the ONC at 1 Myr, with peaks at 7-9 days and 1-2 days (e.g., Herbst et al. 2001).

Kolmogorov-Smirnov tests were run to compare the period distribution of each mass bin to the next (i.e. $0.4-0.6 M_{\odot}$ vs $0.6-0.9 M_{\odot}$, $0.6-0.9 M_{\odot}$ vs $0.9-1.1 M_{\odot}$ and $0.9-1.1 M_{\odot}$ vs $1.1-1.4 M_{\odot}$). The probability that the distributions are drawn from the same overall parental distribution is 0.04, 0.17 and 0.33, respectively. Hence, while the period distribution does not seem to depend on mass at an age of 13 Myr above $0.6 M_{\odot}$, there is a hint for the $0.4-0.6 M_{\odot}$ mass objects to rotate faster in average. This is in agreement with the finding of previous studies indicating a larger fraction of fast rotators among the lowest mass stars (e.g. Herbst et al. 2001, Irwin et al. 2007b, 2008a, 2008b).

The photometric amplitudes of the 508 periodic h Per candidate members are plotted as a function of i'_{CFHT} -band magnitude and period in Fig. 13. The lower envelope of the photometric amplitude is seen to increase with i'_{CFHT} -band magnitude. This trend clearly points to an observational bias, as it is increasingly difficult to detect lower amplitude variables among fainter objects (cf. Fig. 3). The upper envelope of the photometric amplitude, however, also appears to increase towards fainter, i.e., lower mass, objects. This suggests that lower mass stars either have a larger fractional coverage by stellar spots, or that the spot distribution at their surface is more asymmetric than in higher mass stars, thus leading to a larger contrast along the rotational cycle. No correlation is found between photometric amplitude and rotational period in Fig. 13. A K-S test on photometric amplitudes for stars with periods shorter and longer than 1d returns a probability of 0.06 of being drawn from the same distribution. Hence, a weak trend, if any, might be present with median values of 0.034 and 0.029 mag for the photometric amplitudes of fast and slow rotators, respectively. Taken together, these results suggest that the origin of increasing maximum photometric amplitude towards lower mass stars at 13 Myr is not primarily linked to rotation but more likely related to the internal structure of the pre-main sequence objects, and possibly to the extent of their convective zones.

4. Discussion

4.1. Angular momentum distribution at 13 Myr

At 13 Myr, the accretion process has terminated and the stars are no longer magnetically coupled to their disk (Currie et al. 2007a; Fedele et al. 2010). Measurements of rotational periods in the h Per cluster thus provide the initial angular momentum distribution of freely evolving stars. We computed the specific angular momentum of the 508 stars with known rotational periods assuming uniform rotation, i.e., $J/M = I \cdot \Omega/M$, where the stellar moment of inertia I is derived at each mass from Baraffe et al. (1998) 13 Myr models, and $\Omega = 2\pi/P_{rot}$. The resulting distribution of specific stellar angular momenta at 13 Myr is shown as a function of mass in Figure 14. A large dispersion is observed, between $\log(J/M) \sim 15.7 - 17.5$, with a weak trend for increasing J/M with mass. The lower values of the specific angular momentum of solar-mass stars at 13 Myr ($(J/M)_{min} \sim 10^{16} \text{ cm}^2 \text{ s}^{-1}$) are still about an order of magnitude larger than that of the present-day Sun ($J/M = 9.2 \cdot 10^{14} \text{ cm}^2 \text{ s}^{-1}$, Pinto et al. 2011).

Rebull (2001) and Herbst & Mundt (2005) reported the distribution of specific angular momenta for low mass stars in the Orion Nebula Cluster and its flanking fields at an age of ~ 1 Myr. They both find a large dispersion of J/M , with a range of $\log(J/M) \sim 16.0 - 17.7$ and a peak at $\log(J/M) \sim 16.5$ in Rebull (2001)³, and a range of $\log(J/M) \sim 16.2 - 17.5$ with a

³ Rebull (2001) computed angular momenta assuming a gyration factor k^2 , where $I = k^2 MR^2$, of 2/5 corresponding to a solid body rotating

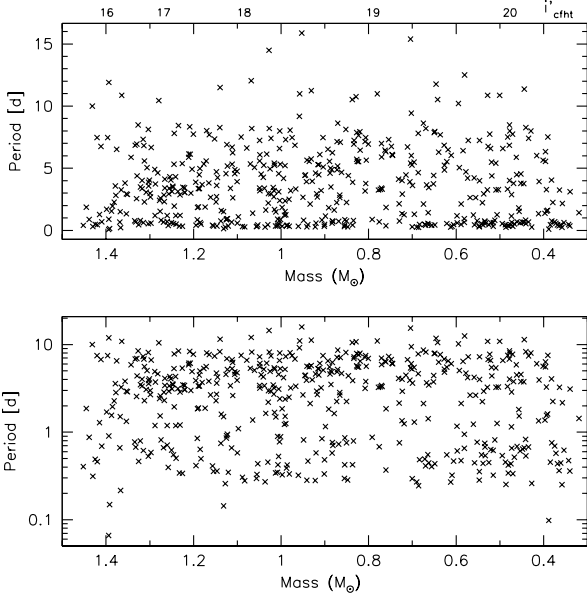


Fig. 11. The periods detected for 508 h Per photometric candidate members (excluding synchronized binaries with period ≤ 1 d) are shown as a function of stellar mass. Periods are plotted on a linear scale in the upper panel, and on a log scale in the lower one. On the top panel, the upper x-axis scale corresponds to i'_{CFHT} -band magnitude.

sphere of uniform density. However, for their sample of fully convective stars, the correct gyration factor is 0.205 (polytrope $n=1.5$, Horedt 2004). We therefore reduced Rebull's J/M value by a factor of 2 to compare with ours.

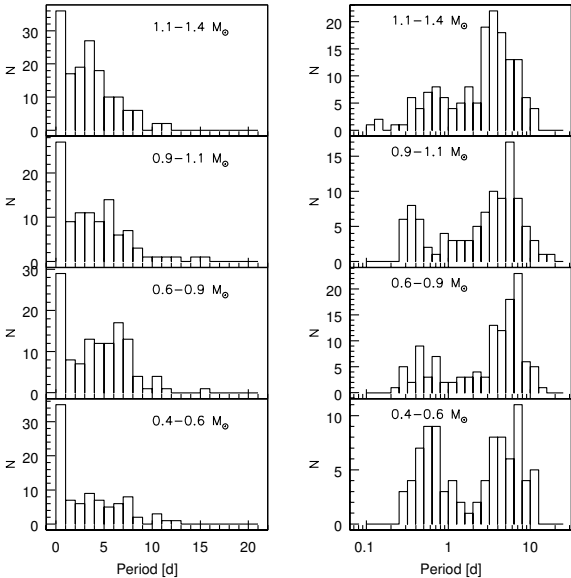


Fig. 12. Histograms of the periods of h Per candidate members in 4 mass bins. *From bottom to top:* 0.4-0.6 M_{\odot} , 0.6-0.9 M_{\odot} , 0.9-1.1 M_{\odot} , and 1.1-1.4 M_{\odot} . The mass bins contain 90, 123, 103, and 152 periodic h Per candidate members, respectively. The histograms are shown on a linear scale on the left panels, and on a logarithmic scale on the right panels.

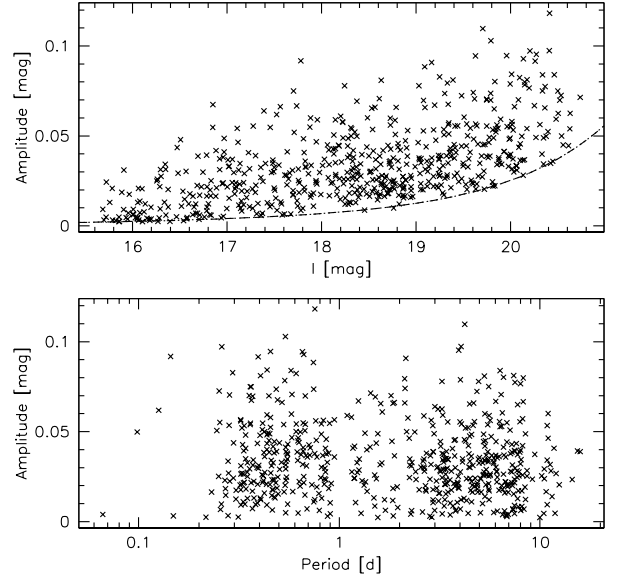


Fig. 13. The photometric amplitudes derived from a sinusoidal fit to the periodic light curves are shown as a function of i'_{CFHT} magnitude (upper panel) and period (lower panel).

peak at $\log(J/M) \sim 16.5$ in Herbst & Mundt (2005)⁴. The scatter in J/M in both studies (1.7 and 1.3 dex, respectively) is roughly similar to what we derive (1.8 dex) for the J/M distribution of h Per low-mass members at 13 Myr. However, the peak of the J/M distribution for h Per members ($\log(J/M) \sim 16.2$) appears to be slightly shifted towards lower values. The decrease of the specific angular momentum of low-mass stars between ~ 1 and 13 Myr presumably reflects angular momentum loss due to the star-disk interaction during the early PMS (Rebull et al. 2004).

Figure 14 also shows the ratio of angular velocity to critical velocity, ω/ω_{crit} , as a function of mass for the 508 periodic h Per candidate members. For a few stars (including HPer-215 and HPer-513; see Section 3.1), this ratio exceeds unity, suggesting the photometric period could reflect either pulsation or orbital motion instead of rotation. The distribution is strongly peaked at $\omega \leq 0.1\omega_{crit}$, with a median value of 0.048, and a tail extending up to $\omega \sim 0.5\omega_{crit}$. Of the 508 periodic members, 492 (97%) have $\omega \leq 0.5\omega_{crit}$. No evidence for a mass dependence is found, except perhaps at masses larger than 1.1 M_{\odot} where the lower envelope of the ω/ω_{crit} distribution may slightly increase. The range and shape of the ω/ω_{crit} distribution we derive for low-mass stars at 13 Myr is qualitatively similar to that reported for similar stars in the ONC cluster at an age of 1 Myr (Stassun et al. 2001). When projected to the ZAMS assuming no angular momentum loss, i.e., $\omega/\omega_{crit} \propto I^{-1}R^{1.5}$, the ω/ω_{crit} ratio increases by a factor of 1.4 to 2.3 over the mass range 0.4-1.4 M_{\odot} . The projected distribution on the ZAMS has a median value of $\omega/\omega_{crit} \sim 0.1$, and 80 stars (16%) have $\omega > 0.5\omega_{crit}$, including 15 stars with $\omega/\omega_{crit} \geq 1$. This suggests that some angular mo-

⁴ Herbst & Mundt (2005) computed the specific angular momentum of the surface shell of ONC stars, using a gyration factor $k^2 \sim 2/3$. For the whole star, however, assuming it is fully convective, rotates as a solid body and neglecting rotational distortion, $k^2 = 0.205$. To compare with our study, we therefore reduced Herbst & Mundt (2005) specific angular momentum values by a factor 3.3, which is appropriate for all but the most rapid rotators.

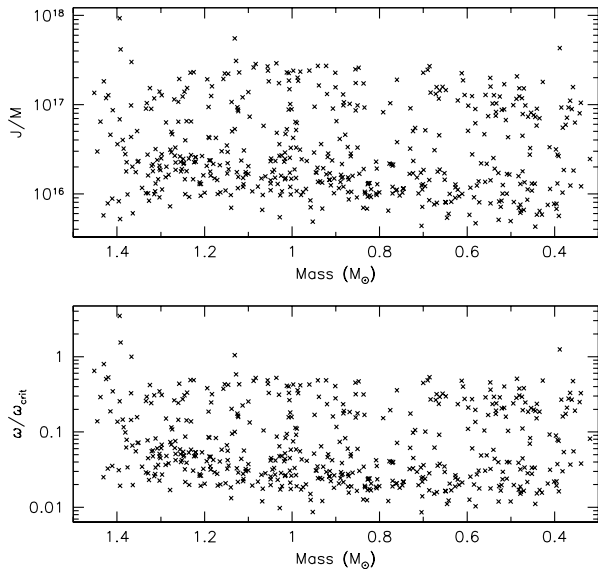


Fig. 14. The specific angular momentum (cm^2s^{-1}) of 508 periodic h Per candidate members is shown as a function of mass in the upper panel. The ratio of their angular velocity to the break-up velocity ($\omega_{crit} = (GM)^{1/2}R^{-3/2}$) is shown as a function of mass in the lower panel.

mentum loss must occur during the late PMS evolution, an issue to which we return in the next section.

4.2. Angular momentum evolution to the ZAMS

The derivation of hundreds of rotational periods for low-mass stars in the 13 Myr-old h Per cluster provides a new time step to investigate pre-main sequence angular momentum evolution. This time step, not previously covered by other cluster studies (e.g. Irwin & Bouvier 2009; Messina et al. 2010, 2011) is particularly interesting as it marks the end of the PMS disk accretion process. Disk accretion is thought to be largely terminated by 10 Myr (Kennedy & Kenyon 2009; Fedele et al. 2010), leaving at most a few percent of stars still actively accreting from their disk in h Per (Currie et al. 2007c). The so-called “disk-locking process” by which stars are prevented from spinning up during their early PMS evolution is therefore over for most of the h Per low mass population. These stars are thus expected to freely spin-up as they contract towards the zero-age main sequence (ZAMS) that they eventually reach at an age of 22, 33, 66, and 100 Myr for a mass of 1.2, 1.0, 0.7, and 0.5 M_{\odot} , respectively. The rotational distribution of h Per members is thus particularly suited to investigate stellar spin-up at the end of PMS evolution and on the approach to the ZAMS.

Figure 15 compares the rotational distribution of h Per members with those of solar-type and lower mass members of various open clusters over the age range from 5 to 150 Myr. At all ages, a significant scatter is seen in the rotational period distributions, which cannot be accounted for by observational errors, but reflects a true dispersion of rotation rates during the PMS. In these period-mass plots, both early-PMS and ZAMS clusters exhibit some similarities with h Per but also striking differences. The upper envelope of the period distribution, located at ~ 10 day in h Per, does not appear to evolve much between 5 and 40 Myr over the mass range from 0.4 to 0.9 M_{\odot} . This suggests that at

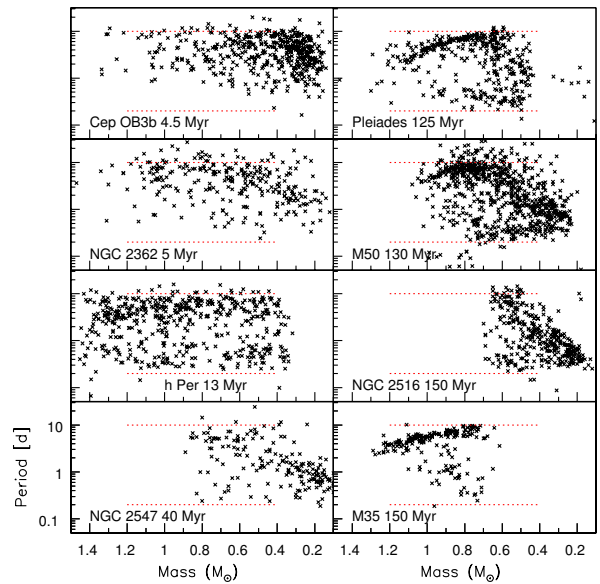


Fig. 15. Period versus mass distributions for clusters with an age ranging from 4 to 150 Myr. The clusters’ name and age are given in each panel. Red dotted lines are drawn at periods of 0.2 and 10 days to guide the eye. References: Cep OB3b: Littlefair et al. (2010); NGC 2362: Irwin et al. (2008a); NGC 2547: Irwin et al. (2008b); Pleiades: Hartman et al. (2010); M 50: Irwin et al. (2009); NGC 2516: Irwin et al. (2007b); M35: Meibom et al. (2009).

least a fraction of slow rotators are prevented from spinning up over this timescale. By the age of the Pleiades (125 Myr) the upper envelope of the distribution has decreased towards faster rotation for masses larger than 0.7 M_{\odot} . A significant fraction of lower mass stars, even at this age, still exhibit long periods, suggesting that the pre-ZAMS spin up is more efficient for solar-mass than for low mass stars.

In contrast, the lower envelope of the period distribution exhibits quite a drastic evolution from 5 Myr to the ZAMS. In h Per, the lower envelope appears rather flat over the mass range 0.4-1.1 M_{\odot} , at a period of ~ 0.2 -0.3d. In younger clusters, the minimum period seems to strongly depend on mass, ranging from ~ 0.4 -0.5d at 0.4-0.6 M_{\odot} to 1.0d or more for solar-type stars. This provides good evidence for PMS spin up for the fast rotators between 5 and 13 Myr. While the mass sampling and period statistics is unfortunately sparser in NGC2547, its 40 Myr-old rotational distribution does not show any clear evolution for the fastest rotators between 13 and 40 Myr over the mass range 0.4-0.8 M_{\odot} . From 13 to 130 Myr, however, the fastest rotators in the 0.8-1.1 M_{\odot} mass range have been spun down, presumably upon their arrival on the ZAMS, while lower mass stars down to 0.4 M_{\odot} still exhibit the same maximum rotation rate of ~ 0.3 d. The most striking difference between the 13 Myr-old h Per cluster and ZAMS clusters at an age of 125-150 Myr, is the lack of mass-dependency in the rotational distribution of the former while the latter exhibit a narrow rotation-mass relationship for masses larger than about 0.7 M_{\odot} . Indeed, the largest scatter of rotation rates over the investigated mass range is observed for the 13 Myr-old h Per cluster, at the end of the PMS accretion phase, a result that supports the role of disk accretion in establishing the initial dispersion of stellar angular momentum in low-mass stars (Bouvier et al. 1993; Rebull et al. 2004).

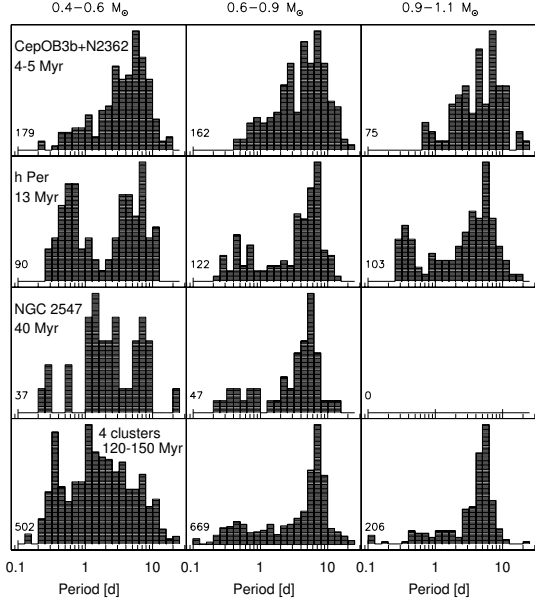


Fig. 16. Histograms of period distributions in 3 mass bins for clusters with an age ranging from 4 to 150 Myr. The clusters’ name and age are given in each panel. *Left:* 0.4-0.6 M_{\odot} , *Middle:* 0.6-0.9 M_{\odot} , *Right:* 0.9-1.1 M_{\odot} . The number of stars in each mass bin is indicated in the lower left corner of the panels.

Table 3. Stellar moment of inertia (I/I_{\odot})

Age (Myr)	0.5 M_{\odot}	0.75 M_{\odot}	1.0 M_{\odot}	1.25 M_{\odot}
5	1.58	3.40	5.61	8.49
13	0.81	1.74	2.89	3.85
40	0.37	0.74	1.00	1.39
130	0.22	0.55	0.95	1.34

A more detailed comparison of the rotational distributions at 4 time steps between the early PMS and the ZAMS is provided in Fig. 16 for 3 mass bins centered at 0.5, 0.75, and 1.0 M_{\odot} , respectively. We do not consider here stars in the mass range 1.1-1.4 M_{\odot} as their rotational period distributions are still missing for most young open clusters. In order to improve statistics, and to smooth out any dependence of rotation on environment (cf. Littlefair et al. 2010), the two 4-5 Myr clusters have been merged, as have been the 4 clusters in the age range 125-150 Myr. The temporal evolution of these distributions can now be compared to the expected PMS spin up in the absence of angular momentum loss. Table 4.2 lists the evolution of the stellar moment of inertia resulting from the star’s contraction and the development of a radiative core. In all 3 mass bins considered here, the reduction of the moment of inertia would translate into a spin up by a factor of ~ 2 from 5 to 13 Myr, and by a factor of ~ 2.5 from 13 to 40 Myr. The observed distributions do suggest some PMS spin up between 5 and 13 Myr in all mass bins, with the bulk of fast rotators ($P < 2d$) shifting towards shorter periods, as expected from the evolution of the stellar structure. The evolution of the fast rotators is less clear from 13 to 40 Myr. This is partly due to the small statistics affecting the distribution of NGC 2547 in the 0.4-0.6 M_{\odot} mass range, although in the better sampled 0.6-0.9 M_{\odot} range, little evolution is observed for fast rotators, contrary to model expectations. Unfortunately, no data exist for NGC 2547 solar-type stars and only a few rotational periods have been published in the 0.9-1.1 M_{\odot} range (Messina

Table 4. Angular momentum model parameters

Mass bin (Stellar model)	Wind braking [†]		Core-envelope coupling
M (M_{\odot})	K ($10^{47} \text{ g cm}^2 \text{ s}$)	ω_{sat} (ω_{\odot})	τ_c (yr)
0.9-1.1 (1.0)	3.75 7.5 5.6	8.0 8.0 8.0	10^6 10^8 $10^8 \cdot (\omega/\omega_{\odot})^{-1}$
0.6-0.9 (0.8)	3.75 15 4.5	6.0 6.0 6.0	10^6 $5 \cdot 10^7$ $5 \cdot 10^8 \cdot (\omega/\omega_{\odot})^{-1}$
0.4-0.6 (0.5)	2.25 4.5 3.75	4.5 4.5 4.5	10^6 $5 \cdot 10^7$ $5 \cdot 10^8 \cdot (\omega/\omega_{\odot})^{-1}$

$$\dagger \left(\frac{dJ}{dt} \right)_{\text{wind}} = \begin{cases} -K \omega^3 \left(\frac{R}{R_{\odot}} \right)^{1/2} \left(\frac{M}{M_{\odot}} \right)^{-1/2}, & \omega < \omega_{\text{sat}} \\ -K \omega \omega_{\text{sat}}^2 \left(\frac{R}{R_{\odot}} \right)^{1/2} \left(\frac{M}{M_{\odot}} \right)^{-1/2}, & \omega \geq \omega_{\text{sat}} \end{cases}$$

et al. 2011). Slow rotators ($P \geq 2d$) as a whole do not appear to spin up as much as fast ones. In the 0.6-0.9 M_{\odot} range, the peak of the slow rotator distribution varies from $\sim 7.5d$ at 5 Myr, to $\sim 6.5d$ at 13 Myr, and $\sim 5.5d$ at 40 Myr, i.e., much less than the reduction of the stellar moment of inertia would imply. Similar conclusions are reached for the other mass bins. Clearly, some angular momentum loss must occur in at least a fraction of slow rotators over the 5-40 Myr age range to compensate for the spin up due to contraction.

While the rotational distributions of fast and slow rotators provide some clues to the angular momentum evolution of PMS stars, the complete distributions have to be modelled to understand the processes at play. We therefore computed angular momentum evolution models starting from the observed 5 Myr rotational distributions as initial conditions and evolved them at ages of 13, 40 and 130 Myr to compare with observations. The models assume all stars are released from their disk at 5 Myr, therefore does not include any “disk locking” process after this age. Angular momentum loss due to stellar winds are included in the way described in Irwin & Bouvier (2009). Core-envelope decoupling is also included in the model through the introduction of a coupling timescale τ_c over which angular momentum is exchanged between the radiative core and the convective envelope (Allain 1998). Previous modelling efforts suggest that τ_c is significantly shorter for rapid rotators than for slow ones (Bouvier 1997; Irwin et al. 2007b; Bouvier 2008; Irwin & Bouvier 2009; Denissenkov et al. 2010; Spada et al. 2011). We illustrate here 3 classes of models: solid-body rotation models ($\tau_c = 1$ Myr), decoupled models with a constant coupling timescale ($\tau_c = 50-100$ Myr), and a velocity-dependent coupling model, with $\tau_c = \tau_{c0} \cdot (\omega/\omega_{\odot})^{-1}$ Myr and $\tau_{c0} = 100-500$ Myr. The other parameters of the models, namely the angular momentum loss scaling and saturation velocity (see Irwin & Bouvier 2009) are summarized in Table 4. Owing to the observed scatter of rotation rates among field stars (Harrison et al. 2012), the models are required to reproduce the angular velocity of the Sun to within 30% for solar-type stars, and up to a factor of 2 lower rotation rates for lower mass stars. In addition, the solar-mass models must comply with heliosismology results that indicate no residual excess rotation in the radiative core of solar-mass stars by the age of the Sun (Thompson et al. 2003). Stellar evolution models for 0.5, 0.8, and 1.0 M_{\odot} stars are taken from Baraffe et al. (1998).

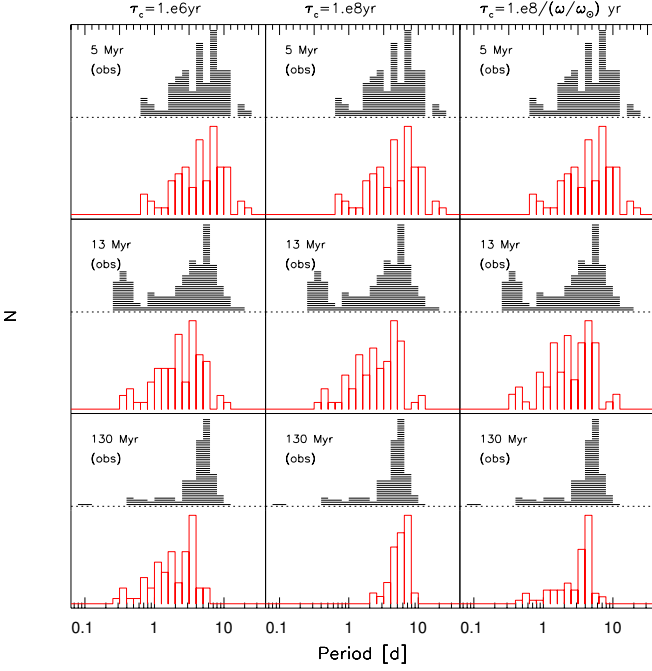


Fig. 17. The initial distribution of periods at 5 Myr (top panels) for 0.9-1.1 M_{\odot} stars is projected to 13 Myr (middle panels) and 130 Myr (bottom panels) using 3 models : strong core-envelope coupling ($\tau_c = 1$ Myr, left panels), weak core-envelope coupling ($\tau_c = 100$ Myr, middle panels), and a velocity-dependent coupling timescale ($\tau_c = 100 \cdot (\omega/\omega_{\odot})^{-1}$ Myr, right panels). The observed distributions are shown as black shaded histograms, the projected ones as red bar histograms.

The results for solar-mass stars are shown in Figure 17 where the initial period distribution at 5 Myr is projected forward in time using the 3 models to ages of 13 and 130 Myr, and compared to the observed distributions at those ages. It is seen that, starting from 5 Myr, the projected distributions at 13 Myr do not depend much of the assumed model. This is because the radiative core only recently developed at this stage, and the amount of core-envelope decoupling hardly impacts on the early PMS rotational evolution. Indeed, the projected distributions at 13 Myr encompass the full range of rotational periods observed for solar-mass stars in the h Per cluster. These results support the hypothesis that most of the disk locking process is over in solar-mass stars by 5-10 Myr (Rebull et al. 2004), which is consistent with current estimates of disk lifetimes (Fedele et al. 2010). Once on the ZAMS, however, significant differences occur between the models. Solid-body rotation models successfully reproduce the fastest ZAMS rotators, but fail to account for the bulk of slow rotators in Pleiades-like clusters. On the opposite, distributions projected with fully decoupled models do yield a population of ZAMS slow rotators, but do not exhibit the observed tail of fast rotators. Only the ω -dependent τ_c model ($\tau_c = 100 \cdot (\omega/\omega_{\odot})^{-1}$ Myr) simultaneously accounts for both the peak of slow rotators and the high-velocity tail observed in ZAMS clusters. This confirms the need for a core-envelope coupling timescale that depends upon the rotation rate. As discussed in Bouvier (2008), the different PMS rotational history of slow and fast rotators may leave imprints in the properties of field stars once their angular velocities have converged on the MS, such as an increased Li dispersion (e.g., Pasquini et al. 1997).

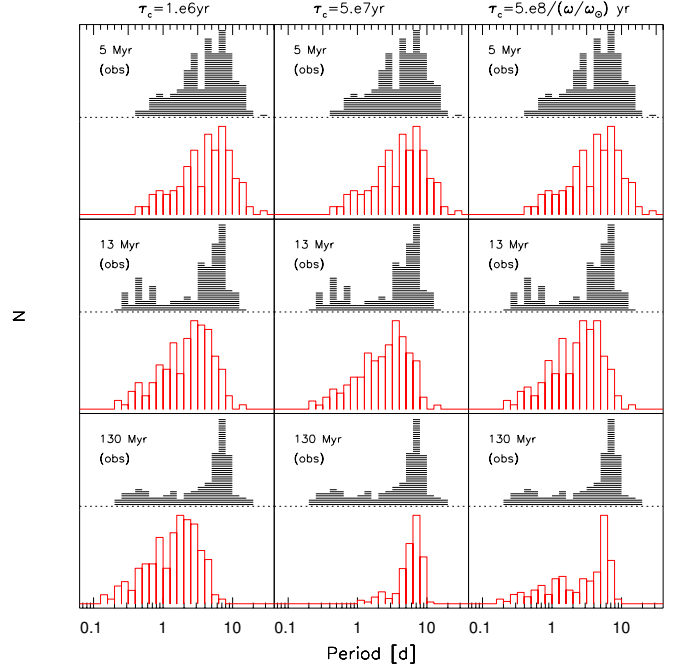


Fig. 18. The initial distribution of periods at 5 Myr (top panels) for 0.6-0.9 M_{\odot} stars is projected to 13 and 130 Myr (top to bottom panels) using 3 models : strong core-envelope coupling ($\tau_c = 1$ Myr, left panels), weak core-envelope coupling ($\tau_c = 50$ Myr, middle panels), and a velocity-dependent coupling timescale ($\tau_c = 500 \cdot (\omega/\omega_{\odot})^{-1}$ Myr, right panels). The observed distributions are shown as black shaded histograms, the projected ones as red bar histograms.

We ran a similar analysis for stars in the mass bin 0.6-0.9 M_{\odot} . The results are shown in Figure 18 and the model parameters are listed in Table 4. Starting from the 5 Myr period distribution, a short coupling timescale between the core and the envelope ($\tau_c=1$ Myr) is required to yield fast rotators on the ZAMS, while a much longer coupling timescale ($\tau_c=50$ Myr) is needed to account for the slow rotators. As for the solar-mass stars, the best results are obtained by assuming a rotation-dependent coupling timescale. Figure 18 shows that a model assuming $\tau_c = 500 \cdot (\omega/\omega_{\odot})^{-1}$ Myr provides a reasonable description of the observed angular momentum evolution of 0.6-0.9 M_{\odot} stars from 5 to 130 Myr. A small fraction of ZAMS stars in this mass range, however, have rotational periods longer than 10 days and up to ~ 20 days, that are not accounted for by the model. Assuming these slow rotators result from an extended disk-locking period during the PMS, this suggests that disk lifetimes may exceed 5 Myr for about 7% of stars in this mass range, a result that would be consistent with current estimates of accretion disk lifetimes (Fedele et al. 2010).

Finally, model simulations were run for the lowest mass bin, 0.4-0.6 M_{\odot} . The results are shown in Figure 19. While a short coupling timescale ($\tau_c=1$ Myr) clearly fails to reproduce slow rotators in this mass range on the ZAMS, the observed evolution of the rotational period distributions can be reproduced by assuming either a longer coupling timescale ($\tau_c=50$ Myr) for all stars or a rotation-dependent core-envelope coupling ($\tau_c = 500 \cdot (\omega/\omega_{\odot})^{-1}$ Myr). This is because, as the convective envelope thickens in the lowest mass bin, surface rotation becomes less sensitive to varying coupling timescales. As in the 0.6-0.9 M_{\odot} bin, a small fraction (6%) of low-mass stars have rotational

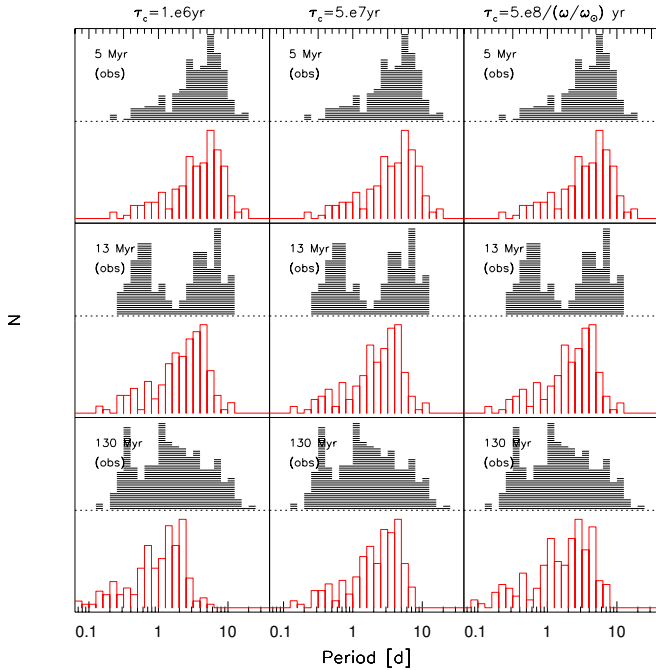


Fig. 19. The initial distribution of periods at 5 Myr (top panels) for $0.4\text{--}0.6 M_{\odot}$ stars is projected to 13 and 130 Myr (top to bottom panels) using 3 models : strong core-envelope coupling ($\tau_c = 1$ Myr, left panels), weak core-envelope coupling ($\tau_c = 50$ Myr, middle panels), and a velocity-dependent coupling timescale ($\tau_c = 500 \cdot (\omega/\omega_{\odot})^{-1}$ Myr, right panels). The observed distributions are shown as black shaded histograms, the projected ones as red bar histograms.

periods in excess of 10 days on the ZAMS, which may indicate a prolonged star-disk coupling during the early PMS, up to 10 Myr. Alternatively, we cannot exclude that some of these slow rotators, which mostly arise from the M50 cluster study by Irwin et al. (2009), may be slowly-rotating field star contaminants.

Applying quantitative statistical analysis, such as 2-sided Kolmogorov-Smirnov tests, indicates that the formal agreement between the observed and model projected rotational distributions is poor. This may result both from shortcomings of the models and from uncertainties in the observed rotational distributions. As to the models, we considered the accretion process to be fully completed by 5 Myr. As discussed above, assuming instead that a small fraction of PMS stars have disk lifetimes in excess of 5 Myr would increase the fraction of slow rotators on the ZAMS and bring the observed and projected distribution in better agreement. As to the observed distribution themselves, they may suffer various biases. We have shown in Section 3.4 that short-period synchronized binaries significantly impact on the h Per rotational distribution and consequently removed them from the analysis. To our knowledge, synchronized binaries have not been identified and similarly discarded in other studies. Field contaminants in the photometric samples may also affect the rotational distributions by increasing the fraction of slow rotators, with long period field stars being uncorrectly classified as cluster members. Finally, environmental conditions may play a role in shaping the initial distribution of angular momenta (e.g. Clarke & Bouvier 2000; Littlefair et al. 2010). Such intrinsic cluster-to-cluster differences would undermine a detailed comparison between observed and projected distributions. Given these numerous sources of uncertainty, we believe it is premature to attempt

to reproduce the detailed shape of the observed rotational distributions. Instead, we merely aimed here at a qualitative agreement between the observed and modeled distributions by trying to best account for the *range* of observed rotational periods as a function of age.

5. Conclusions

We have presented the results of an extensive photometric monitoring campaign in the 13 Myr open cluster h Per to look for variability in the *I*-band. Thanks to the combination of CFHT/MegaCam and Maidanak data, the study is sensitive to periodic variations on timescales of less than 0.2 day to 20 days. Selection of candidate members using empirical isochrones in various CMDs in the optical and the near-infrared found 2287 candidates in the Maidanak camera field of view ($18' \times 18'$). The field contamination is estimated to be around 18% according to the Besançon Galactic model.

The light curves of the candidate cluster members were searched for periodic modulations due to stellar rotation, giving 586 detections over the mass range $0.4 \leq M/M_{\odot} \leq 1.4$. This provides a statistically large sample with uniform completeness of rotational periods for low mass stars at 13 Myr, a time step that was not covered by previous cluster studies. This age is particularly important to understand the angular momentum evolution prior to the ZAMS since it corresponds to the time when most of the stars have dissipated their disk and start to freely spin-up as they contract towards the ZAMS.

The rotation period distribution exhibits a wide dispersion, with most of the measured periods in the range ~ 0.3 to ~ 9 days and a few slow rotators around 15 days. We found that photometric binaries skew the distribution towards short periods, especially in the mass range above $1.2 M_{\odot}$. We suggest that this is due to the presence of synchronized binaries that have a specific rotational evolution due to tidal fields and should therefore be removed to investigate the angular momentum evolution of single stars. The distribution of the remaining 508 rotational periods (excluding the photometric binaries with a period $P < 1$ d) does not show any clear dependence with mass. In particular, the upper and lower envelopes (corresponding respectively to slow and fast rotators) is remarkably flat over the whole mass range.

Comparing the rotational period distribution of h Per members to those of low mass stars in other young clusters allowed us to model the angular momentum evolution of low-mass stars during the PMS up to the ZAMS. Models suggest that core-envelope decoupling occurs on a timescale inversely proportional to surface rotation. Furthermore, models indicate that less than 10% of stars may remain coupled to their disk beyond 5 Myr in order to reproduce the spin evolution to the ZAMS, in agreement with current estimates of disk lifetimes.

Acknowledgements. The authors thank B. Reipurth for giving us access to his CFHT data; K. Zwintz for the pulsation analysis of the 2 fast rotators; A. Scholz for useful discussion about fast rotation from synchronized binaries; F. Mignard for help with the FAMOUS program; and A. Robin for the use of the Besançon Galactic Model. We are also grateful to the CFHT QSO team for service observing and to J.-C. Cuillandre for the pre-reduction of CFHT data. This work has been supported by the EGIDE ECONET 1886YF program as well as by bilateral programs with the Academy of Science in Armenia and Ukraine. J. Bouvier and E. Moraux acknowledge funding from the Agence National Recherche grants ANR-2011-Blanc-SIMI5-6-020-01 “Toupiques: Towards understanding the spin evolution of stars” (<http://ipag.osug.fr/Anr.Toupiques/>) and ANR-2010-JCJC-0501-1 “DESC: Dynamical Evolution of Stellar Clusters” (<http://ipag.osug.fr/emoraux/DESC>) respectively.

References

- Affer, L., Micela, G., Favata, F., Flaccomio, E., & Bouvier, J. 2013, *MNRAS*, 430, 1433
- Aigrain, S., Hodgkin, S., Irwin, J., et al. 2007, *MNRAS*, 375, 29
- Allain, S. 1998, *A&A*, 333, 629
- Baraffe, I., Chabrier, G., Allard, F., & Hauschildt, P. H. 1998, *A&A*, 337, 403
- Baran, A. S., Winiarski, M., Krzesiński, J., et al. 2011, *Acta Astron.*, 61, 37
- Bidelman, W. P. 1943, *ApJ*, 98, 61
- Boulade, O., Charlot, X., Abbon, P., et al. 2003, *Proc. SPIE*, 4841, 72
- Bouvier, J., Cabrit, S., Fernandez, M., Martin, E. L., & Matthews, J. M. 1993, *A&A*, 272, 176
- Bouvier, J. 1997, *Mem. Soc. Astron. Italiana*, 68, 881
- Bouvier, J., Rigaut, F., & Nadeau, D. 1997, *A&A*, 323, 139
- Bouvier, J. 2008, *A&A*, 489, L53
- Bragg, A. E., & Kenyon, S. J. 2005, *AJ*, 130, 134
- Briceno, C., Hartmann, L. W., Stauffer, J. R., et al. 1997, *AJ*, 113, 740
- Capilla, G., & Fabregat, J. 2002, *A&A*, 394, 479
- Chang, S.-W., Protopapas, P., Kim, D.-W., & Byun, Y.-I. 2013, *AJ*, 145, 132
- Clarke, C. J., & Bouvier, J. 2000, *MNRAS*, 319, 457
- Currie, T., Balog, Z., Kenyon, S. J., et al. 2007, *ApJ*, 659, 599
- Currie, T., Kenyon, S. J., Rieke, G., Balog, Z., & Bromley, B. C. 2007, *ApJ*, 663, L105
- Currie, T., Kenyon, S. J., Balog, Z., Bragg, A., & Tokarz, S. 2007, *ApJ*, 669, L33
- Currie, T., Kenyon, S. J., Balog, Z., et al. 2008, *ApJ*, 672, 558
- Currie, T., Evans, N. R., Spitzbart, B. D., et al. 2009, *AJ*, 137, 3210
- Currie, T., Hernandez, J., Irwin, J., et al. 2010, *ApJS*, 186, 191
- Denissenkov, P. A. 2010, *ApJ*, 719, 28
- Dworetzky, M. M. 1983, *MNRAS*, 203, 917
- Fedele, D., van den Ancker, M. E., Henning, T., Jayawardhana, R., & Oliveira, J. M. 2010, *A&A*, 510, A72
- Gallet, F., & Bouvier, J. 2013, *A&A*, submitted
- Harrison, T. E., Coughlin, J. L., Ule, N. M., & López-Morales, M. 2012, *AJ*, 143, 4
- Hartman, J. D., Bakos, G. Á., Kovács, G., & Noyes, R. W. 2010, *MNRAS*, 408, 475
- Herbst, W., Bailer-Jones, C. A. L., & Mundt, R. 2001, *ApJ*, 554, L197
- Herbst, W., & Mundt, R. 2005, *ApJ*, 633, 967
- Horedt, G. P. 2004, *Astrophysics and Space Science Library*, 306
- Horne, J. H., & Baliunas, S. L. 1986, *ApJ*, 302, 757
- Irwin, J., Irwin, M., Aigrain, S., et al. 2007, *MNRAS*, 375, 1449
- Irwin, J., Hodgkin, S., Aigrain, S., et al. 2007, *MNRAS*, 377, 741
- Irwin, J., Hodgkin, S., Aigrain, S., et al. 2008, *MNRAS*, 384, 675
- Irwin, J., Hodgkin, S., Aigrain, S., et al. 2008, *MNRAS*, 383, 1588
- Irwin, J., & Bouvier, J. 2009, *IAU Symposium*, 258, 363
- Irwin, J., Aigrain, S., Bouvier, J., et al. 2009, *MNRAS*, 392, 1456
- Keller, S. C., Grebel, E. K., Miller, G. J., & Yoss, K. M. 2001, *AJ*, 122, 248
- Kennedy, G. M., & Kenyon, S. J. 2009, *ApJ*, 695, 1210
- Littlefair, S. P., Naylor, T., Mayne, N. J., Saunders, E. S., & Jeffries, R. D. 2010, *MNRAS*, 403, 545
- Mayne, N. J., Naylor, T., Littlefair, S. P., Saunders, E. S., & Jeffries, R. D. 2007, *MNRAS*, 375, 1220
- Mayne, N. J., & Naylor, T. 2008, *MNRAS*, 386, 261
- Meibom, S., Mathieu, R. D., & Stassun, K. G. 2009, *ApJ*, 695, 679
- Meibom, S., Barnes, S. A., Latham, D. W., et al. 2011, *ApJ*, 733, L9
- Messina, S., Desidera, S., Turatto, M., Lanzafame, A. C., & Guinan, E. F. 2010, *A&A*, 520, A15
- Messina, S., Desidera, S., Lanzafame, A. C., Turatto, M., & Guinan, E. F. 2011, *A&A*, 532, A10
- Nefs, S. V., Birkby, J. L., Snellen, I. A. G., et al. 2012, *MNRAS*, 425, 950
- Oosterhoff, P. T. 1937, *Annalen van de Sterrewacht te Leiden*, 17, A1
- Palla, F., & Baraffe, I. 2005, *A&A*, 432, L57
- Pasquini, L., Randich, S., & Pallavicini, R. 1997, *A&A*, 325, 535
- Pinto, R. F., Brun, A. S., Jouve, L., & Grappin, R. 2011, *ApJ*, 737, 72
- Rebull, L. M. 2001, *AJ*, 121, 1676
- Rebull, L. M., Wolf, S. C., & Strom, S. E. 2004, *AJ*, 127, 1029
- Roberts, D. H., Lehar, J., & Dreher, J. W. 1987, *AJ*, 93, 968
- Robin, A. C., Reylé, C., Derrière, S., & Picaud, S. 2003, *A&A*, 409, 523
- Rodríguez-López, C., MacDonald, J., & Moya, A. 2012, *MNRAS*, 419, L44
- Saesen, S., Carrier, F., Pigulski, A., et al. 2010, *A&A*, 515, A16
- Scargle, J. D. 1982, *ApJ*, 263, 835
- Siess, L., Dufour, E., & Forestini, M. 2000, *A&A*, 358, 593
- Schild, R. E. 1965, *ApJ*, 142, 979
- Slesnick, C. L., Hillenbrand, L. A., & Massey, P. 2002, *ApJ*, 576, 880
- Spada, F., Lanzafame, A. C., Lanza, A. F., Messina, S., & Collier Cameron, A. 2011, *MNRAS*, 416, 447
- Stassun, K. G., Mathieu, R. D., Vrba, F. J., Mazeh, T., & Henden, A. 2001, *AJ*, 121, 1003
- Taylor, M. B. 2005, *Astronomical Data Analysis Software and Systems XIV*, 347, 29
- Thompson, M. J., Christensen-Dalsgaard, J., Miesch, M. S., & Toomre, J. 2003, *ARA&A*, 41, 599
- Trumpler, R. J. 1926, *PASP*, 38, 350
- Uribe, A., García-Varela, J.-A., Sabogal-Martínez, B.-E., Higuera G., M. A., & Brieva, E. 2002, *PASP*, 114, 233
- van Maanen, A. 1911, *Recherches Astronomiques de l'Observatoire d'Utrecht*, 5, 1

Appendix A: Phased light curves of the 586 periodic h Per candidate members

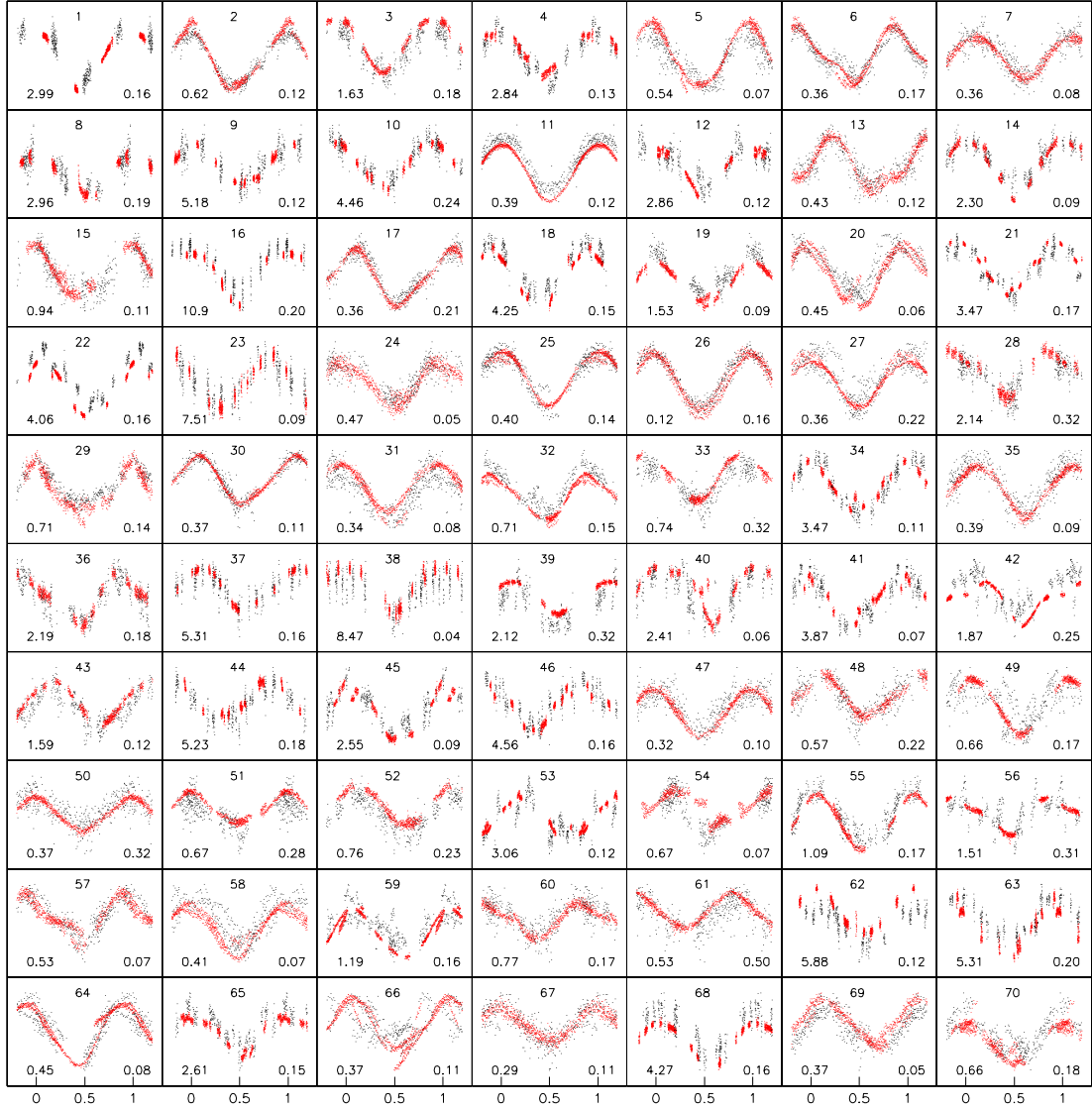


Fig. A.1. The phased light curves of periodic h Per candidate members (red dots : CFHT, back dots : Maitanak). The object number is given in each panel (top) as well as the period (in days, bottom left) and amplitude (in magnitude, bottom right). The light-curves are ordered by decreasing periodogram peak power.

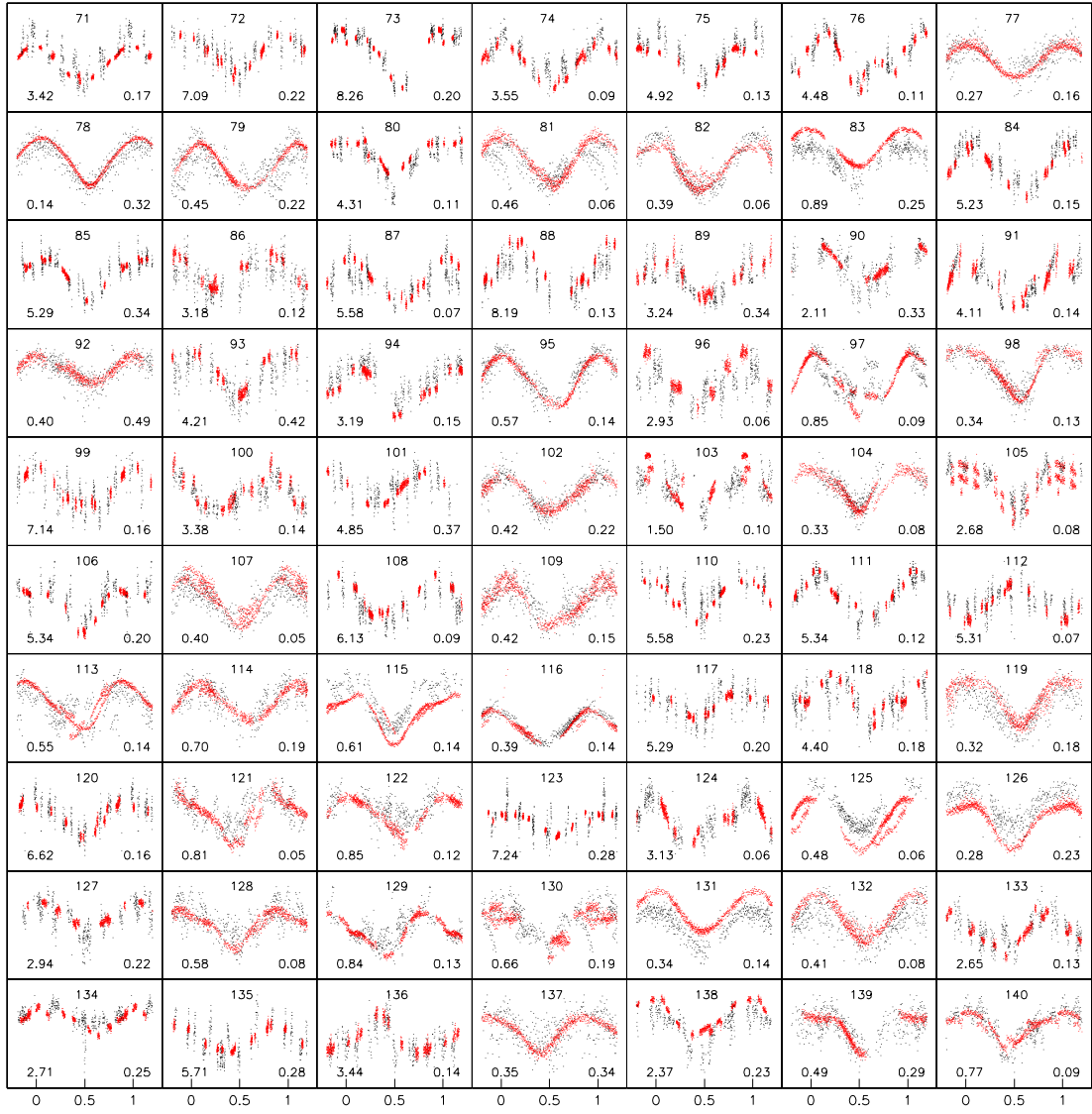


Fig. A.2. Fig. A.1 ct'd.

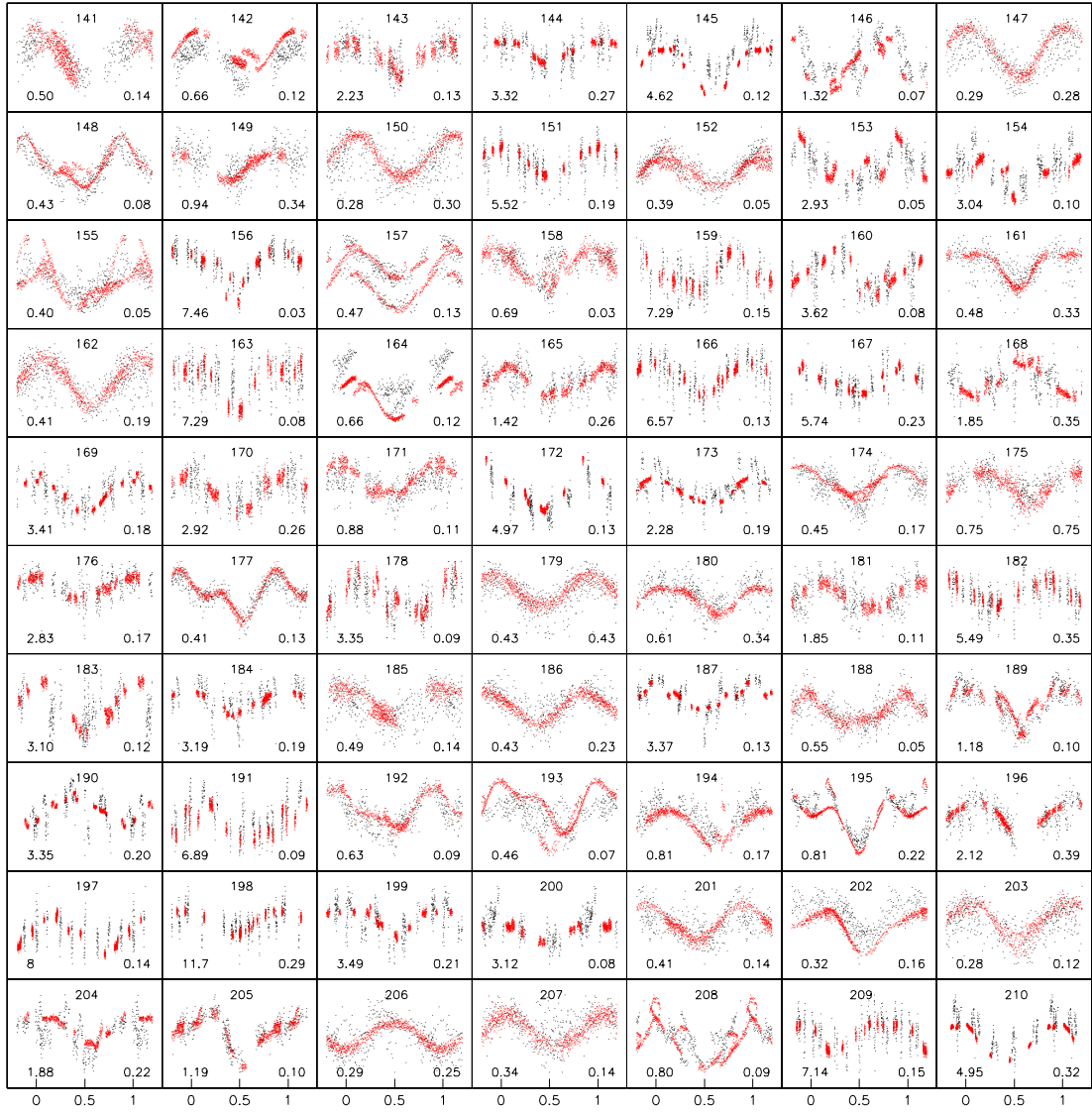


Fig. A.3. Fig. A.1 ct'd.

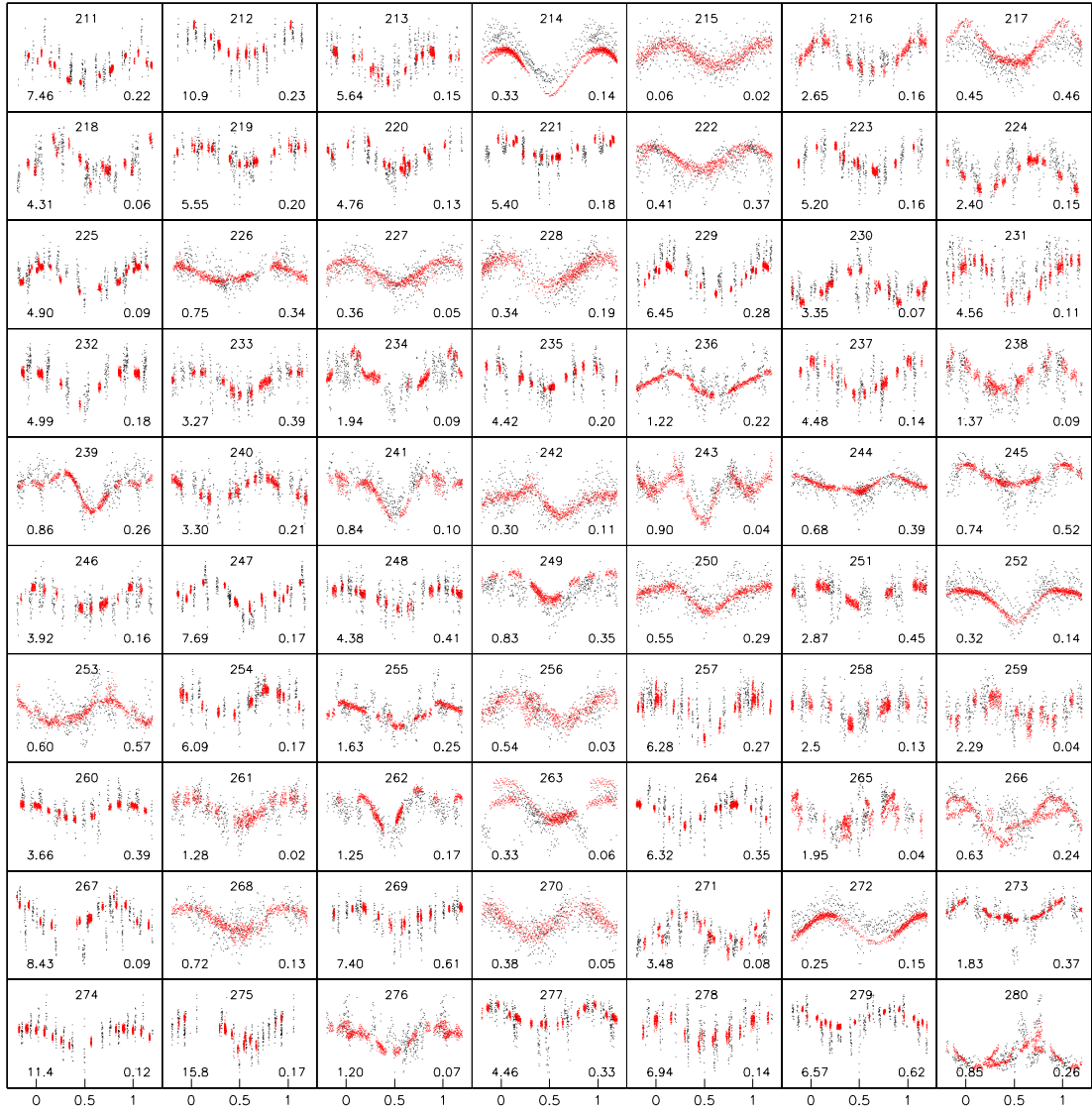


Fig. A.4. Fig. A.1 ct'd.

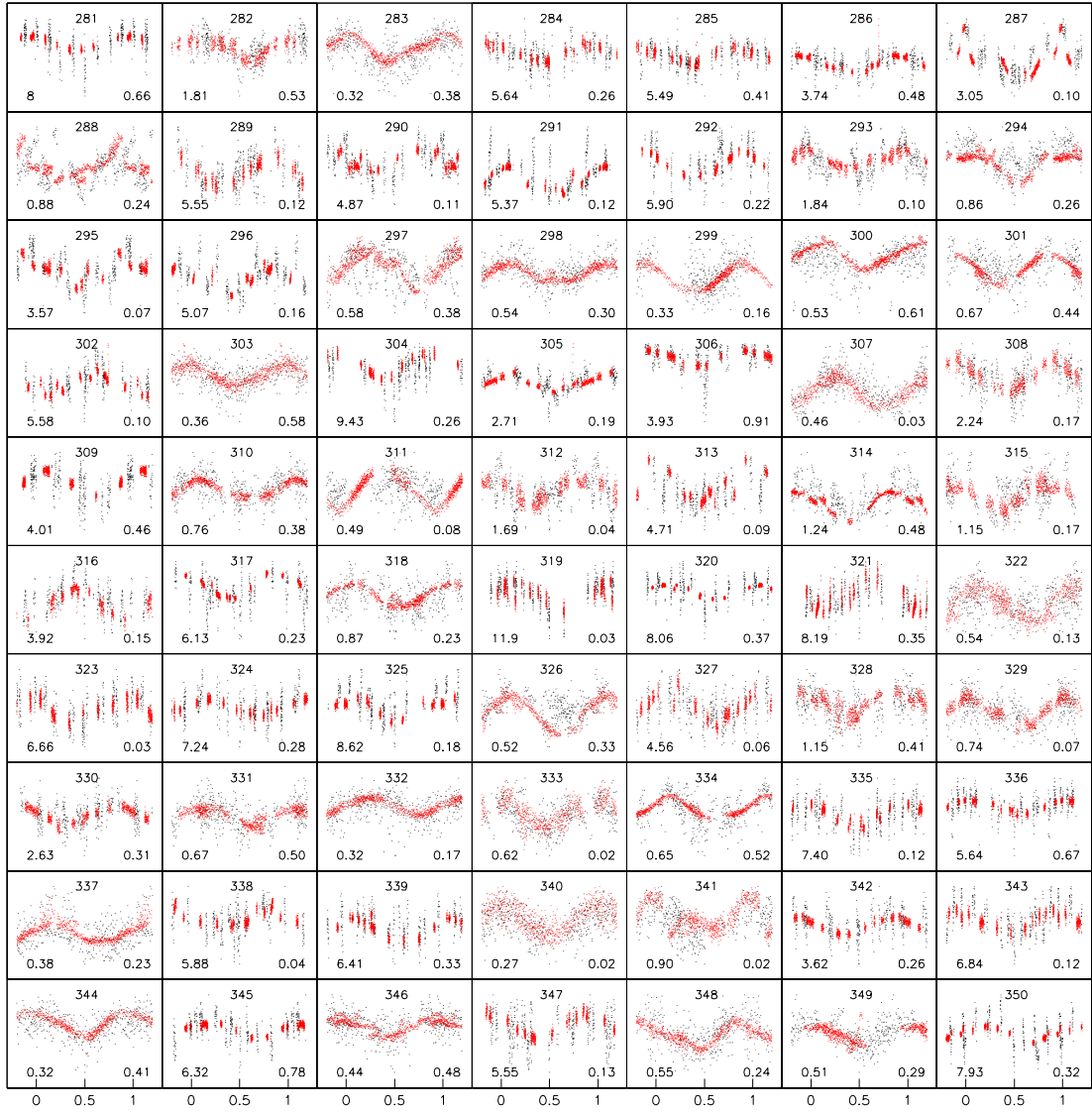


Fig. A.5. Fig. A.1 ct'd.

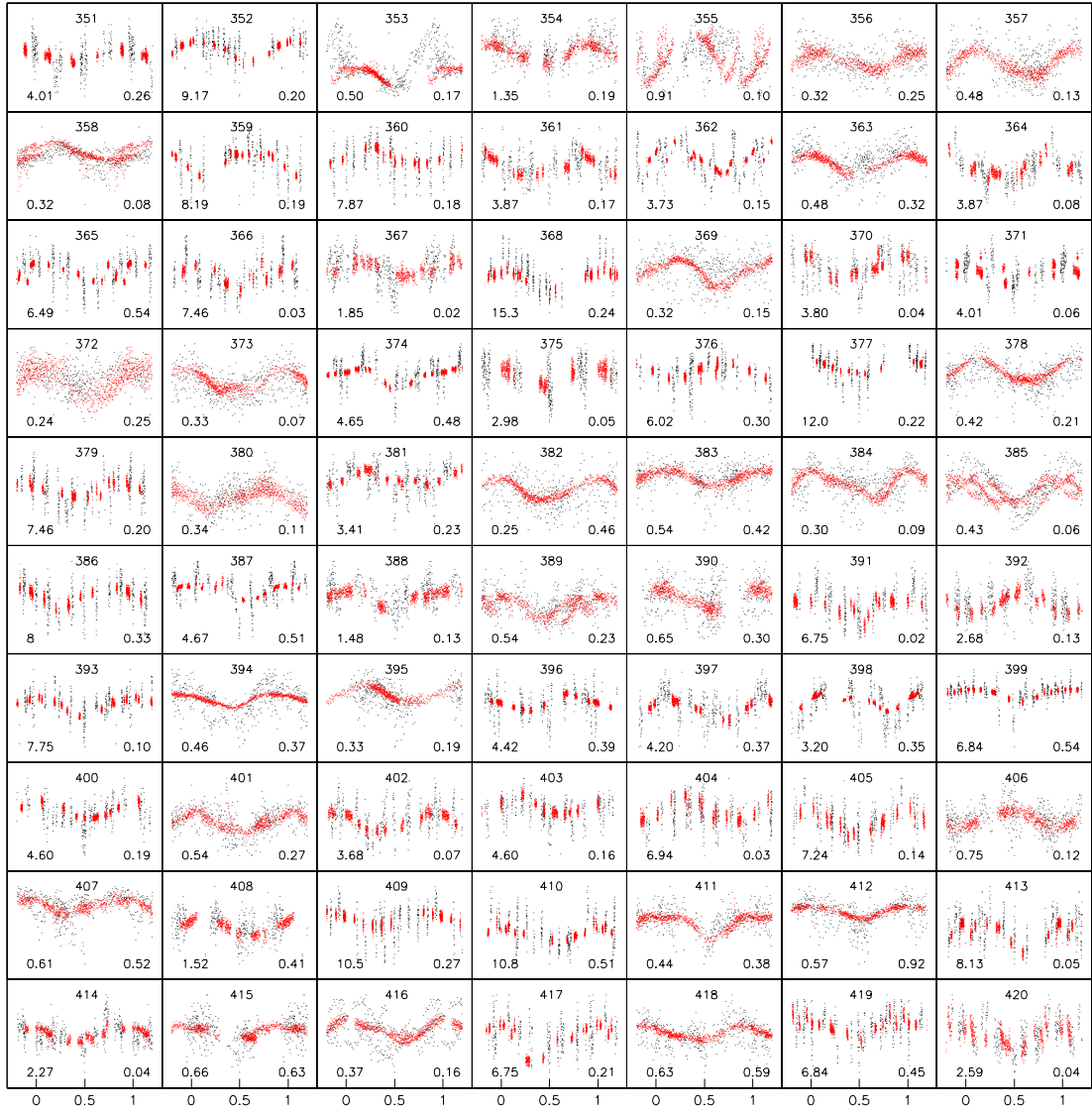


Fig. A.6. Fig. A.1 ct'd.

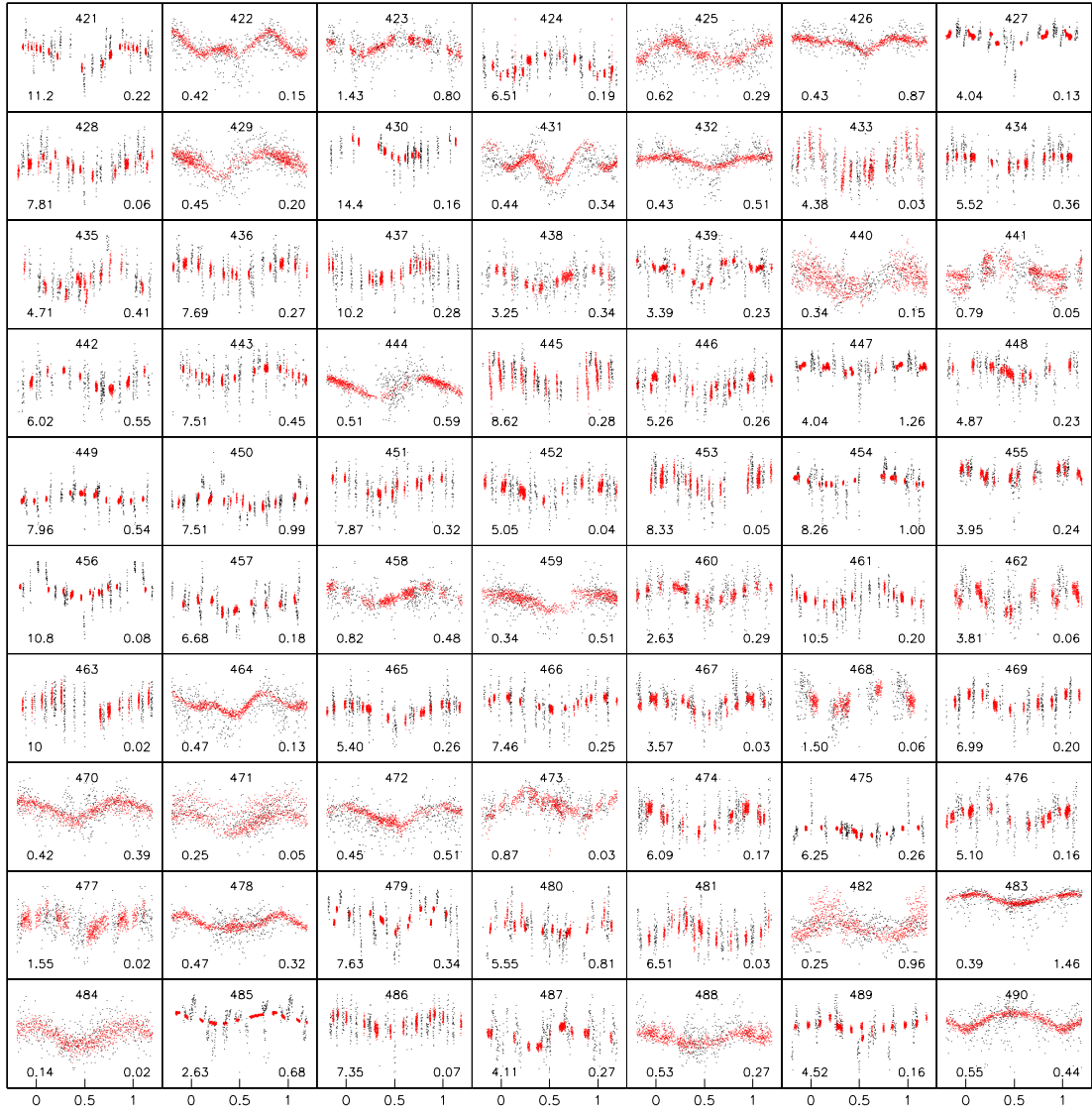


Fig. A.7. Fig. A.1 ct'd.

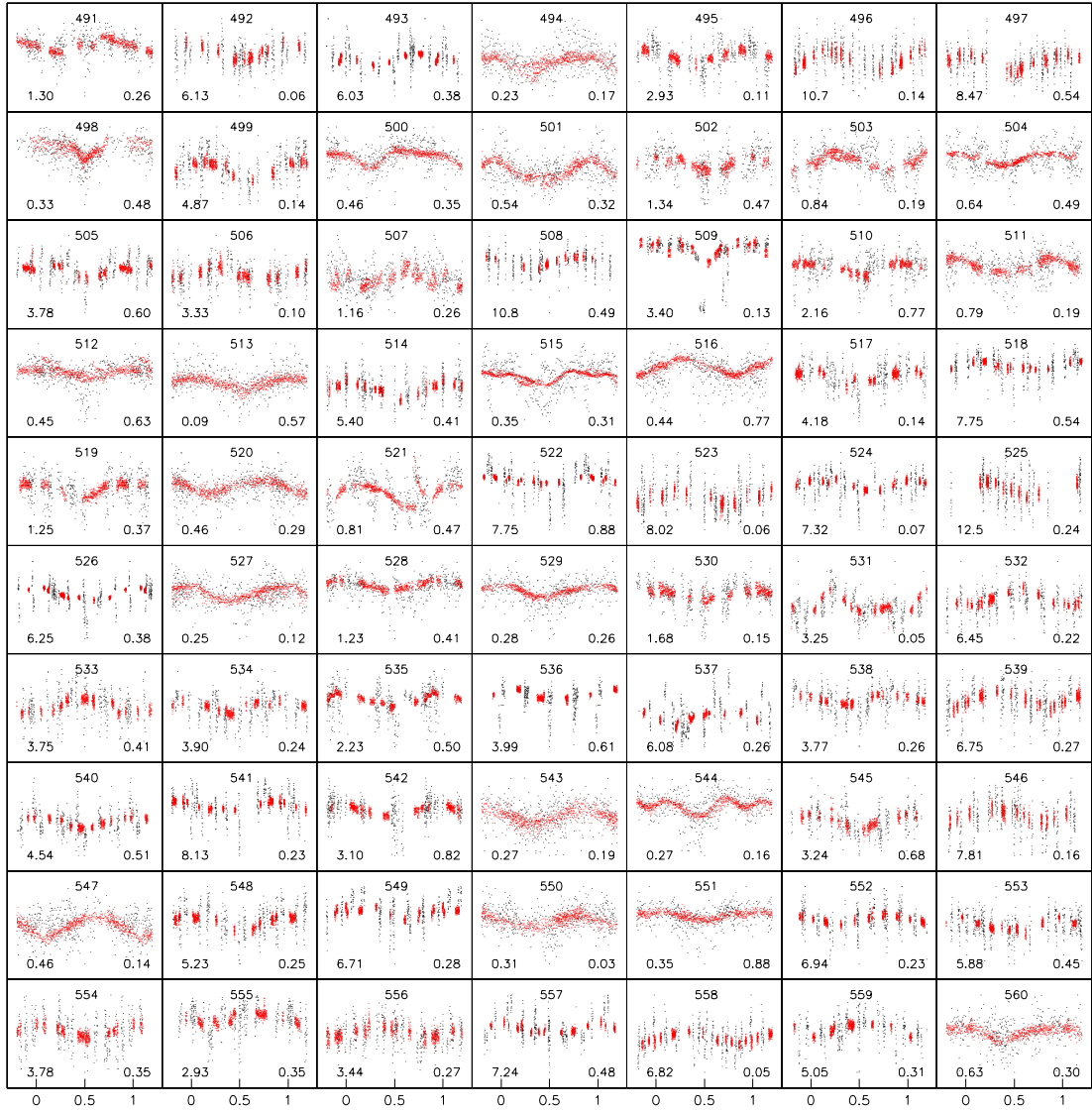


Fig. A.8. Fig. A.1 ct'd.

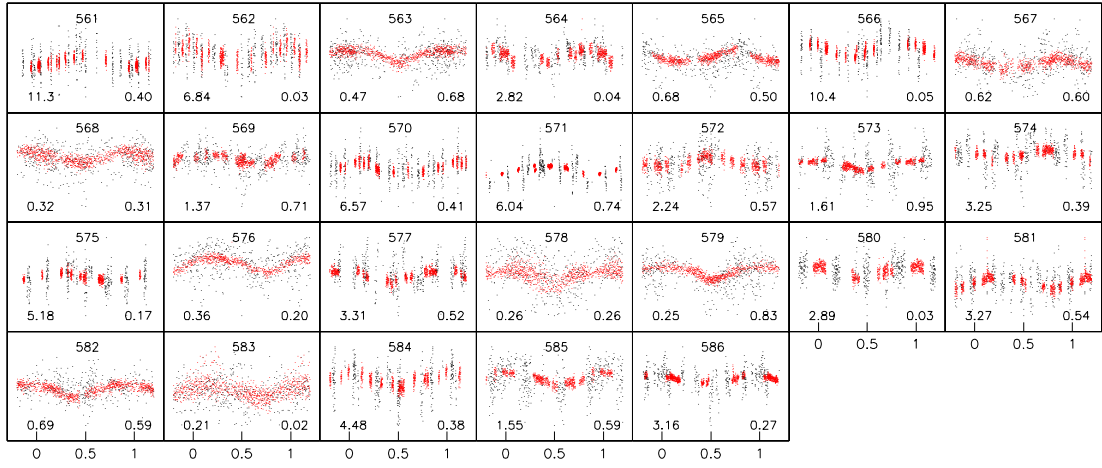


Fig. A.9. Fig. A.1 ct'd.

Table 2. List of periodic objects ordered by periodogram peak power. The binary flag is set to 2 if the object has been identified as a binary in the $V_{CFHT} - K$ CMD and to 1 otherwise. The V and I_c magnitudes as well as the membership flag (column before last) are from Currie et al. (2010). The near infrared photometry has been obtained with WIRCcam at CFHT and is from Cardoso et al. (in prep.). The last column indicates whether the object has been detected in H α (Currie et al. 2007b) and/or in X-rays (Currie et al. 2009; C. Argiroffo priv. com)

HPer -ID	RA (deg)	DEC (deg)	V_{CFHT} (mag)	Period (d)	Power	FAP	amplitude (mag)	mass M_{\odot}	binary flag	V (mag)	I_c (mag)	J (mag)	H (mag)	K (mag)	Memb. flag	Other
1	02:19:20.17	+57:11:51.4	17.35	2.99	476.0	<0.001	0.064	1.21	1	-	-	15.72	15.09	14.90	-	X
2	02:19:38.13	+57:12:32.3	17.11	0.625	463.3	<0.001	0.046	1.25	1	18.32	16.63	15.48	14.83	14.63	3	X
3	02:18:11.37	+57:14:40.8	18.21	1.64	430.6	<0.001	0.061	1.03	1	-	-	16.41	15.67	15.46	-	-
4	02:18:17.31	+57:07:35.3	17.02	2.85	430.5	<0.001	0.037	1.27	1	18.10	16.63	15.48	14.85	14.70	3	-
5	02:18:31.14	+57:03:53.3	16.43	0.541	430.4	<0.001	0.029	1.34	2	17.57	16.10	14.94	14.33	14.17	3	X
6	02:18:19.07	+57:02:28.5	16.85	0.361	426.4	<0.001	0.055	1.29	2	18.16	16.40	15.10	14.40	14.20	3	X
7	02:19:23.99	+57:02:24.8	16.71	0.364	426.2	<0.001	0.022	1.31	2	17.88	16.25	15.10	14.45	14.27	3	-
8	02:18:54.21	+57:00:30.6	18.14	2.97	424.3	<0.001	0.049	1.03	1	19.70	17.75	16.10	15.35	15.15	3	-
9	02:18:50.23	+56:59:57.8	17.83	5.18	413.4	<0.001	0.033	1.12	1	19.09	17.43	16.12	15.42	15.28	3	-
10	02:19:46.17	+57:09:39.0	18.50	4.46	408.1	<0.001	0.065	0.94	1	20.23	18.03	16.54	15.71	15.42	1	-
11	02:18:49.08	+57:11:12.9	16.42	0.391	407.4	<0.001	0.043	1.34	2	17.57	16.00	14.89	14.27	14.06	3	X
12	02:18:00.05	+57:13:06.7	17.20	2.87	405.1	<0.001	0.032	1.23	1	-	-	15.66	15.07	14.90	-	-
13	02:19:48.85	+57:15:09.0	18.10	0.436	403.5	<0.001	0.040	1.05	1	19.31	17.54	16.34	15.60	15.36	1	-
14	02:18:37.09	+57:05:53.2	16.99	2.30	402.9	<0.001	0.033	1.27	1	17.91	16.42	15.40	14.78	14.56	3	X
15	02:19:36.85	+57:03:17.0	17.78	0.946	401.5	<0.001	0.036	1.12	1	19.09	17.31	15.99	15.25	15.04	3	X
16	02:19:44.74	+57:14:37.7	18.42	11.0	397.0	<0.001	0.060	0.96	1	19.82	17.94	16.65	15.86	15.63	1	-
17	02:19:25.76	+57:09:24.2	17.68	0.360	396.4	<0.001	0.075	1.15	1	18.98	17.19	15.85	15.20	14.93	3	X
18	02:18:29.88	+57:14:24.3	17.68	4.26	395.9	<0.001	0.052	1.14	1	18.86	17.13	15.90	15.25	15.02	3	-
19	02:19:17.02	+57:15:45.1	16.93	1.53	393.2	<0.001	0.024	1.28	1	18.02	16.46	15.38	14.80	14.61	3	-
20	02:18:52.71	+57:11:29.6	16.09	0.451	392.7	<0.001	0.021	1.39	2	17.29	15.75	14.61	14.10	13.93	3	X
21	02:18:38.27	+56:59:42.3	17.22	3.47	390.8	<0.001	0.055	1.22	1	-	-	15.74	15.06	14.87	-	X
22	02:19:20.91	+57:13:12.3	17.07	4.07	390.6	<0.001	0.054	1.25	1	18.28	16.71	15.50	14.91	14.72	3	X
23	02:19:48.62	+57:13:10.9	17.93	7.52	389.8	<0.001	0.030	1.09	1	19.12	17.38	16.24	15.51	15.28	1	-
24	02:19:54.81	+57:03:03.8	16.06	0.473	388.7	<0.001	0.014	1.39	2	17.02	15.66	14.68	14.17	14.05	3	-
25	02:19:15.00	+57:09:05.0	16.51	0.402	387.5	<0.001	0.048	1.34	2	-	-	14.96	14.33	14.09	-	X
26	02:18:14.52	+57:09:31.8	17.51	0.126	386.0	<0.001	0.062	1.18	2	-	-	15.34	14.64	14.30	-	X
27	02:18:57.60	+57:03:31.7	16.77	0.365	384.8	<0.001	0.067	1.29	2	-	-	15.12	14.54	14.32	-	X
28	02:19:46.36	+57:07:30.9	19.11	2.15	383.6	<0.001	0.091	0.73	1	21.06	18.70	16.95	16.08	15.87	1	-
29	02:19:32.76	+57:05:44.1	17.00	0.712	383.2	<0.001	0.037	1.26	1	18.23	16.60	15.36	14.75	14.56	3	X
30	02:17:58.31	+57:08:38.2	16.27	0.372	381.9	<0.001	0.034	1.36	2	-	-	14.86	14.32	14.14	-	-
31	02:18:48.73	+57:11:27.5	16.80	0.348	379.1	<0.001	0.025	1.30	2	-	-	15.19	14.56	14.34	-	-
32	02:18:18.03	+57:16:58.2	16.90	0.717	378.7	<0.001	0.041	1.27	2	18.12	16.47	15.24	14.52	14.31	3	-
33	02:19:51.52	+57:08:33.6	19.20	0.743	378.4	<0.001	0.088	0.76	2	21.20	18.60	16.77	15.95	15.64	1	X
34	02:19:20.52	+57:09:25.4	17.10	3.47	378.1	<0.001	0.035	1.25	1	18.37	16.76	15.50	14.91	14.68	0	X
35	02:18:58.23	+57:13:55.2	17.04	0.395	375.6	<0.001	0.030	1.26	1	18.29	16.60	15.44	14.86	14.62	3	-
36	02:19:23.99	+57:09:08.5	18.18	2.20	371.4	<0.001	0.058	1.03	1	19.48	17.71	16.36	15.64	15.36	1	X
37	02:19:46.02	+57:03:41.4	18.31	5.32	367.4	<0.001	0.042	1.00	1	19.65	17.80	16.48	15.75	15.57	1	-
38	02:19:57.71	+57:10:37.4	16.58	8.47	367.2	<0.001	0.012	1.33	1	17.56	16.13	15.19	14.67	14.50	1	-
39	02:18:03.08	+57:16:15.9	18.60	2.12	364.8	<0.001	0.066	0.93	1	20.10	18.08	16.56	15.77	15.52	1	-
40	02:19:21.38	+57:05:14.6	16.93	2.42	364.7	<0.001	0.023	1.28	1	18.09	16.50	15.34	14.82	14.66	3	X

Table 2. Continued.

HPer -ID	RA (deg)	DEC (deg)	i_{CFHT} (mag)	Period (d)	Power	FAP	amplitude (mag)	mass M_{\odot}	binary flag	V (mag)	Ic (mag)	J (mag)	H (mag)	K (mag)	Memb. flag	Other
41	02:18:30.58	+57:04:54.0	16.74	3.88	364.5	<0.001	0.022	1.30	1	17.86	16.42	15.30	14.76	14.58	3	X
42	02:18:58.25	+57:01:40.5	17.52	1.88	364.4	<0.001	0.066	1.17	1	-	-	15.85	15.26	15.07	-	X
43	02:19:45.54	+57:02:53.5	17.73	1.60	364.1	<0.001	0.032	1.14	2	18.97	17.18	15.88	15.11	14.89	3	X
44	02:18:31.49	+57:06:39.6	18.14	5.24	363.3	<0.001	0.044	1.04	1	19.54	17.73	16.33	15.65	15.46	1	-
45	02:18:03.02	+57:06:37.3	16.56	2.55	360.7	<0.001	0.030	1.33	2	17.74	16.07	14.78	14.10	13.91	3	X
46	02:19:03.12	+57:11:26.5	17.79	4.57	360.3	<0.001	0.048	1.12	1	19.03	17.31	16.09	15.38	15.14	0	-
47	02:18:36.48	+57:01:15.3	17.11	0.323	360.2	<0.001	0.031	1.25	2	18.34	16.69	15.39	14.77	14.58	3	X, H _q
48	02:18:06.60	+57:15:14.8	18.67	0.578	359.4	<0.001	0.060	0.88	1	20.23	18.16	16.65	15.84	15.61	1	-
49	02:18:54.77	+57:03:38.9	17.85	0.661	359.0	<0.001	0.055	1.11	1	19.21	17.44	15.95	15.27	15.10	3	X
50	02:18:33.74	+57:11:46.1	19.08	0.370	358.3	<0.001	0.070	0.76	1	20.90	18.58	16.90	16.13	15.84	1	-
51	02:19:25.25	+57:02:37.8	18.07	0.674	353.0	<0.001	0.051	1.05	2	19.68	17.58	16.03	15.29	15.07	3	X
52	02:18:15.22	+57:05:07.8	18.76	0.764	352.8	<0.001	0.056	0.88	1	20.38	18.20	16.66	15.86	15.60	1	-
53	02:19:57.83	+57:00:44.8	16.70	3.07	352.3	<0.001	0.030	1.31	1	17.67	16.29	15.29	14.77	14.59	3	-
54	02:18:21.70	+57:06:52.2	16.49	0.674	351.5	<0.001	0.015	1.33	1	17.54	16.13	15.03	14.48	14.31	3	X
55	02:18:29.95	+57:01:09.1	17.95	1.10	349.9	<0.001	0.059	1.10	1	19.25	17.50	16.03	15.32	15.11	3	-
56	02:17:59.20	+57:16:32.6	18.35	1.51	349.5	<0.001	0.069	0.99	1	19.94	17.89	16.44	15.62	15.40	1	-
57	02:18:29.48	+57:10:19.2	16.72	0.530	349.1	<0.001	0.016	1.30	1	17.89	16.39	15.26	14.67	14.45	3	X
58	02:19:13.07	+57:12:35.6	16.27	0.415	348.3	<0.001	0.022	1.36	2	-	-	14.60	14.04	13.83	-	X
59	02:18:22.10	+56:59:32.2	16.83	1.19	348.1	<0.001	0.042	1.29	1	-	-	15.40	14.81	14.65	-	X
60	02:18:13.94	+57:12:52.7	18.31	0.774	345.8	<0.001	0.036	1.00	1	-	-	16.40	15.69	15.45	-	-
61	02:18:17.79	+57:10:51.6	19.83	0.539	343.9	<0.001	0.103	0.53	1	22.42	19.10	17.38	16.55	16.25	1	-
62	02:19:54.24	+57:03:48.2	17.37	5.88	343.7	<0.001	0.032	1.21	1	18.50	16.84	15.64	14.97	14.76	3	X
63	02:19:51.56	+57:10:00.9	17.82	5.32	343.4	<0.001	0.060	1.11	1	-	-	16.17	15.44	15.20	-	X
64	02:19:21.84	+57:02:07.1	15.85	0.460	342.0	<0.001	0.031	1.42	1	16.81	15.49	14.56	14.10	13.95	3	X
65	02:18:55.22	+57:11:29.0	17.85	2.62	341.5	<0.001	0.034	1.11	1	19.32	17.41	15.97	15.29	15.06	3	X
66	02:18:05.38	+57:01:28.5	16.34	0.371	340.7	<0.001	0.031	1.36	2	17.34	15.90	14.85	14.30	14.14	3	H _q
67	02:19:47.77	+57:12:59.9	18.08	0.296	338.9	<0.001	0.024	1.06	1	19.45	17.60	16.30	15.54	15.32	1	-
68	02:18:23.82	+57:13:47.0	18.16	4.27	338.7	<0.001	0.045	1.04	1	19.56	17.76	16.35	15.62	15.40	1	-
69	02:18:47.47	+57:01:38.6	16.28	0.376	337.5	<0.001	0.013	1.36	2	17.39	15.94	14.82	14.24	14.08	3	X
70	02:19:08.05	+57:06:08.6	17.57	0.661	336.6	<0.001	0.041	1.16	2	19.01	17.10	15.68	14.93	14.72	1	X
71	02:18:20.74	+56:59:58.8	17.29	3.42	335.2	<0.001	0.039	1.22	1	18.30	16.79	15.77	15.16	14.99	0	-
72	02:19:16.74	+57:12:04.6	18.76	7.09	334.8	<0.001	0.051	0.86	1	20.47	18.25	16.64	15.82	15.55	1	-
73	02:18:44.07	+57:08:56.1	17.69	8.26	333.2	<0.001	0.067	1.14	1	18.75	17.10	16.09	15.44	15.21	1	X
74	02:18:47.98	+57:13:58.5	17.12	3.56	332.7	<0.001	0.023	1.25	2	18.38	16.66	15.41	14.72	14.50	3	X
75	02:19:12.96	+56:59:33.0	17.39	4.93	332.0	<0.001	0.035	1.20	1	-	-	15.78	15.15	14.97	-	-
76	02:18:46.56	+57:13:53.8	17.43	4.48	331.8	<0.001	0.030	1.19	2	18.93	17.05	15.69	14.91	14.70	3	X
77	02:18:29.41	+57:15:59.0	18.00	0.279	330.7	<0.001	0.034	1.08	1	19.48	17.50	16.08	15.32	15.09	3	-
78	02:20:00.95	+57:11:24.8	17.75	0.144	330.5	<0.001	0.092	1.13	1	18.96	17.24	16.26	15.59	15.32	1	-
79	02:19:18.12	+57:01:32.9	18.19	0.454	330.4	<0.001	0.058	1.03	1	-	-	16.26	15.55	15.31	-	X
80	02:19:46.10	+57:05:47.6	16.95	4.31	329.1	<0.001	0.024	1.25	1	17.99	16.50	15.38	14.81	14.65	1	X
81	02:18:09.29	+57:03:23.6	16.60	0.463	328.1	<0.001	0.018	1.33	1	17.55	16.12	15.08	14.54	14.37	3	X
82	02:18:27.18	+57:11:07.5	15.78	0.392	327.6	<0.001	0.021	1.49	2	16.77	15.38	14.35	13.77	13.60	1	X
83	02:19:43.65	+57:06:05.7	18.31	0.895	326.5	<0.001	0.055	1.01	1	19.82	17.78	16.27	15.47	15.25	1	-
84	02:18:31.19	+57:10:56.0	18.26	5.24	326.1	<0.001	0.049	1.01	1	19.67	17.84	16.52	15.77	15.54	1	-

Table 2. Continued.

HPer -ID	RA (deg)	DEC (deg)	i_{CFHT} (mag)	Period (d)	Power	FAP	amplitude (mag)	mass M_{\odot}	binary flag	V (mag)	Ic (mag)	J (mag)	H (mag)	K (mag)	Memb. flag	Other
85	02:20:02.25	+57:03:49.2	18.57	5.29	325.5	<0.001	0.081	0.91	1	20.28	18.17	16.69	15.81	15.61	1	-
86	02:18:26.22	+57:09:21.9	18.16	3.18	325.5	<0.001	0.029	1.05	1	19.43	17.64	16.38	15.71	15.47	1	-
87	02:18:35.13	+57:04:06.7	16.70	5.59	325.3	<0.001	0.017	1.31	1	17.62	16.29	15.31	14.79	14.65	0	-
88	02:18:30.64	+57:10:08.7	18.06	8.20	324.7	<0.001	0.042	1.07	1	19.43	17.67	16.33	15.58	15.36	1	X
89	02:18:44.90	+57:10:05.4	18.96	3.25	322.5	<0.001	0.078	0.78	1	-	-	16.92	16.11	15.82	-	X
90	02:18:29.63	+57:07:14.2	19.37	2.12	321.9	<0.001	0.079	0.67	1	-	-	17.17	16.37	16.13	-	-
91	02:19:33.09	+57:09:44.0	17.02	4.12	320.3	<0.001	0.033	1.26	1	18.09	16.58	15.45	14.93	14.73	3	X
92	02:18:24.46	+57:09:28.5	19.38	0.405	318.5	<0.001	0.081	0.65	1	21.55	18.82	17.10	16.35	16.04	1	X
93	02:19:53.35	+57:07:22.1	19.72	4.22	317.9	<0.001	0.110	0.56	1	21.93	19.13	17.35	16.55	16.28	1	-
94	02:18:19.80	+57:12:24.4	18.23	3.19	317.5	<0.001	0.044	1.02	1	19.70	17.71	16.27	15.52	15.27	1	-
95	02:18:32.38	+57:14:29.2	17.91	0.580	316.8	<0.001	0.047	1.10	1	19.28	17.50	16.04	15.28	15.05	1	-
96	02:18:31.43	+57:05:36.2	17.08	2.93	316.2	<0.001	0.018	1.26	2	18.34	16.69	15.37	14.70	14.49	3	X
97	02:19:14.09	+57:01:47.7	16.30	0.853	313.9	<0.001	0.027	1.36	2	17.39	15.85	14.72	14.07	13.90	3	X
98	02:18:53.61	+57:10:04.6	17.20	0.342	313.9	<0.001	0.041	1.23	1	18.43	16.73	15.64	14.96	14.76	1	X
99	02:18:35.88	+57:12:12.5	18.77	7.14	313.0	<0.001	0.038	0.87	1	20.39	18.30	16.69	15.89	15.63	1	-
100	02:19:07.67	+57:11:03.4	17.82	3.39	312.1	<0.001	0.029	1.12	2	19.28	17.37	15.85	15.13	14.86	1	X
101	02:18:06.86	+57:05:15.0	19.47	4.85	311.0	<0.001	0.072	0.63	1	21.61	18.84	17.03	16.26	16.00	1	-
102	02:18:24.49	+57:08:28.9	18.28	0.423	310.1	<0.001	0.050	1.01	1	-	-	16.43	15.72	15.46	-	-
103	02:19:08.85	+57:06:59.0	16.25	1.50	309.7	<0.001	0.026	1.37	1	17.14	15.84	14.85	14.40	14.28	3	X
104	02:19:10.54	+57:15:45.1	17.03	0.337	308.9	<0.001	0.022	1.25	2	18.31	16.60	15.37	14.68	14.46	3	-
105	02:18:15.55	+57:13:54.8	16.75	2.69	308.4	<0.001	0.020	1.30	1	17.82	16.42	15.35	14.79	14.62	3	-
106	02:18:48.39	+57:07:40.2	18.04	5.35	306.4	<0.001	0.045	1.07	1	-	-	16.36	15.60	15.38	-	X
107	02:18:03.79	+57:01:41.7	15.70	0.404	305.9	<0.001	0.013	1.45	1	16.47	15.33	14.51	14.02	13.87	1	-
108	02:19:16.62	+57:13:41.4	17.39	6.14	305.9	<0.001	0.025	1.21	1	18.51	16.87	15.69	15.10	14.90	1	X
109	02:18:34.71	+57:10:33.1	18.78	0.424	305.4	<0.001	0.036	0.85	1	20.49	18.28	16.70	15.91	15.63	1	X
110	02:19:38.04	+57:07:04.3	18.07	5.59	305.2	<0.001	0.059	1.05	1	19.52	17.59	16.20	15.47	15.27	1	X
111	02:19:15.75	+57:13:02.8	17.56	5.35	304.4	<0.001	0.034	1.18	1	18.79	17.05	15.87	15.18	14.98	0	X
112	02:18:33.30	+57:02:23.0	17.10	5.32	303.2	<0.001	0.014	1.24	2	18.51	16.73	15.41	14.71	14.52	3	X
113	02:18:56.02	+57:07:22.5	16.88	0.552	301.7	<0.001	0.037	1.28	2	18.05	16.45	15.24	14.59	14.46	3	X
114	02:19:14.30	+57:16:07.6	18.70	0.707	300.3	<0.001	0.043	0.88	1	20.23	18.22	16.73	15.88	15.62	1	-
115	02:19:57.12	+57:16:39.4	16.66	0.617	299.9	<0.001	0.039	1.31	1	17.60	16.09	15.41	14.73	14.41	3	-
116	02:19:39.36	+57:09:45.4	16.25	0.397	299.3	<0.001	0.031	1.36	2	17.33	15.84	14.76	14.20	14.00	3	X
117	02:19:34.29	+57:00:09.3	18.62	5.29	296.9	<0.001	0.034	0.92	1	20.12	18.10	16.84	16.06	15.79	1	-
118	02:18:07.60	+57:11:31.8	18.85	4.41	295.5	<0.001	0.042	0.85	2	20.83	18.23	16.49	15.69	15.41	1	-
119	02:19:05.11	+57:09:58.0	18.34	0.327	295.1	<0.001	0.052	1.00	1	-	-	16.38	15.65	15.40	-	-
120	02:19:18.31	+57:08:35.9	18.00	6.62	294.2	<0.001	0.037	1.08	1	19.37	17.49	16.07	15.43	15.15	1	X
121	02:18:02.35	+57:08:45.6	16.04	0.817	293.5	<0.001	0.013	1.39	2	-	-	14.59	14.04	13.86	-	X
122	02:18:34.79	+57:13:13.7	17.95	0.856	292.5	<0.001	0.023	1.10	2	19.36	17.42	16.00	15.26	15.02	1	-
123	02:18:58.25	+57:09:38.0	18.13	7.25	291.7	<0.001	0.043	1.05	2	-	-	16.17	15.40	15.10	-	X
124	02:19:41.70	+57:06:13.4	17.18	3.13	291.5	<0.001	0.016	1.24	1	18.35	16.79	15.51	14.86	14.70	0	X
125	02:18:21.01	+57:06:07.4	15.86	0.489	291.0	<0.001	0.019	1.42	1	16.80	15.55	14.57	14.13	13.99	3	X
126	02:18:22.17	+57:09:16.5	18.51	0.282	290.6	<0.001	0.054	0.94	1	20.09	18.09	16.64	15.83	15.58	1	-
127	02:18:54.85	+57:05:31.5	18.61	2.94	290.4	<0.001	0.039	0.92	2	20.43	18.06	16.42	15.62	15.37	1	X
128	02:18:31.14	+57:13:30.4	16.81	0.586	290.1	<0.001	0.017	1.30	1	17.88	16.38	15.29	14.73	14.55	3	X

Table 2. Continued.

HPer -ID	RA (deg)	DEC (deg)	i_{CFHT} (mag)	Period (d)	Power	FAP	amplitude (mag)	mass M_{\odot}	binary flag	V (mag)	Ic (mag)	J (mag)	H (mag)	K (mag)	Memb. flag	Other
129	02:19:18.63	+57:01:39.2	17.45	0.849	289.8	<0.001	0.030	1.19	1	18.56	16.91	15.75	15.05	14.83	3	X
130	02:19:20.43	+57:04:39.3	18.21	0.660	289.7	<0.001	0.039	1.01	2	19.92	17.74	16.08	15.33	15.08	1	X
131	02:19:36.30	+57:02:23.6	17.84	0.348	288.8	<0.001	0.033	1.12	1	19.13	17.34	15.96	15.26	15.06	3	-
132	02:19:19.05	+57:12:55.6	17.63	0.419	288.2	<0.001	0.023	1.16	2	18.91	17.11	15.71	15.02	14.77	3	X
133	02:19:02.95	+57:14:01.2	17.61	2.66	288.2	<0.001	0.028	1.16	1	18.89	17.17	15.99	15.37	15.14	0	-
134	02:18:49.64	+57:15:07.6	18.20	2.72	287.4	<0.001	0.038	1.02	1	19.64	17.78	16.40	15.65	15.43	1	-
135	02:19:41.32	+57:05:17.1	18.87	5.71	287.2	<0.001	0.047	0.83	1	-	-	16.81	15.97	15.74	-	-
136	02:19:19.64	+57:08:41.9	18.25	3.45	286.5	<0.001	0.030	1.02	1	-	-	16.31	15.55	15.27	-	X
137	02:19:58.67	+57:10:58.2	19.75	0.356	285.3	<0.001	0.070	0.55	1	21.91	19.11	17.35	16.48	16.20	1	-
138	02:18:26.21	+57:03:11.2	18.39	2.38	285.1	<0.001	0.050	0.99	1	19.78	17.85	16.42	15.68	15.47	1	X
139	02:19:24.76	+57:10:19.4	19.32	0.493	284.7	<0.001	0.068	0.67	1	21.42	18.69	17.01	16.26	15.95	1	X
140	02:17:58.71	+57:04:43.0	16.53	0.773	284.7	<0.001	0.019	1.33	1	17.53	16.11	15.06	14.51	14.34	1	X
141	02:19:50.43	+57:10:50.8	18.42	0.503	284.4	<0.001	0.044	0.96	2	20.35	17.87	16.14	15.32	15.03	1	X
142	02:19:21.71	+57:13:15.2	17.00	0.665	283.3	<0.001	0.022	1.27	1	18.13	16.56	15.37	14.80	14.59	3	X
143	02:19:23.59	+57:15:33.8	18.82	2.24	282.7	<0.001	0.024	0.87	2	-	-	16.51	15.71	15.41	-	-
144	02:19:34.94	+57:00:06.2	19.06	3.32	281.8	<0.001	0.038	0.77	1	20.92	18.54	16.99	16.14	15.87	1	-
145	02:19:56.30	+57:01:07.3	16.86	4.63	281.8	<0.001	0.031	1.28	1	18.06	16.49	15.37	14.73	14.56	3	-
146	02:19:22.74	+57:06:21.6	16.32	1.33	281.6	<0.001	0.020	1.35	1	17.40	15.93	14.92	14.41	14.28	3	X
147	02:18:13.19	+57:07:46.6	19.22	0.294	281.4	<0.001	0.083	0.70	1	21.16	18.67	16.99	16.09	15.85	1	-
148	02:19:03.03	+57:04:51.9	16.05	0.433	279.3	<0.001	0.021	1.39	2	17.11	15.66	14.61	14.11	13.94	3	X
149	02:18:05.33	+57:10:51.6	19.59	0.946	279.2	<0.001	0.056	0.58	1	-	-	17.23	16.39	16.10	-	-
150	02:18:07.84	+57:08:50.3	19.73	0.284	279.1	<0.001	0.070	0.55	1	-	-	17.23	16.42	16.13	-	-
151	02:19:53.17	+57:03:08.1	18.88	5.52	278.0	<0.001	0.034	0.82	1	20.44	18.29	16.82	16.04	15.84	1	-
152	02:18:17.96	+57:12:21.6	16.16	0.391	277.9	<0.001	0.010	1.38	2	17.17	15.71	14.61	14.01	13.80	3	X
153	02:18:21.74	+57:04:37.3	16.33	2.93	277.7	<0.001	0.010	1.35	1	17.34	16.00	15.01	14.52	14.37	3	X
154	02:19:34.58	+57:05:06.1	17.29	3.05	276.7	<0.001	0.023	1.22	1	18.58	16.87	15.64	15.01	14.84	3	X
155	02:19:08.89	+57:03:57.7	16.09	0.406	276.6	<0.001	0.012	1.38	2	17.10	15.68	14.64	14.10	13.94	3	X
156	02:19:12.60	+57:13:21.4	15.89	7.46	276.0	<0.001	0.009	1.42	2	16.87	15.50	14.53	14.04	13.91	3	-
157	02:19:02.44	+57:14:29.9	16.90	0.474	276.0	<0.001	0.038	1.27	2	18.26	16.50	15.15	14.50	14.25	3	X
158	02:19:43.76	+57:05:31.9	15.95	0.691	275.7	<0.001	0.007	1.41	1	16.81	15.53	14.65	14.17	14.05	2	-
159	02:18:15.01	+57:12:13.3	19.10	7.30	275.3	<0.001	0.031	0.75	1	20.71	18.64	17.01	16.19	15.92	0	-
160	02:19:37.66	+57:04:37.7	17.69	3.62	274.9	<0.001	0.018	1.15	1	18.88	17.19	15.94	15.33	15.15	1	X
161	02:18:32.93	+57:08:27.4	19.30	0.485	274.6	<0.001	0.073	0.68	1	21.10	18.74	17.06	16.25	15.97	1	-
162	02:18:37.15	+57:09:05.6	19.23	0.413	274.4	<0.001	0.051	0.67	1	-	-	17.04	16.22	15.89	-	X
163	02:18:46.57	+57:13:37.5	18.36	7.30	273.8	<0.001	0.020	0.99	1	19.83	17.96	16.53	15.79	15.55	1	-
164	02:19:18.35	+56:59:17.3	16.23	0.665	273.6	<0.001	0.025	1.37	1	17.17	15.81	14.86	14.40	14.24	3	X
165	02:19:55.82	+57:04:01.6	19.36	1.42	273.0	<0.001	0.041	0.66	2	21.47	18.75	16.92	16.11	15.82	1	-
166	02:19:47.78	+57:03:38.7	18.27	6.58	272.5	<0.001	0.026	1.00	1	19.72	17.78	16.40	15.68	15.48	1	-
167	02:19:03.97	+57:05:48.2	18.56	5.75	272.5	<0.001	0.037	0.93	1	20.21	18.02	16.44	15.68	15.40	1	X
168	02:18:20.82	+57:00:53.0	19.13	1.85	272.4	<0.001	0.066	0.75	1	-	-	16.80	16.01	15.73	-	-
169	02:18:58.43	+57:13:38.1	18.14	3.41	268.7	<0.001	0.035	1.05	1	19.51	17.67	16.33	15.61	15.37	1	X
170	02:20:01.46	+57:02:54.1	19.12	2.92	266.3	<0.001	0.053	0.72	1	20.89	18.66	16.99	16.16	15.92	1	-
171	02:18:29.54	+57:03:10.2	17.74	0.886	266.2	<0.001	0.018	1.13	2	19.07	17.28	15.87	15.15	14.92	1	X
172	02:18:44.26	+57:11:39.1	17.49	4.98	265.9	<0.001	0.032	1.18	1	-	-	15.84	15.23	15.00	-	X

Table 2. Continued.

HPer -ID	RA (deg)	DEC (deg)	i_{CFHT} (mag)	Period (d)	Power	FAP	amplitude (mag)	mass M_{\odot}	binary flag	V (mag)	Ic (mag)	J (mag)	H (mag)	K (mag)	Memb. flag	Other
173	02:19:19.86	+57:04:36.2	17.68	2.29	264.5	<0.001	0.031	1.15	1	18.90	17.16	15.84	15.20	15.00	3	X
174	02:19:19.08	+57:03:19.3	18.07	0.459	264.2	<0.001	0.034	1.07	2	19.68	17.56	16.00	15.19	14.95	3	X
175	02:18:24.76	+57:10:56.2	20.46	0.756	262.8	<0.001	0.118	0.38	1	23.08	19.73	17.93	17.06	16.77	1	-
176	02:19:34.45	+57:15:14.8	18.75	2.83	262.3	<0.001	0.023	0.87	2	-	-	16.56	15.69	15.40	-	-
177	02:19:25.37	+57:14:32.3	17.63	0.412	262.0	<0.001	0.026	1.16	1	18.90	17.18	15.95	15.25	15.04	1	-
178	02:18:20.31	+57:12:22.2	17.42	3.36	261.1	<0.001	0.021	1.19	1	18.65	17.07	15.83	15.20	14.98	0	X
179	02:19:03.46	+57:12:40.5	20.02	0.437	259.9	<0.001	0.084	0.47	1	22.59	19.44	17.47	16.63	16.33	1	-
180	02:18:19.44	+57:11:47.9	19.56	0.610	259.9	<0.001	0.054	0.60	1	21.79	18.96	17.23	16.42	16.15	1	-
181	02:19:50.82	+57:04:07.3	18.31	1.85	259.9	<0.001	0.018	1.00	1	19.80	17.87	16.39	15.64	15.40	1	-
182	02:18:33.69	+57:10:17.6	19.79	5.49	259.8	<0.001	0.054	0.52	1	-	-	17.50	16.74	16.45	-	-
183	02:17:56.64	+57:10:14.1	18.33	3.11	259.5	<0.001	0.031	1.00	2	-	-	16.01	15.21	14.92	-	-
184	02:18:26.33	+57:05:20.2	18.40	3.19	259.3	<0.001	0.028	0.98	1	19.85	17.91	16.50	15.72	15.48	1	-
185	02:19:48.85	+57:01:23.6	18.72	0.494	258.9	<0.001	0.025	0.88	2	20.54	18.13	16.37	15.59	15.33	1	-
186	02:19:17.88	+57:13:52.5	19.39	0.436	258.5	<0.001	0.043	0.65	1	21.34	18.85	17.07	16.27	15.97	1	-
187	02:18:49.60	+57:08:59.0	17.06	3.38	257.1	<0.001	0.021	1.25	2	18.33	16.64	15.44	14.78	14.55	3	X
188	02:18:34.89	+57:09:39.8	17.11	0.553	255.9	<0.001	0.010	1.25	1	18.27	16.71	15.54	14.92	14.71	3	X
189	02:18:11.77	+57:10:34.3	17.09	1.19	255.3	<0.001	0.024	1.24	2	18.44	16.69	15.36	14.63	14.42	3	X
190	02:19:07.96	+57:06:51.5	17.46	3.36	254.4	<0.001	0.035	1.19	1	-	-	15.82	15.28	15.09	-	X
191	02:19:05.66	+57:00:39.6	17.80	6.90	253.5	<0.001	0.019	1.12	1	19.13	17.36	16.01	15.30	15.12	1	X
192	02:19:03.23	+57:01:20.5	17.49	0.638	252.9	<0.001	0.020	1.18	1	18.80	17.01	15.73	15.07	14.87	3	-
193	02:19:07.57	+57:06:09.2	15.97	0.467	252.9	<0.001	0.018	1.41	2	16.92	15.52	14.55	14.08	13.94	3	X
194	02:18:19.29	+57:03:43.2	18.49	0.816	252.7	<0.001	0.030	0.95	1	20.13	17.99	16.44	15.63	15.41	1	X
195	02:19:00.64	+57:10:20.1	16.96	0.814	252.2	<0.001	0.049	1.27	2	18.10	16.51	15.41	14.72	14.49	3	X
196	02:19:22.49	+57:13:19.5	19.61	2.13	252.1	<0.001	0.074	0.59	1	21.67	19.05	17.23	16.40	16.10	1	-
197	02:18:10.61	+57:16:28.0	18.29	8.00	251.3	<0.001	0.032	1.00	2	20.12	17.71	16.12	15.28	15.01	0	-
198	02:19:46.25	+57:11:48.8	19.42	11.8	249.0	<0.001	0.041	0.64	2	21.75	18.80	16.93	16.13	15.82	1	-
199	02:19:35.50	+57:07:00.6	18.69	3.50	248.9	<0.001	0.034	0.89	1	20.35	18.12	16.60	15.76	15.54	1	X
200	02:18:49.89	+57:01:12.8	17.09	3.12	248.2	<0.001	0.011	1.25	1	18.23	16.75	15.56	14.94	14.80	3	X
201	02:19:40.12	+57:03:55.4	18.58	0.418	247.1	<0.001	0.025	0.93	2	20.27	17.99	16.32	15.50	15.24	1	X
202	02:19:48.81	+57:05:26.3	18.10	0.330	247.0	<0.001	0.043	1.05	1	19.57	17.63	16.25	15.44	15.25	1	-
203	02:19:26.52	+57:12:31.7	18.59	0.281	246.6	<0.001	0.027	0.92	1	20.19	18.10	16.47	15.70	15.44	1	-
204	02:18:43.18	+57:07:23.1	17.19	1.88	246.2	<0.001	0.036	1.19	1	18.26	16.70	15.64	15.01	14.74	3	X
205	02:19:25.15	+57:09:48.3	17.01	1.19	246.1	<0.001	0.024	1.26	2	18.13	16.60	15.40	14.77	14.54	3	X
206	02:19:25.79	+57:05:25.3	18.77	0.297	245.9	<0.001	0.044	0.86	1	20.55	18.30	16.69	15.84	15.61	1	-
207	02:19:51.89	+57:15:05.1	18.79	0.348	245.8	<0.001	0.027	0.84	2	-	-	16.46	15.66	15.35	-	-
208	02:19:14.75	+57:04:29.6	15.72	0.808	245.5	<0.001	0.024	1.54	1	16.41	15.37	14.61	14.23	14.13	3	-
209	02:19:42.06	+57:06:04.9	18.93	7.14	245.2	<0.001	0.028	0.81	1	20.57	18.37	16.88	16.07	15.87	1	-
210	02:18:51.92	+57:06:56.7	18.21	4.95	245.1	<0.001	0.078	1.02	1	19.72	17.74	16.43	15.67	15.52	1	X
211	02:19:13.91	+57:05:32.1	18.41	7.46	245.0	<0.001	0.040	0.97	1	19.86	17.88	16.48	15.76	15.56	1	X
212	02:19:11.89	+57:16:01.4	19.02	11.0	244.8	<0.001	0.046	0.78	1	20.70	18.44	16.96	16.11	15.88	1	-
213	02:19:46.03	+57:00:48.3	18.54	5.65	244.5	<0.001	0.026	0.94	1	19.99	17.98	16.65	15.90	15.67	1	-
214	02:19:24.51	+57:01:53.3	16.76	0.334	244.3	<0.001	0.039	1.30	2	17.87	16.34	15.18	14.52	14.34	3	-
215	02:19:59.96	+57:10:12.4	16.02	0.0663	242.2	<0.001	0.004	1.39	1	16.95	15.59	14.66	14.25	14.04	3	-
216	02:19:26.64	+57:11:05.4	18.48	2.66	240.4	<0.001	0.030	0.95	1	19.98	18.01	16.52	15.76	15.51	1	X

Table 2. Continued.

HPer -ID	RA (deg)	DEC (deg)	i_{CFHT} (mag)	Period (d)	Power	FAP	amplitude (mag)	mass M_{\odot}	binary flag	V (mag)	Ic (mag)	J (mag)	H (mag)	K (mag)	Memb. flag	Other
217	02:19:17.42	+57:13:52.9	19.96	0.454	239.7	<0.001	0.094	0.49	1	-	-	17.47	16.61	16.31	-	-
218	02:18:22.22	+57:04:47.4	17.15	4.31	238.6	<0.001	0.012	1.24	1	18.27	16.80	15.69	15.11	14.95	3	-
219	02:19:50.27	+57:06:48.6	18.88	5.56	237.3	<0.001	0.025	0.82	1	20.54	18.27	16.77	15.98	15.76	1	-
220	02:19:50.24	+57:06:17.1	17.93	4.76	237.3	<0.001	0.024	1.10	1	19.43	17.53	16.01	15.29	15.10	1	X
221	02:19:55.75	+57:06:50.9	18.27	5.41	235.7	<0.001	0.026	1.01	1	19.62	17.72	16.32	15.61	15.41	1	X
222	02:19:06.28	+57:08:37.6	17.43	0.415	235.6	<0.001	0.055	1.19	1	-	-	15.69	15.09	14.83	-	X
223	02:18:32.15	+57:08:39.8	18.36	5.21	235.4	<0.001	0.026	0.99	1	-	-	16.51	15.75	15.49	-	-
224	02:18:07.55	+57:06:54.4	18.29	2.40	235.3	<0.001	0.028	1.00	1	19.79	17.82	16.45	15.69	15.46	1	-
225	02:19:40.42	+56:59:43.3	16.83	4.90	235.3	<0.001	0.016	1.29	1	-	-	15.48	14.95	14.75	-	-
226	02:18:07.33	+57:09:20.9	19.17	0.755	235.2	<0.001	0.038	0.73	1	-	-	17.00	16.14	15.88	-	-
227	02:18:51.80	+57:11:14.9	16.06	0.369	233.8	<0.001	0.007	1.39	2	17.11	15.61	14.57	13.98	13.76	3	X
228	02:19:41.01	+57:10:07.9	19.33	0.342	232.4	<0.001	0.035	0.67	2	-	-	16.78	15.96	15.66	-	-
229	02:18:43.78	+57:08:42.3	18.88	6.45	231.7	<0.001	0.053	0.82	1	-	-	16.95	16.21	15.89	-	-
230	02:19:35.44	+57:11:18.4	16.64	3.36	231.0	<0.001	0.012	1.32	1	17.64	16.23	15.16	14.63	14.45	3	X
231	02:19:35.29	+57:09:49.3	18.31	4.57	230.4	<0.001	0.022	1.00	2	19.98	17.75	16.23	15.42	15.13	1	-
232	02:19:46.83	+57:03:20.1	18.71	5.00	229.7	<0.001	0.036	0.89	1	20.30	18.22	16.72	15.94	15.72	1	-
233	02:19:37.99	+57:07:11.5	19.91	3.28	229.0	<0.001	0.059	0.50	2	-	-	17.34	16.49	16.20	-	-
234	02:19:23.34	+57:11:24.6	17.13	1.95	228.4	<0.001	0.019	1.24	2	18.11	16.58	15.42	14.78	14.57	3	X
235	02:18:50.86	+57:06:15.9	18.51	4.42	228.0	<0.001	0.030	0.94	1	20.04	18.08	16.62	15.89	15.70	1	X
236	02:19:16.84	+57:03:10.8	18.36	1.23	227.5	<0.001	0.033	0.99	1	19.83	17.88	16.49	15.72	15.50	1	X
237	02:19:14.13	+57:00:02.1	18.63	4.48	227.4	<0.001	0.024	0.91	1	20.30	18.06	16.50	15.70	15.47	1	-
238	02:18:30.10	+57:13:32.9	18.07	1.38	226.9	<0.001	0.017	1.06	2	19.72	17.53	16.04	15.22	14.95	1	-
239	02:17:55.58	+57:11:33.1	18.81	0.861	226.9	<0.001	0.046	0.85	1	20.34	18.24	16.70	15.88	15.62	1	-
240	02:19:50.23	+57:12:37.0	19.02	3.30	226.1	<0.001	0.029	0.77	1	20.74	18.48	16.97	16.13	15.85	1	-
241	02:19:31.42	+57:09:11.6	17.74	0.847	225.6	<0.001	0.024	1.13	2	19.34	17.27	15.77	15.02	14.76	3	X
242	02:18:02.50	+57:05:11.1	17.96	0.306	225.4	<0.001	0.017	1.09	1	-	-	16.20	15.47	15.24	-	-
243	02:19:22.24	+57:13:56.2	16.63	0.900	223.9	<0.001	0.010	1.32	2	17.75	16.21	14.99	14.42	14.21	3	X
244	02:18:31.45	+57:04:39.3	19.03	0.683	222.8	<0.001	0.037	0.77	1	20.80	18.49	16.89	16.06	15.80	1	-
245	02:18:47.01	+57:06:42.7	19.76	0.746	222.7	<0.001	0.074	0.53	1	22.50	19.24	17.25	16.49	16.20	1	-
246	02:18:00.27	+57:09:46.2	18.54	3.92	222.4	<0.001	0.019	0.94	1	20.06	18.07	16.59	15.81	15.56	1	-
247	02:18:47.38	+57:08:42.5	17.59	7.69	221.9	<0.001	0.028	1.16	1	-	-	15.90	15.23	14.97	-	X
248	02:18:22.58	+57:14:45.1	19.85	4.39	221.6	<0.001	0.052	0.52	1	22.56	19.26	17.34	16.55	16.24	1	-
249	02:19:03.50	+57:13:08.0	19.36	0.833	221.6	<0.001	0.056	0.67	2	21.23	18.69	16.95	16.14	15.83	1	-
250	02:18:13.49	+57:00:24.6	19.33	0.553	221.3	<0.001	0.043	0.66	1	21.33	18.75	16.99	16.18	15.92	1	-
251	02:18:45.12	+57:13:11.1	20.01	2.87	221.3	<0.001	0.056	0.47	1	22.31	19.50	17.58	16.80	16.47	1	-
252	02:19:24.26	+57:05:55.8	17.29	0.327	221.2	<0.001	0.027	1.21	2	18.63	16.86	15.57	14.91	14.70	3	X
253	02:18:21.34	+57:13:43.0	20.08	0.609	218.6	<0.001	0.082	0.45	1	-	-	17.59	16.83	16.53	-	-
254	02:18:31.46	+57:14:36.2	18.63	6.10	218.2	<0.001	0.028	0.91	2	20.51	18.09	16.42	15.64	15.35	1	-
255	02:19:20.03	+57:00:19.6	18.73	1.63	218.1	<0.001	0.033	0.88	1	20.41	18.14	16.62	15.83	15.58	1	-
256	02:19:03.58	+57:04:03.0	15.82	0.541	217.8	<0.001	0.005	1.43	2	16.64	15.45	14.51	14.11	13.92	3	X
257	02:18:16.07	+57:07:21.2	19.44	6.29	217.1	<0.001	0.056	0.64	1	-	-	17.20	16.38	16.11	-	-
258	02:18:15.06	+57:14:43.9	18.39	2.50	216.8	<0.001	0.018	0.98	1	-	-	16.44	15.65	15.41	-	-
259	02:19:51.30	+57:09:28.5	16.66	2.29	214.3	<0.001	0.006	1.31	1	17.65	16.27	15.31	14.84	14.63	0	-
260	02:18:58.98	+57:16:06.0	19.32	3.66	214.1	<0.001	0.041	0.67	1	21.24	18.78	17.13	16.26	15.99	1	-

Table 2. Continued.

HPer -ID	RA (deg)	DEC (deg)	i_{CFHT} (mag)	Period (d)	Power	FAP	amplitude (mag)	mass M_{\odot}	binary flag	V (mag)	Ic (mag)	J (mag)	H (mag)	K (mag)	Memb. flag	Other
261	02:18:42.75	+57:14:19.1	15.91	1.29	213.4	<0.001	0.004	1.41	2	16.72	15.53	14.61	14.11	13.94	3	-
262	02:18:35.97	+57:13:18.9	18.38	1.25	213.2	<0.001	0.029	0.99	1	19.82	17.89	16.40	15.64	15.40	1	-
263	02:19:33.92	+57:03:31.5	16.49	0.332	213.1	<0.001	0.011	1.34	2	17.61	16.08	14.91	14.31	14.15	3	X
264	02:18:49.71	+57:00:06.2	19.05	6.33	212.5	<0.001	0.053	0.76	1	-	-	16.98	16.19	15.97	-	-
265	02:18:17.39	+57:07:30.9	16.09	1.96	211.9	<0.001	0.008	1.38	2	17.13	15.75	14.67	14.16	14.03	3	X
266	02:19:38.99	+57:06:53.4	19.08	0.630	211.6	<0.001	0.044	0.75	2	21.33	18.42	16.59	15.77	15.48	1	X
267	02:18:53.89	+57:01:34.1	17.19	8.43	211.0	<0.001	0.019	1.23	1	-	-	15.53	14.89	14.73	-	X
268	02:18:54.16	+57:15:11.7	18.77	0.730	210.9	<0.001	0.020	0.87	1	20.37	18.20	16.65	15.86	15.62	1	-
269	02:18:30.13	+57:06:35.9	20.18	7.41	210.8	<0.001	0.081	0.43	1	22.64	19.59	17.64	16.86	16.59	1	-
270	02:19:26.59	+57:09:37.0	16.98	0.382	210.6	<0.001	0.009	1.27	2	18.14	16.55	15.36	14.73	14.52	3	X
271	02:19:26.77	+57:00:12.2	16.59	3.48	210.5	<0.001	0.016	1.32	1	17.52	16.14	15.39	14.80	14.59	3	-
272	02:18:52.34	+57:04:35.2	17.74	0.250	210.5	<0.001	0.025	1.14	2	19.14	17.29	15.84	15.10	14.84	3	X
273	02:19:21.07	+57:07:29.3	18.70	1.83	210.4	<0.001	0.045	0.89	1	20.25	18.23	16.64	15.87	15.69	1	X
274	02:19:32.83	+57:16:43.3	17.72	11.5	210.4	<0.001	0.014	1.14	1	18.99	17.24	16.00	15.29	15.06	1	-
275	02:18:44.00	+57:13:21.4	18.46	15.9	209.9	<0.001	0.039	0.95	2	20.42	17.93	16.26	15.47	15.16	1	X
276	02:17:56.52	+57:10:37.0	17.22	1.21	209.9	<0.001	0.011	1.23	1	18.19	16.75	15.74	15.23	15.04	0	-
277	02:18:53.55	+57:09:56.6	19.18	4.46	209.3	<0.001	0.047	0.71	1	-	-	17.14	16.32	16.05	-	-
278	02:19:58.46	+57:05:14.6	18.86	6.94	209.2	<0.001	0.021	0.83	1	20.70	18.36	16.80	15.96	15.71	1	-
279	02:19:18.12	+57:02:09.2	19.86	6.58	209.0	<0.001	0.080	0.52	1	21.88	19.19	17.49	16.65	16.36	1	-
280	02:19:43.09	+57:00:45.0	17.79	0.854	208.7	<0.001	0.041	1.12	1	-	-	16.16	15.48	15.25	-	-
281	02:18:25.86	+57:11:25.5	20.17	8.00	208.5	<0.001	0.077	0.43	1	22.64	19.52	17.73	16.92	16.62	1	-
282	02:18:52.95	+57:13:48.8	20.06	1.81	206.8	<0.001	0.070	0.46	1	-	-	17.44	16.73	16.42	-	-
283	02:18:05.14	+57:07:17.7	19.51	0.322	206.8	<0.001	0.057	0.61	1	21.59	18.99	17.21	16.34	16.08	1	-
284	02:18:01.32	+57:02:29.8	18.90	5.65	205.9	<0.001	0.026	0.81	1	20.59	18.44	16.93	16.11	15.88	1	-
285	02:18:16.36	+57:02:56.4	19.27	5.49	204.7	<0.001	0.039	0.70	1	-	-	17.05	16.27	16.00	-	-
286	02:19:51.46	+57:03:10.8	19.39	3.75	204.5	<0.001	0.045	0.65	1	21.26	18.75	17.13	16.26	16.04	1	-
287	02:19:32.90	+57:06:01.8	17.27	3.06	204.2	<0.001	0.019	1.22	1	18.46	16.83	15.59	15.04	14.87	0	X
288	02:19:33.51	+57:09:50.6	18.31	0.885	203.2	<0.001	0.038	1.00	1	-	-	16.35	15.64	15.37	-	-
289	02:18:32.12	+57:10:56.4	18.50	5.56	202.8	<0.001	0.021	0.94	1	20.07	18.07	16.67	15.88	15.64	1	-
290	02:18:31.03	+57:01:56.2	17.87	4.88	202.4	<0.001	0.018	1.11	1	19.09	17.40	16.17	15.47	15.26	1	-
291	02:18:51.37	+57:11:16.2	17.26	5.38	202.3	<0.001	0.021	1.23	1	18.38	16.84	15.70	15.05	14.86	1	X
292	02:18:35.42	+57:03:41.6	19.03	5.90	202.2	<0.001	0.035	0.77	1	20.75	18.52	16.93	16.11	15.91	1	X
293	02:18:47.14	+57:09:12.2	17.42	1.85	202.0	<0.001	0.012	1.19	1	18.62	16.97	15.83	15.20	14.97	0	X
294	02:19:51.31	+57:07:36.9	19.02	0.863	200.5	<0.001	0.038	0.78	2	21.18	18.46	16.66	15.81	15.56	1	X
295	02:19:08.05	+57:11:12.7	16.77	3.57	200.2	<0.001	0.010	1.30	2	17.88	16.32	15.15	14.58	14.37	3	X
296	02:19:34.66	+57:13:06.9	18.08	5.08	199.8	<0.001	0.024	1.06	1	19.36	17.62	16.30	15.59	15.39	1	-
297	02:18:24.90	+57:02:06.1	18.51	0.580	199.3	<0.001	0.071	0.92	1	-	-	16.58	15.66	15.48	-	-
298	02:18:08.87	+57:02:08.9	19.28	0.543	199.0	<0.001	0.034	0.69	2	-	-	16.76	15.98	15.70	-	-
299	02:18:07.84	+57:07:34.6	18.65	0.333	198.9	<0.001	0.026	0.90	1	20.26	18.14	16.68	15.86	15.65	1	-
300	02:18:50.71	+57:15:07.6	20.17	0.535	198.7	<0.001	0.078	0.44	1	22.52	19.62	17.56	16.78	16.49	1	-
301	02:18:01.64	+57:02:40.9	19.79	0.677	198.2	<0.001	0.070	0.53	1	21.85	19.20	17.48	16.64	16.39	1	-
302	02:18:55.07	+57:15:22.2	17.55	5.59	197.8	<0.001	0.012	1.17	2	19.13	17.11	15.56	14.80	14.59	3	X
303	02:18:54.69	+57:14:43.5	20.49	0.363	197.7	<0.001	0.075	0.36	2	22.92	19.83	17.76	16.95	16.64	1	-
304	02:19:32.43	+57:12:56.8	19.25	9.43	197.1	<0.001	0.037	0.70	1	20.95	18.62	17.03	16.20	15.94	1	-

Table 2. Continued.

HPer -ID	RA (deg)	DEC (deg)	i_{CFHT} (mag)	Period (d)	Power	FAP	amplitude (mag)	mass M_{\odot}	binary flag	V (mag)	Ic (mag)	J (mag)	H (mag)	K (mag)	Memb. flag	Other
305	02:18:03.23	+57:06:33.0	17.56	2.71	196.4	<0.001	0.017	1.15	1	—	—	15.83	15.06	14.86	—	—
306	02:18:55.33	+57:06:33.2	20.25	3.94	196.2	<0.001	0.095	0.41	1	23.14	19.59	17.73	17.01	16.72	1	X
307	02:19:31.58	+57:05:02.6	15.99	0.464	195.9	<0.001	0.006	1.40	2	16.95	15.54	14.58	14.04	13.90	3	X
308	02:19:38.26	+57:08:28.7	18.80	2.25	195.8	<0.001	0.031	0.85	1	20.40	18.30	16.81	15.95	15.72	1	—
309	02:18:01.15	+57:06:00.0	20.02	4.02	195.5	<0.001	0.079	0.48	1	22.34	19.35	17.52	16.81	16.52	1	—
310	02:18:09.29	+57:07:02.3	19.71	0.769	195.3	<0.001	0.045	0.55	1	21.98	19.15	17.28	16.45	16.21	1	X
311	02:18:12.92	+57:10:54.7	17.51	0.496	195.0	<0.001	0.015	1.18	1	18.71	17.08	15.87	15.22	15.00	3	—
312	02:19:23.54	+57:04:26.3	16.01	1.70	194.8	<0.001	0.006	1.40	2	16.87	15.56	14.66	14.13	13.98	3	X
313	02:18:33.66	+57:00:21.9	17.70	4.72	194.6	<0.001	0.020	1.15	2	19.13	17.22	15.80	15.05	14.84	3	—
314	02:18:08.07	+56:59:36.7	19.20	1.25	194.6	<0.001	0.067	0.72	1	—	—	17.12	16.28	16.04	—	—
315	02:19:25.34	+57:07:11.1	18.66	1.16	193.2	<0.001	0.028	0.90	1	20.17	18.02	16.61	15.82	15.60	1	—
316	02:19:26.20	+57:05:11.3	17.90	3.92	192.9	<0.001	0.025	1.10	1	—	—	16.11	15.44	15.23	—	X
317	02:18:58.15	+57:09:41.1	18.19	6.14	192.8	<0.001	0.036	1.03	2	—	—	16.15	15.37	15.10	—	X
318	02:18:07.51	+57:01:08.9	18.99	0.872	192.7	<0.001	0.033	0.79	1	20.74	18.47	16.91	16.09	15.85	1	—
319	02:18:09.34	+57:11:54.5	15.99	1.19	191.9	<0.001	0.005	1.39	2	17.09	15.61	14.56	13.94	13.77	1	—
320	02:20:00.82	+56:59:31.8	18.38	8.06	190.9	<0.001	0.034	0.98	1	19.72	17.85	16.73	15.91	15.63	1	—
321	02:19:32.82	+57:13:22.8	19.38	8.20	190.5	<0.001	0.057	0.67	1	—	—	17.18	16.33	16.04	—	—
322	02:18:36.93	+57:14:17.1	18.50	0.543	189.9	<0.001	0.023	0.91	2	20.64	18.03	16.38	15.58	15.29	1	—
323	02:18:24.39	+57:04:50.9	16.77	6.67	189.4	<0.001	0.006	1.30	1	17.77	16.41	15.40	14.90	14.74	0	—
324	02:18:18.16	+57:06:07.0	19.65	7.25	189.3	<0.001	0.028	0.57	1	21.70	19.08	17.32	16.50	16.23	1	—
325	02:19:42.26	+57:01:34.1	18.73	8.62	188.9	<0.001	0.025	0.87	1	20.29	18.18	16.75	15.99	15.77	1	—
326	02:19:26.47	+57:06:22.2	18.55	0.528	188.1	<0.001	0.054	1.00	1	20.13	18.04	16.47	15.73	15.51	1	X
327	02:18:04.66	+57:09:18.8	17.88	4.57	187.0	<0.001	0.011	1.11	1	19.28	17.38	16.06	15.37	15.12	1	—
328	02:18:16.87	+57:13:11.3	20.01	1.15	186.6	<0.001	0.058	0.47	1	22.46	19.39	17.57	16.78	16.49	1	—
329	02:18:06.64	+57:09:58.4	17.72	0.747	186.3	<0.001	0.011	1.14	1	19.06	17.32	15.94	15.26	15.03	3	—
330	02:19:08.05	+57:12:14.3	19.68	2.64	185.6	<0.001	0.035	0.57	2	22.17	19.02	17.17	16.32	16.00	1	—
331	02:18:16.22	+57:14:18.5	20.17	0.677	185.4	<0.001	0.054	0.43	1	—	—	17.63	16.87	16.58	—	—
332	02:19:33.97	+57:06:21.4	18.45	0.323	185.1	<0.001	0.018	0.96	1	20.04	18.00	16.43	15.63	15.41	1	X
333	02:19:43.10	+57:13:17.5	15.71	0.623	184.7	<0.001	0.005	1.54	1	16.33	15.31	14.60	14.28	14.16	3	—
334	02:18:53.71	+57:04:45.9	19.62	0.655	184.6	<0.001	0.094	0.58	1	—	—	17.20	16.46	16.17	—	—
335	02:19:43.53	+57:02:14.1	18.25	7.41	184.2	<0.001	0.015	1.02	1	19.50	17.64	16.33	15.60	15.39	1	X
336	02:18:50.88	+57:15:18.5	20.33	5.65	183.8	<0.001	0.056	0.40	1	23.01	19.71	17.64	16.84	16.54	1	—
337	02:18:32.14	+57:16:00.8	18.35	0.389	183.8	<0.001	0.030	0.99	1	—	—	16.43	15.62	15.38	—	—
338	02:18:53.49	+56:59:43.1	16.43	5.88	183.7	<0.001	0.005	1.34	1	—	—	15.05	14.53	14.40	—	—
339	02:18:49.25	+57:10:56.8	19.61	6.41	183.3	<0.001	0.071	0.58	1	—	—	17.21	16.42	16.10	—	—
340	02:19:49.48	+57:12:17.0	15.65	0.279	182.7	<0.001	0.003	1.60	1	16.33	15.29	14.52	14.23	14.08	3	—
341	02:19:37.84	+57:13:28.0	16.01	0.902	182.6	<0.001	0.004	1.39	1	16.86	15.62	14.77	14.34	14.20	1	X
342	02:18:47.44	+57:15:36.1	19.23	3.62	182.3	<0.001	0.028	0.70	1	21.05	18.67	17.03	16.19	15.92	1	—
343	02:19:40.20	+57:02:36.0	18.40	6.85	182.2	<0.001	0.020	0.97	1	20.00	17.95	16.50	15.72	15.49	1	—
344	02:18:16.73	+57:09:51.8	19.87	0.323	181.2	<0.001	0.056	0.51	1	—	—	17.40	16.56	16.27	—	—
345	02:18:15.46	+57:09:23.3	20.34	6.33	181.1	<0.001	0.084	0.40	1	22.76	19.68	17.85	17.12	16.77	1	—
346	02:19:57.05	+56:59:53.6	19.75	0.440	180.8	<0.001	0.049	0.54	1	22.17	19.15	17.35	16.49	16.17	1	—
347	02:18:09.53	+57:03:58.1	18.69	5.56	180.6	<0.001	0.018	0.89	1	—	—	16.60	15.82	15.58	—	—
348	02:19:41.33	+57:13:32.5	19.51	0.551	180.5	<0.001	0.035	0.62	1	21.48	18.87	17.21	16.38	16.09	1	—

Table 2. Continued.

HPer -ID	RA (deg)	DEC (deg)	i_{CFHT} (mag)	Period (d)	Power	FAP	amplitude (mag)	mass M_{\odot}	binary flag	V (mag)	Ic (mag)	J (mag)	H (mag)	K (mag)	Memb. flag	Other
349	02:19:42.68	+56:59:57.6	19.12	0.515	179.2	<0.001	0.033	0.74	2	21.46	18.50	16.72	15.98	15.67	1	-
350	02:18:51.73	+57:01:30.2	18.89	7.94	178.8	<0.001	0.039	0.82	1	-	-	16.83	16.01	15.81	-	X
351	02:18:33.69	+56:59:32.0	19.17	4.02	178.8	<0.001	0.027	0.72	1	-	-	16.88	16.08	15.80	-	-
352	02:17:58.35	+57:06:33.0	18.47	9.17	178.5	<0.001	0.024	0.96	1	19.96	17.94	16.52	15.79	15.59	1	-
353	02:19:14.58	+57:06:06.6	17.16	0.504	176.3	<0.001	0.029	1.24	1	18.16	16.70	15.62	15.00	14.81	1	X
354	02:19:37.14	+57:11:17.2	19.18	1.35	175.2	<0.001	0.022	0.72	1	21.20	18.60	16.88	16.04	15.75	1	-
355	02:19:47.45	+57:03:57.2	17.79	0.912	174.9	<0.001	0.021	1.12	1	18.93	17.23	15.96	15.26	15.05	1	X
356	02:19:35.44	+57:16:34.0	19.30	0.323	174.5	<0.001	0.026	0.68	1	21.24	18.67	16.94	16.09	15.81	1	-
357	02:18:11.45	+57:12:56.2	18.66	0.483	174.3	<0.001	0.022	0.90	1	20.19	18.17	16.69	15.91	15.65	1	-
358	02:19:22.63	+57:09:52.6	15.63	0.323	173.9	<0.001	0.009	1.59	1	16.37	15.27	14.44	14.11	13.93	3	X
359	02:19:25.60	+57:05:47.2	18.20	8.20	173.9	<0.001	0.026	1.03	1	19.62	17.71	16.32	15.61	15.40	1	X
360	02:19:58.00	+57:06:37.7	18.88	7.87	173.8	<0.001	0.025	0.83	1	20.56	18.30	16.78	15.98	15.77	1	-
361	02:18:53.78	+57:15:01.4	18.83	3.88	172.2	<0.001	0.020	0.84	1	20.53	18.33	16.75	15.95	15.70	1	-
362	02:18:58.41	+57:06:11.1	16.83	3.73	172.0	<0.001	0.021	1.29	1	-	-	15.42	14.91	14.76	-	X
363	02:18:30.59	+57:00:48.1	19.32	0.487	171.8	<0.001	0.039	0.68	2	-	-	16.87	16.05	15.77	-	-
364	02:18:12.42	+57:03:56.4	17.45	3.88	171.7	<0.001	0.011	1.19	1	18.72	17.05	15.78	15.14	14.96	3	X
365	02:18:19.46	+57:01:23.6	19.50	6.49	171.6	<0.001	0.060	0.62	1	21.62	18.98	17.25	16.47	16.22	1	-
366	02:19:03.27	+57:05:47.8	16.00	7.46	171.1	<0.001	0.004	1.40	1	16.89	15.60	14.71	14.27	14.09	3	-
367	02:18:32.00	+57:02:27.3	15.73	1.86	170.8	<0.001	0.003	1.45	1	16.55	15.40	14.54	14.10	13.96	3	X
368	02:18:23.17	+57:05:47.0	19.23	15.4	169.5	<0.001	0.039	0.70	1	21.15	18.66	16.95	16.14	15.85	1	-
369	02:20:00.33	+57:14:35.4	18.16	0.326	169.4	<0.001	0.021	1.04	2	19.81	17.65	16.20	15.36	15.11	1	-
370	02:18:46.33	+57:02:35.6	16.35	3.80	169.1	<0.001	0.006	1.36	1	-	-	15.01	14.55	14.41	-	-
371	02:19:46.76	+57:11:33.3	16.61	4.02	168.7	<0.001	0.007	1.32	1	17.74	16.24	15.18	14.64	14.45	3	X
372	02:19:51.00	+57:13:17.5	19.44	0.245	168.6	<0.001	0.051	0.69	1	21.00	18.63	17.11	16.28	15.98	1	-
373	02:18:50.34	+57:10:36.2	17.25	0.339	168.2	<0.001	0.010	1.23	1	18.48	16.84	15.62	14.97	14.78	0	-
374	02:18:36.91	+57:06:27.8	19.30	4.65	167.1	<0.001	0.054	0.69	1	-	-	17.09	16.27	16.06	-	X
375	02:19:22.39	+57:09:08.3	16.77	2.99	166.7	<0.001	0.006	1.30	2	17.91	16.37	15.18	14.57	14.32	3	X
376	02:19:16.54	+57:15:32.6	19.22	6.02	166.6	<0.001	0.037	0.70	2	21.41	18.69	16.86	16.01	15.67	1	-
377	02:18:42.97	+57:07:33.6	18.06	12.0	166.4	<0.001	0.027	1.07	2	19.72	17.59	16.16	15.30	15.05	1	X
378	02:18:24.75	+57:09:42.1	18.87	0.426	166.4	<0.001	0.027	0.84	1	-	-	16.81	16.00	15.72	-	-
379	02:18:26.84	+56:59:20.6	18.62	7.46	165.8	<0.001	0.023	0.90	1	20.16	18.11	16.74	15.97	15.75	1	-
380	02:18:15.62	+57:05:28.2	18.29	0.349	165.7	<0.001	0.013	1.01	1	19.79	17.82	16.42	15.63	15.40	1	-
381	02:18:25.30	+57:13:28.8	19.05	3.41	165.2	<0.001	0.023	0.77	1	20.82	18.40	16.86	16.06	15.79	1	-
382	02:20:01.41	+57:12:04.4	19.98	0.254	164.8	<0.001	0.055	0.49	1	22.09	19.33	17.59	16.70	16.41	1	-
383	02:18:47.40	+57:11:40.7	19.92	0.540	164.4	<0.001	0.041	0.49	1	22.03	19.40	17.55	16.73	16.42	0	-
384	02:18:10.66	+57:02:19.3	17.29	0.305	163.7	<0.001	0.012	1.22	2	-	-	15.59	14.87	14.68	-	-
385	02:18:52.57	+57:04:25.3	15.88	0.435	162.9	<0.001	0.009	1.40	2	-	-	14.57	13.92	13.74	-	X
386	02:18:46.86	+57:11:36.2	20.01	8.00	162.2	<0.001	0.040	0.48	1	22.69	19.35	17.43	16.70	16.37	1	-
387	02:18:00.23	+56:59:45.6	18.75	4.67	161.4	<0.001	0.066	0.86	1	-	-	16.77	15.96	15.73	-	-
388	02:19:57.51	+57:07:16.1	18.24	1.49	161.4	<0.001	0.013	1.01	1	19.74	17.81	16.36	15.61	15.42	1	-
389	02:18:09.89	+57:04:58.9	19.13	0.545	161.1	<0.001	0.025	0.74	2	-	-	16.71	15.86	15.60	-	-
390	02:19:40.72	+57:04:05.1	20.04	0.657	160.8	<0.001	0.032	0.47	1	22.41	19.40	17.48	16.66	16.37	1	-
391	02:19:32.87	+56:59:48.7	15.89	6.76	160.4	<0.001	0.004	1.41	1	16.78	15.52	14.66	14.16	14.01	3	-
392	02:18:35.41	+57:15:08.8	18.60	2.69	160.1	<0.001	0.018	0.92	1	20.12	18.10	16.66	15.89	15.65	1	-

Table 2. Continued.

HPer -ID	RA (deg)	DEC (deg)	i_{CFHT} (mag)	Period (d)	Power	FAP	amplitude (mag)	mass M_{\odot}	binary flag	V (mag)	Ic (mag)	J (mag)	H (mag)	K (mag)	Memb. flag	Other
393	02:19:16.94	+57:04:31.3	17.41	7.75	158.7	<0.001	0.013	1.20	1	18.53	16.93	15.78	15.18	15.00	1	X
394	02:18:47.27	+57:07:16.3	18.51	0.468	158.4	<0.001	0.042	0.94	1	-	-	16.54	15.74	15.51	-	-
395	02:17:56.26	+57:09:03.5	18.38	0.333	157.9	<0.001	0.021	0.98	1	-	-	16.41	15.69	15.40	-	-
396	02:20:00.73	+57:02:19.7	19.40	4.42	156.7	<0.001	0.038	0.65	1	21.23	18.81	17.17	16.34	16.07	1	-
397	02:18:53.42	+57:05:19.5	19.66	4.20	155.5	<0.001	0.045	0.57	1	21.77	19.10	17.35	16.52	16.26	1	-
398	02:19:15.70	+57:06:57.7	18.64	3.21	155.1	<0.001	0.042	0.91	1	-	-	16.66	15.87	15.63	-	-
399	02:19:06.36	+57:02:25.5	19.47	6.85	153.7	<0.001	0.044	0.63	1	21.49	18.92	17.28	16.44	16.18	1	-
400	02:18:23.94	+57:12:50.4	18.70	4.61	153.6	<0.001	0.020	0.89	1	20.23	18.17	16.73	15.95	15.69	1	-
401	02:18:33.32	+57:07:12.4	19.21	0.541	153.2	<0.001	0.031	0.70	2	21.43	18.64	16.81	16.03	15.73	1	X
402	02:18:01.06	+57:13:54.6	17.51	3.69	152.9	<0.001	0.009	1.18	1	18.73	17.09	15.71	15.03	14.82	1	-
403	02:18:18.92	+57:04:41.0	18.58	4.61	152.9	<0.001	0.016	0.92	1	20.11	18.11	16.61	15.85	15.61	1	X
404	02:19:21.62	+57:14:18.3	16.55	6.94	152.9	<0.001	0.004	1.33	1	17.48	16.12	15.15	14.64	14.47	1	-
405	02:18:25.53	+57:10:33.5	18.83	7.25	152.7	<0.001	0.022	0.83	1	-	-	16.91	16.09	15.86	-	-
406	02:18:29.89	+57:05:33.8	18.81	0.755	152.4	<0.001	0.012	0.85	1	20.60	18.29	16.64	15.83	15.56	1	X
407	02:19:01.42	+57:10:28.3	19.53	0.610	150.7	<0.001	0.050	0.61	2	-	-	17.04	16.27	15.96	-	-
408	02:19:36.76	+57:14:00.1	20.07	1.53	150.5	<0.001	0.044	0.46	2	-	-	17.35	16.62	16.28	-	-
409	02:18:44.69	+57:09:18.4	19.43	10.5	150.3	<0.001	0.029	0.64	2	21.83	18.84	17.02	16.22	15.89	1	X
410	02:18:24.70	+57:09:08.5	19.81	10.9	150.3	<0.001	0.053	0.53	1	-	-	17.55	16.77	16.44	-	-
411	02:18:53.37	+57:16:19.8	19.70	0.447	150.0	<0.001	0.045	0.56	1	21.88	19.10	17.28	16.44	16.15	1	-
412	02:18:09.02	+57:03:51.5	20.47	0.575	149.4	0.001	0.084	0.37	1	-	-	17.88	17.08	16.78	-	-
413	02:19:39.61	+56:59:51.2	16.77	8.13	149.4	0.001	0.008	1.30	1	17.77	16.34	15.33	14.79	14.59	3	-
414	02:18:46.75	+57:02:57.2	16.10	2.27	149.3	0.001	0.004	1.38	1	17.02	15.77	14.83	14.40	14.24	1	-
415	02:17:57.11	+57:10:00.5	20.12	0.665	149.2	0.001	0.093	0.44	1	22.48	19.45	17.50	16.73	16.40	1	-
416	02:19:05.37	+57:09:01.7	16.67	0.374	149.1	0.001	0.022	1.32	2	-	-	15.09	14.43	14.19	-	X
417	02:18:38.52	+56:59:39.4	19.11	6.76	148.5	0.001	0.036	0.75	1	-	-	17.03	16.19	15.97	-	-
418	02:18:31.74	+57:03:25.1	20.14	0.640	148.0	0.001	0.050	0.45	1	22.35	19.51	17.63	16.81	16.51	1	X
419	02:19:09.13	+57:05:57.1	19.98	6.85	147.5	0.001	0.055	0.48	1	22.09	19.21	17.54	16.70	16.42	1	X
420	02:19:24.66	+57:15:36.1	16.87	2.60	147.3	0.001	0.005	1.27	1	17.90	16.43	15.44	14.88	14.72	3	X
421	02:18:23.61	+57:12:40.5	18.56	11.2	147.2	0.001	0.032	0.93	1	-	-	16.68	15.90	15.68	-	-
422	02:18:22.94	+57:13:04.9	18.39	0.423	147.2	0.001	0.016	0.99	1	19.96	17.90	16.44	15.68	15.43	1	-
423	02:19:36.12	+57:08:30.1	20.69	1.43	146.7	0.001	0.071	0.32	1	23.49	20.03	18.02	17.21	16.86	1	X
424	02:18:07.07	+57:06:41.4	18.69	6.52	146.3	0.001	0.018	0.89	1	20.30	18.11	16.55	15.76	15.52	1	X
425	02:18:06.02	+57:11:16.8	19.85	0.620	145.8	0.001	0.034	0.51	1	22.12	19.25	17.38	16.61	16.31	1	-
426	02:18:23.25	+57:15:47.0	20.47	0.436	145.2	0.001	0.059	0.37	1	22.92	19.78	17.76	17.01	16.66	1	-
427	02:19:00.90	+57:04:49.0	16.77	4.05	144.8	0.001	0.012	1.30	2	18.00	16.37	15.17	14.56	14.36	3	X
428	02:18:35.81	+57:03:17.2	17.13	7.81	144.0	0.001	0.008	1.24	1	18.15	16.73	15.70	15.15	15.02	0	-
429	02:19:46.91	+57:02:03.8	19.31	0.455	143.5	0.001	0.027	0.68	2	21.36	18.68	16.78	15.97	15.68	1	-
430	02:19:32.90	+57:05:23.0	18.23	14.5	143.4	0.001	0.023	1.03	2	19.94	17.71	16.17	15.37	15.12	1	-
431	02:20:00.49	+57:03:28.2	19.34	0.447	142.6	0.001	0.038	0.66	1	21.12	18.78	17.04	16.20	15.96	1	-
432	02:19:18.35	+57:05:25.3	19.60	0.436	141.5	0.001	0.048	0.59	2	22.19	18.95	16.98	16.17	15.86	1	-
433	02:19:34.96	+57:06:12.8	16.55	4.39	141.0	0.001	0.005	1.33	1	-	-	15.11	14.64	14.50	-	-
434	02:20:00.47	+57:02:04.8	19.50	5.52	140.9	0.001	0.033	0.62	1	21.55	18.95	17.21	16.37	16.14	1	-
435	02:18:02.23	+57:03:59.7	19.58	4.72	140.6	0.001	0.056	0.58	1	-	-	17.28	16.42	16.15	-	-
436	02:18:32.93	+57:09:36.5	19.45	7.69	140.4	0.002	0.024	0.64	1	-	-	17.30	16.50	16.20	-	-

Table 2. Continued.

HPer -ID	RA (deg)	DEC (deg)	i_{CFHT} (mag)	Period (d)	Power	FAP	amplitude (mag)	mass M_{\odot}	binary flag	V (mag)	Ic (mag)	J (mag)	H (mag)	K (mag)	Memb. flag	Other
437	02:19:32.65	+57:11:16.8	19.58	10.2	140.4	0.002	0.025	0.59	1	21.50	19.02	17.39	16.55	16.26	1	-
438	02:19:39.45	+57:09:40.9	19.90	3.26	140.3	0.002	0.038	0.51	1	22.06	19.31	17.50	16.68	16.38	1	-
439	02:18:22.74	+57:01:48.9	18.17	3.39	140.2	0.002	0.026	1.04	1	-	-	16.28	15.57	15.35	-	-
440	02:18:32.49	+57:13:39.1	18.26	0.343	139.7	0.002	0.018	1.01	1	-	-	16.48	15.76	15.49	-	-
441	02:19:54.04	+57:04:53.1	16.63	0.795	139.6	0.002	0.006	1.32	1	17.50	16.19	15.29	14.86	14.72	0	X
442	02:19:43.74	+57:02:52.5	20.27	6.02	139.5	0.002	0.067	0.41	1	22.75	19.61	17.63	16.79	16.52	1	X
443	02:19:42.50	+57:02:07.9	19.98	7.52	139.3	0.002	0.039	0.48	1	22.29	19.38	17.48	16.64	16.35	1	-
444	02:17:59.45	+57:07:19.2	20.05	0.518	139.3	0.002	0.066	0.47	1	-	-	17.61	16.85	16.59	-	-
445	02:19:23.08	+57:11:35.1	19.15	8.62	138.0	0.002	0.028	0.67	1	-	-	16.98	16.17	15.88	-	-
446	02:18:30.64	+57:09:33.5	19.24	5.26	137.6	0.002	0.028	0.70	2	-	-	16.81	16.05	15.73	-	X
447	02:18:25.53	+57:03:37.2	20.41	4.05	137.0	0.002	0.097	0.38	1	23.09	19.77	17.92	17.14	16.82	1	-
448	02:18:33.91	+57:11:50.2	18.71	4.88	136.4	0.002	0.021	0.87	1	20.47	18.27	16.76	15.96	15.72	1	-
449	02:19:06.75	+57:05:54.6	19.40	7.96	136.0	0.002	0.055	0.65	1	21.38	18.85	17.20	16.40	16.14	1	X
450	02:18:31.56	+57:01:30.2	20.30	7.52	135.9	0.002	0.077	0.39	1	-	-	17.83	17.03	16.76	-	-
451	02:18:02.24	+57:00:16.5	19.40	7.87	135.8	0.002	0.028	0.65	1	21.36	18.77	17.12	16.38	16.11	1	-
452	02:19:24.24	+57:03:15.8	16.70	5.05	135.6	0.002	0.005	1.31	1	17.67	16.33	15.38	14.94	14.79	0	-
453	02:19:53.35	+57:09:06.2	17.36	8.33	135.1	0.002	0.007	1.21	2	18.71	16.87	15.59	14.92	14.67	3	-
454	02:18:36.37	+57:03:52.1	20.15	8.26	134.9	0.003	0.080	0.44	1	22.40	19.55	17.66	16.86	16.60	1	-
455	02:19:02.99	+57:13:01.6	18.56	3.95	134.8	0.003	0.019	0.93	2	20.40	18.03	16.35	15.55	15.24	1	X
456	02:19:01.12	+57:09:58.4	16.26	10.9	134.7	0.003	0.009	1.36	1	17.19	15.86	14.92	14.48	14.28	1	X
457	02:19:24.33	+57:04:18.9	17.85	6.69	134.2	0.003	0.016	1.11	1	19.29	17.35	15.95	15.21	15.00	3	X
458	02:18:35.46	+57:15:05.3	20.17	0.827	133.5	0.003	0.037	0.44	1	22.55	19.64	17.59	16.81	16.52	1	-
459	02:18:36.22	+57:16:11.3	19.99	0.341	133.5	0.003	0.048	0.48	1	22.25	19.38	17.53	16.68	16.37	1	-
460	02:19:49.57	+57:10:20.1	19.71	2.63	133.3	0.003	0.030	0.56	1	21.93	19.10	17.42	16.52	16.23	1	X
461	02:19:08.24	+57:02:34.5	18.83	10.5	133.3	0.003	0.024	0.84	1	20.50	18.31	16.82	16.05	15.80	1	-
462	02:18:44.17	+57:12:47.5	17.59	3.82	133.2	0.003	0.007	1.16	1	18.81	17.17	15.94	15.29	15.06	1	X
463	02:18:28.13	+57:00:06.6	15.83	10.0	133.1	0.003	0.002	1.43	2	16.74	15.46	14.56	14.00	13.85	3	-
464	02:18:57.26	+57:11:15.8	17.55	0.479	132.2	0.004	0.013	1.17	2	-	-	15.66	14.93	14.70	-	X
465	02:19:22.16	+57:12:52.9	19.23	5.41	131.4	0.005	0.029	0.70	2	21.35	18.69	16.86	16.05	15.72	1	-
466	02:17:56.78	+57:06:31.1	18.94	7.46	131.3	0.005	0.022	0.81	1	-	-	16.96	16.15	15.94	-	-
467	02:18:18.99	+57:10:19.9	16.14	3.57	130.4	0.005	0.004	1.38	1	16.96	15.77	14.86	14.39	14.22	3	-
468	02:19:31.00	+57:14:31.7	17.76	1.50	130.1	0.005	0.009	1.13	2	19.29	17.27	15.84	15.06	14.82	3	X
469	02:18:34.50	+57:11:10.8	19.03	6.99	129.9	0.005	0.020	0.77	1	20.87	18.48	17.00	16.23	15.97	1	-
470	02:18:36.22	+57:13:47.4	20.01	0.421	129.9	0.005	0.038	0.48	1	-	-	17.48	16.67	16.39	-	-
471	02:18:14.88	+57:13:22.6	17.30	0.256	129.7	0.005	0.007	1.22	2	18.59	16.79	15.43	14.68	14.44	1	-
472	02:19:53.44	+57:12:43.6	20.40	0.454	129.5	0.005	0.052	0.38	1	-	-	17.79	16.95	16.60	-	-
473	02:19:36.74	+56:59:59.2	15.79	0.873	128.9	0.006	0.003	1.44	1	16.41	15.42	14.77	14.41	14.28	3	-
474	02:18:02.78	+57:10:22.7	19.10	6.10	128.8	0.006	0.022	0.75	1	21.06	18.53	16.82	16.01	15.72	1	-
475	02:19:34.14	+57:10:44.4	17.87	6.25	128.6	0.006	0.017	1.11	1	19.15	17.39	16.09	15.40	15.19	1	-
476	02:18:09.14	+57:10:13.3	18.65	5.10	128.1	0.006	0.016	0.90	1	-	-	16.72	15.93	15.67	-	-
477	02:18:02.91	+57:10:37.0	16.03	1.56	128.0	0.006	0.002	1.39	1	16.88	15.68	14.82	14.41	14.27	3	-
478	02:19:36.21	+57:14:55.0	19.60	0.473	127.3	0.006	0.023	0.59	1	21.77	19.00	17.21	16.39	16.09	1	-
479	02:18:51.36	+57:04:13.1	18.91	7.63	127.3	0.006	0.043	0.82	1	-	-	16.84	16.06	15.84	-	X
480	02:19:12.08	+57:06:01.8	20.28	5.56	127.2	0.006	0.075	0.40	1	-	-	17.80	17.03	16.76	-	-

Table 2. Continued.

HPer -ID	RA (deg)	DEC (deg)	i_{CFHT} (mag)	Period (d)	Power	FAP	amplitude (mag)	mass M_{\odot}	binary flag	V (mag)	Ic (mag)	J (mag)	H (mag)	K (mag)	Memb. flag	Other
481	02:18:33.83	+57:15:01.0	16.19	6.52	126.9	0.006	0.004	1.38	2	-	-	14.77	14.25	14.11	-	-
482	02:18:45.40	+57:14:23.9	20.27	0.260	126.9	0.006	0.097	0.43	1	-	-	18.65	17.82	17.59	-	-
483	02:19:06.68	+57:11:02.6	20.29	0.395	126.8	0.006	0.091	0.41	2	23.72	19.63	17.64	16.75	16.44	1	-
484	02:19:44.07	+57:03:11.9	16.04	0.149	126.8	0.006	0.003	1.39	1	16.85	15.64	14.76	14.35	14.22	3	-
485	02:19:00.50	+57:06:46.6	18.76	2.64	126.0	0.006	0.059	0.87	1	-	-	16.79	16.06	15.84	-	-
486	02:19:55.09	+57:09:33.2	17.65	7.35	125.9	0.006	0.007	1.15	1	18.85	17.18	16.03	15.39	15.15	1	-
487	02:19:18.34	+57:04:56.4	19.15	4.12	125.8	0.006	0.035	0.73	1	20.99	18.64	17.01	16.21	15.99	1	X
488	02:19:21.39	+57:13:44.3	19.52	0.537	125.7	0.006	0.020	0.61	2	21.89	18.86	16.90	16.10	15.78	1	-
489	02:19:43.54	+57:16:41.9	18.15	4.52	125.6	0.006	0.017	1.04	1	19.73	17.62	16.29	15.47	15.18	1	-
490	02:19:36.10	+57:09:11.6	19.77	0.550	124.3	0.007	0.038	0.54	1	21.98	19.15	17.37	16.59	16.23	1	-
491	02:19:57.75	+57:04:03.0	19.27	1.30	123.9	0.007	0.023	0.69	2	21.54	18.62	16.79	15.96	15.70	1	-
492	02:19:58.20	+57:10:32.2	17.33	6.14	123.5	0.007	0.006	1.21	2	18.72	16.89	15.61	14.88	14.62	3	-
493	02:19:23.73	+57:03:01.3	19.12	6.03	123.2	0.007	0.030	0.74	1	20.90	18.57	17.06	16.20	15.97	1	X
494	02:20:03.18	+57:11:45.0	18.50	0.231	123.0	0.007	0.016	0.95	2	20.46	17.93	16.32	15.43	15.12	1	-
495	02:18:02.60	+57:09:46.4	18.24	2.93	122.6	0.008	0.012	1.02	1	-	-	16.30	15.55	15.30	-	-
496	02:18:45.57	+57:13:02.8	18.86	10.8	121.9	0.009	0.017	0.83	2	20.90	18.30	16.63	15.79	15.49	1	-
497	02:17:56.75	+57:10:54.7	19.98	8.47	121.7	0.009	0.049	0.48	1	22.21	19.38	17.58	16.72	16.42	1	-
498	02:18:29.49	+57:10:42.1	19.82	0.336	121.1	0.009	0.053	0.47	1	-	-	17.46	16.65	16.31	-	-
499	02:19:17.65	+57:13:16.4	18.71	4.88	120.6	0.009	0.020	0.88	1	20.26	18.18	16.69	15.91	15.65	1	-
500	02:18:01.61	+57:10:55.5	19.54	0.468	120.3	0.009	0.033	0.61	1	21.64	18.98	17.13	16.34	16.07	1	-
501	02:18:14.67	+57:04:00.5	19.69	0.543	120.3	0.009	0.039	0.56	2	21.75	19.05	17.08	16.29	15.99	1	X
502	02:18:33.95	+57:10:39.7	20.29	1.34	120.1	0.009	0.049	0.41	1	-	-	17.82	17.02	16.72	-	-
503	02:19:21.82	+57:07:07.2	18.64	0.842	118.4	0.009	0.021	0.91	1	20.22	18.15	16.65	15.87	15.67	1	X
504	02:18:03.08	+57:15:34.0	19.56	0.645	118.2	0.009	0.037	0.60	2	21.86	18.90	16.91	16.11	15.81	1	-
505	02:18:25.64	+57:09:05.4	20.12	3.79	118.0	0.009	0.045	0.45	1	-	-	17.62	16.90	16.54	-	X
506	02:19:37.14	+57:12:25.1	18.45	3.33	117.4	0.009	0.009	0.97	2	20.36	17.93	16.22	15.40	15.12	1	-
507	02:18:36.80	+57:14:30.3	19.57	1.17	116.4	0.01	0.041	0.60	1	-	-	17.34	16.52	16.27	-	-
508	02:18:03.27	+57:08:23.3	19.95	10.9	115.2	0.01	0.034	0.50	1	22.29	19.37	17.60	16.81	16.52	1	-
509	02:18:17.30	+57:06:59.6	16.99	3.40	115.2	0.01	0.015	1.26	2	18.08	16.55	15.36	14.66	14.47	3	X
510	02:19:24.22	+57:13:24.3	20.53	2.16	114.8	0.01	0.050	0.36	1	-	-	17.91	17.13	16.81	-	-
511	02:19:23.74	+57:14:01.8	18.86	0.792	114.7	0.01	0.016	0.83	1	20.49	18.27	16.75	15.94	15.68	1	-
512	02:19:01.95	+57:00:43.1	19.79	0.450	113.9	0.01	0.049	0.52	1	22.14	19.20	17.33	16.58	16.29	1	-
513	02:18:19.68	+57:16:06.8	20.38	0.0983	113.6	0.01	0.050	0.39	1	-	-	17.60	16.89	16.62	-	-
514	02:19:35.98	+57:08:56.1	19.86	5.41	113.0	0.01	0.037	0.51	1	22.05	19.27	17.54	16.69	16.39	1	-
515	02:19:11.00	+57:09:29.5	17.65	0.357	111.7	0.011	0.029	1.15	1	18.95	17.26	15.87	15.22	14.96	1	X
516	02:19:53.09	+57:03:50.4	20.56	0.446	111.3	0.011	0.070	0.36	1	23.03	19.83	17.89	17.08	16.80	1	-
517	02:18:11.00	+57:02:46.1	18.35	4.18	111.2	0.011	0.013	0.99	1	19.73	17.88	16.55	15.79	15.58	1	-
518	02:19:33.64	+57:14:08.6	20.03	7.75	111.0	0.011	0.037	0.47	1	22.24	19.36	17.66	16.83	16.52	1	-
519	02:18:33.63	+57:14:37.1	19.89	1.26	110.9	0.011	0.035	0.51	1	22.19	19.25	17.51	16.67	16.39	1	-
520	02:19:39.05	+57:10:57.4	19.65	0.463	110.8	0.011	0.023	0.58	2	21.97	19.00	17.02	16.24	15.93	1	-
521	02:19:15.60	+57:02:46.3	19.85	0.814	110.8	0.011	0.054	0.51	1	22.06	19.22	17.39	16.62	16.33	1	-
522	02:19:20.87	+57:10:42.8	19.85	7.75	110.1	0.011	0.065	0.52	1	22.37	19.40	17.48	16.64	16.34	1	-
523	02:18:34.62	+57:13:29.8	17.57	8.03	109.9	0.011	0.006	1.17	2	-	-	15.77	15.02	14.80	-	-
524	02:18:04.19	+57:15:38.3	16.65	7.32	109.8	0.011	0.007	1.32	1	17.64	16.22	15.23	14.65	14.49	1	-

Table 2. Continued.

HPer -ID	RA (deg)	DEC (deg)	i_{CFHT} (mag)	Period (d)	Power	FAP	amplitude (mag)	mass M_{\odot}	binary flag	V (mag)	Ic (mag)	J (mag)	H (mag)	K (mag)	Memb. flag	Other
525	02:18:08.28	+57:13:42.2	19.63	12.5	109.5	0.011	0.020	0.58	1	—	—	17.22	16.42	16.13	—	—
526	02:19:06.22	+57:04:41.6	18.73	6.25	109.5	0.011	0.036	0.88	1	20.31	18.21	16.74	15.97	15.73	1	X
527	02:18:32.05	+57:11:57.8	17.80	0.259	109.4	0.011	0.010	1.13	1	19.02	17.32	16.08	15.37	15.15	0	—
528	02:18:05.73	+57:09:01.3	19.70	1.23	108.6	0.011	0.027	0.56	1	21.80	19.08	17.39	16.64	16.31	1	—
529	02:19:16.04	+57:04:59.5	18.84	0.285	108.1	0.011	0.022	0.85	1	—	—	16.72	15.90	15.67	—	—
530	02:18:36.67	+57:08:29.9	18.28	1.68	107.8	0.011	0.012	1.01	1	—	—	16.49	15.75	15.50	—	X
531	02:18:25.19	+57:12:05.3	16.25	3.26	107.4	0.011	0.004	1.37	1	17.14	15.86	14.93	14.48	14.33	3	—
532	02:19:38.21	+57:00:29.7	19.05	6.45	107.3	0.011	0.020	0.76	1	20.88	18.49	16.97	16.17	15.91	1	—
533	02:19:51.82	+57:01:54.1	20.13	3.76	107.1	0.011	0.036	0.44	1	22.37	19.48	17.64	16.84	16.58	1	—
534	02:19:06.94	+57:05:36.5	19.22	3.91	106.6	0.012	0.021	0.70	1	21.07	18.66	17.04	16.23	15.97	1	—
535	02:18:36.21	+57:13:05.3	19.78	2.23	105.8	0.012	0.046	0.54	1	22.15	19.23	17.40	16.58	16.29	1	—
536	02:19:31.99	+57:08:49.3	19.76	4.00	105.2	0.012	0.055	0.55	1	—	—	17.39	16.53	16.20	—	—
537	02:18:31.12	+57:12:19.3	18.12	6.08	104.7	0.012	0.027	1.05	2	—	—	16.09	15.35	15.06	—	—
538	02:18:32.96	+56:59:32.8	18.94	3.77	103.5	0.014	0.020	0.81	1	—	—	16.94	16.14	15.87	—	—
539	02:18:24.39	+57:05:50.1	19.82	6.76	103.3	0.014	0.022	0.53	2	22.34	19.20	17.21	16.45	16.15	1	—
540	02:19:33.86	+57:14:59.6	20.09	4.55	103.0	0.014	0.036	0.45	1	—	—	17.70	16.90	16.59	—	—
541	02:19:21.43	+57:05:36.9	18.81	8.13	102.6	0.014	0.017	0.85	2	20.83	18.25	16.52	15.69	15.43	1	—
542	02:18:45.36	+57:13:54.2	20.61	3.11	102.2	0.014	0.062	0.34	1	23.51	19.99	18.11	17.34	17.02	1	—
543	02:19:37.25	+57:10:55.5	19.25	0.271	101.4	0.015	0.018	0.69	1	21.16	18.79	17.00	16.20	15.90	1	—
544	02:19:09.21	+57:04:36.4	18.19	0.272	101.0	0.015	0.015	1.04	1	19.66	17.70	16.25	15.48	15.24	1	X
545	02:18:45.42	+57:07:51.8	20.58	3.25	101.0	0.015	0.062	0.36	1	—	—	18.07	17.26	16.92	—	—
546	02:19:52.62	+57:08:38.0	19.24	7.81	100.8	0.015	0.017	0.69	1	21.46	18.67	16.96	16.10	15.79	1	—
547	02:18:23.88	+57:03:28.4	18.58	0.461	100.0	0.015	0.014	0.93	2	20.37	18.05	16.31	15.52	15.26	1	X
548	02:19:34.87	+57:01:25.4	19.49	5.24	99.8	0.015	0.026	0.63	1	21.44	18.84	17.27	16.44	16.14	1	—
549	02:19:25.89	+57:10:43.0	19.22	6.72	98.7	0.015	0.022	0.71	1	21.05	18.66	17.04	16.25	15.96	1	—
550	02:18:07.95	+57:03:59.3	15.81	0.314	98.1	0.015	0.002	1.43	1	16.50	15.47	14.73	14.40	14.29	3	—
551	02:18:32.37	+57:09:48.3	20.56	0.360	96.8	0.016	0.054	0.34	1	—	—	17.87	17.10	16.77	—	—
552	02:18:33.58	+57:07:38.6	18.96	6.94	96.3	0.016	0.016	0.80	1	—	—	16.89	16.08	15.85	—	X
553	02:18:04.70	+57:04:20.5	20.08	5.88	95.2	0.016	0.033	0.46	1	22.39	19.41	17.63	16.84	16.57	1	—
554	02:18:05.61	+57:03:29.8	20.03	3.79	94.6	0.016	0.030	0.47	1	—	—	17.47	16.71	16.41	—	—
555	02:19:38.65	+57:09:02.3	19.78	2.93	94.5	0.016	0.039	0.54	2	22.25	19.13	17.20	16.43	16.08	1	—
556	02:18:19.73	+57:06:57.3	19.35	3.45	94.1	0.016	0.021	0.66	1	21.18	18.86	17.23	16.39	16.15	1	—
557	02:18:25.96	+57:04:13.1	19.73	7.25	93.2	0.017	0.039	0.55	1	—	—	17.34	16.51	16.22	—	—
558	02:19:52.04	+57:02:19.1	16.65	6.83	92.9	0.018	0.004	1.31	1	17.67	16.25	15.21	14.68	14.54	3	—
559	02:18:28.61	+57:07:26.0	19.59	5.05	91.3	0.019	0.024	0.59	1	21.84	18.98	17.19	16.42	16.15	1	—
560	02:19:12.01	+57:13:25.5	19.83	0.631	91.2	0.019	0.022	0.52	1	21.98	19.18	17.40	16.55	16.26	1	—
561	02:19:50.23	+57:10:56.8	20.14	11.4	88.8	0.024	0.028	0.44	1	22.35	19.45	17.69	16.87	16.55	1	—
562	02:19:43.02	+57:13:10.9	16.53	6.85	88.7	0.024	0.003	1.33	2	17.73	16.05	14.94	14.26	14.09	3	—
563	02:19:40.15	+57:09:57.4	20.63	0.475	87.0	0.025	0.045	0.34	1	—	—	17.94	17.16	16.82	—	—
564	02:19:18.72	+57:05:33.4	16.15	2.82	86.9	0.025	0.003	1.38	2	17.21	15.74	14.65	14.11	13.96	3	—
565	02:19:45.17	+57:05:07.4	20.06	0.686	84.7	0.027	0.031	0.46	1	22.47	19.43	17.50	16.68	16.40	1	—
566	02:18:37.46	+57:07:40.0	16.92	10.4	84.6	0.027	0.004	1.28	1	18.04	16.54	15.41	14.78	14.63	3	—
567	02:18:43.48	+57:10:32.6	20.56	0.622	83.8	0.028	0.045	0.35	1	—	—	18.01	17.25	16.94	—	—
568	02:19:51.85	+57:03:41.4	19.73	0.320	83.5	0.029	0.020	0.55	2	22.26	19.01	17.01	16.22	15.90	1	X

Table 2. Continued.

HPer -ID	RA (deg)	DEC (deg)	i_{CFHT} (mag)	Period (d)	Power	FAP	amplitude (mag)	mass M_{\odot}	binary flag	V (mag)	Ic (mag)	J (mag)	H (mag)	K (mag)	Memb. flag	Other
569	02:18:32.86	+57:06:24.5	20.31	1.37	82.7	0.029	0.040	0.40	1	23.07	19.68	17.72	16.98	16.64	1	-
570	02:18:08.83	+57:05:22.4	19.93	6.58	82.5	0.03	0.041	0.49	1	22.06	19.29	17.56	16.73	16.44	1	-
571	02:19:23.18	+57:02:10.8	19.53	6.04	81.5	0.031	0.044	0.61	1	21.58	18.92	17.31	16.48	16.21	1	-
572	02:18:32.09	+57:11:15.3	20.38	2.25	81.4	0.031	0.035	0.38	1	22.97	19.84	17.91	17.18	16.87	1	X
573	02:20:02.66	+57:04:26.3	20.39	1.61	79.6	0.034	0.065	0.39	1	22.83	19.74	17.77	16.97	16.69	1	-
574	02:18:48.55	+57:10:30.4	19.80	3.26	78.8	0.035	0.024	0.53	1	21.99	19.17	17.49	16.68	16.37	1	-
575	02:19:42.62	+57:09:05.4	18.75	5.18	78.4	0.036	0.010	0.87	1	20.40	18.27	16.76	15.98	15.69	1	-
576	02:19:41.12	+57:07:53.4	18.86	0.369	77.9	0.036	0.017	0.84	2	20.90	18.24	16.53	15.67	15.38	1	X
577	02:18:48.88	+57:07:41.7	19.93	3.31	77.8	0.036	0.033	0.48	1	22.03	19.35	17.59	16.73	16.45	1	X
578	02:18:18.44	+57:07:22.1	19.52	0.269	77.6	0.036	0.023	0.61	1	-	-	17.19	16.37	16.08	-	X
579	02:19:10.80	+57:05:25.5	20.53	0.252	77.6	0.036	0.072	0.36	1	23.10	19.85	17.80	17.01	16.69	1	X
580	02:18:42.78	+57:14:13.4	16.36	2.89	77.4	0.036	0.002	1.35	1	17.27	15.98	15.01	14.51	14.35	3	X
581	02:19:48.49	+57:03:17.6	20.35	3.28	77.0	0.038	0.034	0.39	1	22.83	19.64	17.75	16.93	16.66	1	-
582	02:19:06.94	+57:14:08.8	20.45	0.694	76.6	0.04	0.036	0.37	1	-	-	17.87	17.06	16.72	-	-
583	02:19:36.57	+57:02:53.1	16.26	0.216	75.7	0.044	0.002	1.37	1	17.17	15.83	14.86	14.40	14.24	3	X
584	02:19:33.01	+57:06:48.4	20.03	4.48	74.7	0.045	0.034	0.46	1	22.37	19.42	17.45	16.68	16.39	1	-
585	02:19:16.17	+56:59:23.5	20.38	1.56	72.8	0.049	0.049	0.39	1	22.84	19.70	17.72	16.94	16.66	1	-
586	02:19:58.23	+57:07:22.7	18.94	3.16	72.5	0.049	0.016	0.81	1	20.73	18.41	16.83	15.98	15.77	1	-